TAMPEREEN TEKNILLINEN YLIOPISTO
TAMPERE UNIVERSITY OF TECHNOLOGY

UJJWAL DATTA

ENHANCED OPERATIONAL PERFORMANCE OF SIIRTOVERKKOMALLI USING STATIC COMPENSATORS AND BESS EQUIPMENT

Master of Science thesis

Examiner: Dr. Prof. Enrique Acha
Examiner and topic approved by the Faculty Council of the Faculty of Computing and Electrical Engineering on June 8th, 2016

ABSTRACT

UJJWAL DATTA: Enhanced operational performance of Siirtoverkkomalli using Static Compensators and BESS equipment
Tampere University of technology
Master of Science Thesis, 66 pages, 12 Appendix pages
August 2016
Master of Science (Tech) in Electrical Engineering
Major: Smart Grid
Examiner: Prof. Enrique Acha

Keywords: Facts devices (SVC, STATCOM, BESS), Batteries, Voltage Stabilization, Frequency Stabilization, Converters.

This thesis reports on an investigation of the impact of static var compensators (SVC) and static compensators (STATCOM) on the voltage and frequency stability of *practical* transmission system. It also explores an application of a battery energy storage system (BESS) which serves the purpose of stabilizing an otherwise unstable power transmission network.

A mismatch of energy production and consumption at a given area results in power exports over long distances, sometimes across borders. Power exporting and system stability are some of the major concerns in the transport of electrical energy. It has been acknowledged that FACTS devices are a possible way forward to ensure high throughputs of power with enhanced stability. FACTS equipment has lived up-to its promise in cases where system stability has been a concern. BESS application in power transmission is a new area of study which is just commencing to be explored.

The thesis assesses the impact of the SVC and STATCOM on Siirtoverkkomalli and Nordic-32 in an equivalent form. It includes a comparative study of both FACTS devices under unstable network conditions. Preliminary assessments have indicated that, BESS are very effective means for providing frequency and voltage support during load variations. In this thesis, BESS is applied in Siirtoverkkomalli to assess whether or not BESS can be effective to stabilize an otherwise unstable network.

It has been found that using both the SVC and STATCOM in a transmission system significantly improves stability. The comparison shows that the STATCOM is very effective, outperforming the better known SVC. On the other hand, when a BESS is applied in Siirtoverkkomalli, it shows that it has great potential in stabilizing an otherwise unstable system. Hence, a BESS can perform multiple functions, it provides stability support, similar to the SVC or STATCOM, but it can provide frequency support during load changing periods.

PREFACE

I would like to thank Professor Enrique Acha for his endless support, thoughtful suggestions, encouragement which broaden my thoughts and enriched my skills throughout the thesis period.

I would like to thank my parents for their unconditional support and inspiration throughout my entire life as well into higher education.

At last but not the least, Fingrid Oyj, for their support and opportunity to work in a project with them and experienced somewhat a real network dynamics analysis.

Tampere, 1.8.2016

Ujjwal Datta

CONTENTS

ABBREVIATIONS AND NOTATIONS

NOTATIONS

Synchronous generator

$E_d^{"}$ = d-axis component of the sub-transient internal e.m.f proportional to total flux linkage in the q-axis damper winding

$E_q^{"}$ = q-axis component of the sub-transient internal e.m.f proportional to total flux linkage in the d-axis damper winding

$E_q^{'}$ = q-axis component of the transient internal e.m.f proportional to the field winding flux linkage

E_{fd} = generator field voltage

e_t = generator terminal voltage in d-q axis frame –of-reference

E_t = generator terminal voltage in D-Q axis frame –of-reference

i_g = generator armature current in d-q axis frame –of-reference

X_d, X_q = synchronous reactance in d and q axis, respectively

$X_d^{'}, X_q^{'}$ = transient synchronous reactance in d and q axis, respectively

$X_d^{"}, X_q^{"}$ = sub-transient synchronous reactance in d and q axis, respectively

$\tau_{do}^{'}$ = open circuit d-axis transient time constant

$\tau_{qo}^{"}$ = open circuit q-axis sub-transient time constant

δ = rotor angle

ω = rotor speed

P_e = electrical power injected into the grid system

P_m = mechanical power supplied by the governor to the generator

H = inertia constant

Static var compensator

B_c = capacitive suceptance

X_L = inductive reactance

X_C = capacitive reactance

Reactive tie-line system

X_t = reactive tie-line reactance

i_t = current injected at the infinite bus

ABBREVIATIONS

SVC=Static var compensator

STATCOM=Static compensator

BESS=Battery energy storage system

SOC=State of charge

VSI=Voltage source inverter

VSC=Voltage source converter

AC=Alternating current

DC=Direct current

LiC_6= Lithiated graphite

GTO=Gate turn-off thyristor

IGBT=Insulated gate bipolar thyristor

IGCT= Integrated gate-commutated thyristor

1 Introduction

Growing population and industrialization has led to large increases in electrical energy demand; requiring the installation of a large number of central generating stations of large rating. Electrical energy is the most malleable and efficient form of energy to deliver to the end user, compared to any other form of energy i.e. gas, oil, heat. Electricity sources may be divided into renewable and non-renewable. At present, nearly 80% of the total electricity generation comes from non-renewable sources, whereas about 20% comes from hydro and other renewable energy sources [1].

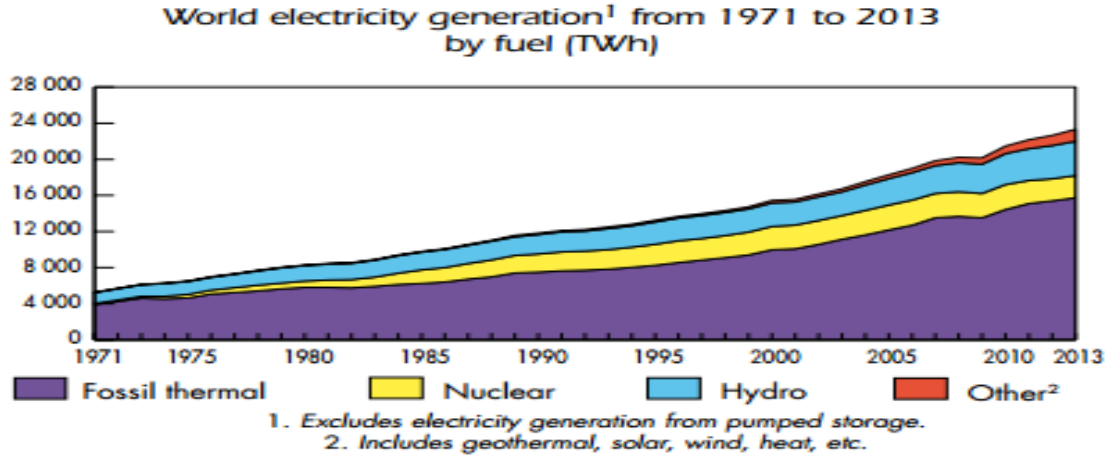

Figure 1-1 Electricity generation by fuel [1]

Due to the fact that electricity generation and consumption clusters are not always located near to each other, electricity transmission over long distances is a necessity, although distributed generation is expected to increase in near future. The latter is expected to bring about benefits to transmission assets since it will relieve congestion and bring down power transmission losses. Note that congestion worse during peak demand; particularly one of the heavily loaded lines undergoes disconnection due to a short-circuit fault or relay mal-operation. In extreme but quite realistic situations, faults in heavily loaded or congested lines may cause total power system blackouts.

System stability may be enhanced by the use of FACTS devices. Several FATCS devices have proved to be effective in stabilizing power systems undergoing a variety of faulted conditions. Static Var Compensators, Static Compensator, Unified Power Flow Controller (UPFC) and a few others, each with their own characteristics, have been inexistence for two decades. They provide reactive power support during the fault time to stabilize the power system. The first generations of FACTS devices are able to provide reactive power, not active power, hence, they cannot provide system frequency support during load changing.

Technological development, environmental awareness and policy support have increased very considerably the penetration of renewable energy. Renewable energy generation from solar PV and wind currently stand at 1.3% and 2.5% respectively of the total global electricity demand [2] [3]. Increased penetration of renewable energy sources, which have an intermittent nature, poses certain concerns to power systems operators. Fluctuations in the power output of renewable energy sources make the system frequency more difficult to stabilize. Moreover, renewable electrical energy is not considered a resolute source due to its dependency on weather conditions. Hence, continuity of supply cannot be guaranteed and the system reliability becomes a matter of great concern.

The current thought is that energy storage system integration with renewable energy sources will make up for a more reliable and secure way of energy supply, leading to a primer generation. Energy storage in the form of chemical storage is not a new concept by any means. Energy storage systems take charge, stores and discharges the energy with relatively low power loss, significantly improving the overall system performance; it flattens load-demand curve [4]. Also, storage systems are able to reduce the fluctuations in the power output of renewable energy sources. They would charge during the day time when demand is low and release energy during peak times and at night.

There are multiple energy storage systems available with different physical characteristics which make a direct comparison between the various storage systems, more complex. The key parameters includes energy density per mass and volume, cycle efficiency, permissible number of charge-discharge cycles, lifetime, time of reverse and response time level, optimal power output, optimal stored energy etc. [4].

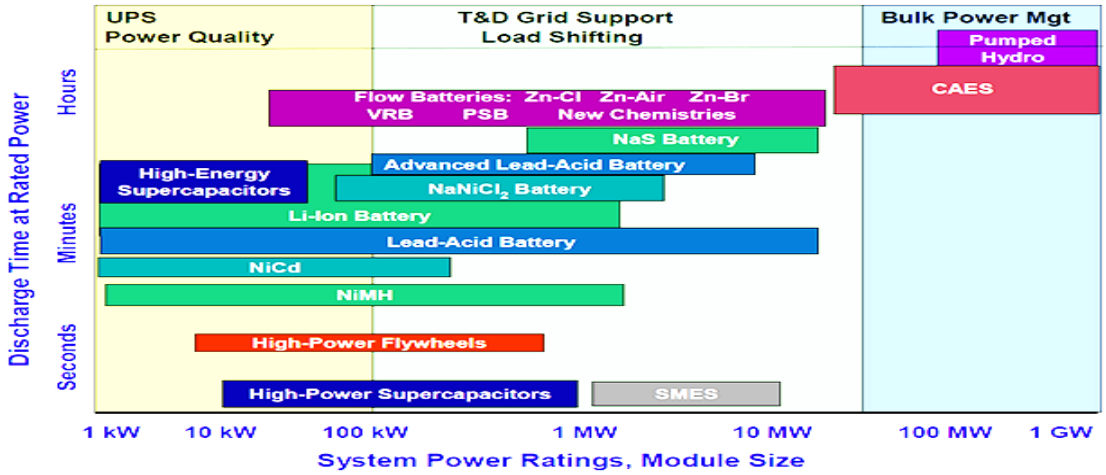

Figure 1-2 Comparison of existing energy storage technologies [5]

From *Figure 1-2*, it can be observed that selection of a particular storage system depends on energy storage capacity and discharge time. A deep study of energy storage system can be found in [4] and [6].

Battery Energy Storage Systems, which belong to the second generation of FACTS equipment, can provide effective system frequency and voltage support. For certain purposes, they may be thought of as being static generators; the range of operational and environmental benefits over the traditional fossil fuel based power plants. BSS produce lower Co_2 emissions. Carbon-dioxide productions per kilowatt-hour when generating electricity with fossil fuels are Coal (Bituminous) 939g of Co_2 per kWh, natural gas 553g of Co_2 per kWh, Distillate oil (No. 2) 744g Co_2 per kWh [7]. Co_2 emission by the BESS depends on the type of battery being used i.e. lead-acid batteries accounts 59g Co_2/kWh and lithium-ion battery storage results 20g Co_2/kWh [8].

1.1 State-of-the-art of Static var compensator and Static Compensator

With the advent of competitive deregulated electricity markets, utilities are bound to integrate into their systems, generation sources and loads in whatever location they may exist within their jurisdiction. Economic power flows demand the system to operate at maximum power transport capacity and this can lead to voltage security problems and congestion in the network. The traditional solution to energy demand increases has been to construct new transmission lines and power plants, but due to the growing expense of power transmission infrastructure, well-grounded environmental concerns and legislation, it is getting more difficult to obtain permission to construct new transmission lines.

Alternatively, reactive power compensation in transmission networks yields effective voltage support to reduce voltage fluctuations and to improve system stability, enabling maximum power transmissions in the compensated transmission lines. A case in point is the SVC which provides rapid reactive power supply owing to its thyristor valve switching compared to mechanical switches. SVCs can regulate voltage according to its droop setting at or near constant value, improving system performance [9]. They can also reduce losses while increasing the transfer capability and mitigation of active power oscillations [10]. More details and an in-depth explanation of the SVC operations and performance improvement may be found in [9] [11] [12] [13]. SVCs are found in transmission and industrial installations; in fact they have been used for quite a long time. However, compared to the new breed of reactive power consumptions, they are found to have limited operational flexibility and their popularity is decreasing.

The STATCOM is a more advanced form of FACTS devices, design to control reactive power, supports in such a way that it acts independently of AC voltage [14]. Hence, the STATCOM provides rated capacitive and inductive power irrespective to system AC voltage. The major attributes of the STATCOM compared to an equivalent SVC, are quick response, smaller rating, less installation space requirement, lower loss, lower low-order harmonics and higher operational flexibility. They have been in operation since the mid1980s, starting at 20MVAR ratings [15]. Since then they have been replacing SVCs and other slow-acting controllers in the power system. The power semiconductor devices used in STATCOMs were GTOs, but further developments gradually moved the technology to use IGBTs, IGCTs.

The STATCOM is a mature piece of technology which has found several applications including power quality improvement [16], [17], reactive power control, voltage regulation [18], [19], transmission line capacity enhancement, dynamic stability improvement [20], [21]. The STATCOM is not only used at the transmission level, it is being used more and more in distribution applications. Application of STATCOMs in wind farms has great prospects, to support the grid-connection of wind farms to the transmission network.

1.2 State-of-the-art of battery energy storage technology and modeling/simulation

The STATCOM with an integrated energy storage system on its DC side becomes a static generator which can be controlled to supply or absorb both active and reactive powers. In fact it provides a similar function to synchronous generator but with an improved response time because of its absence of moving parts. When a DC power source is fitted to a STATCOM, such as a battery pack, the arrangement is termed Battery Energy Storage System (BES/BESS).The traditional STATCOM has been designed to absorb/injects only reactive power.

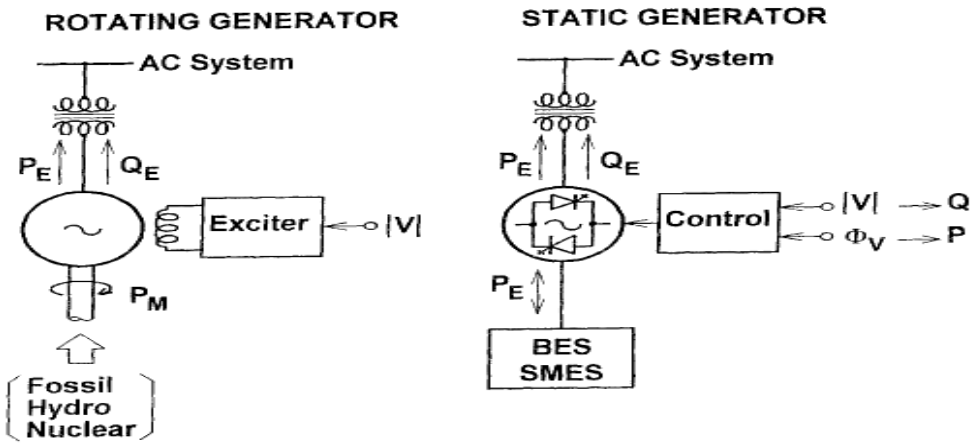

Figure 1-3 Rotating and Static genrator [22]

The BESS can be connected at all voltage levels of the power system, provided suitable power electronics converters and the transformers are employed. A BESS can provide both technical and economic benefits, including frequency control capability in the power system by controlling the rate of charging and discharging of the battery, reduce transmission congestion [23] which is beneficial for utility companies, cuts cost for customers and compensates peak time generations, decreasing the expense of electricity generation.

The growing popularity of BESS stems from the rapid technological improvements in batteries. The Li-ion battery first appeared in the market in 1991; they had an immediate and growing popularity because of their higher energy density, low maintenance, and low self-discharge. Despite of having fragility, temperature, environmental and protection issues; suitable packaging reduces the negatives of Li-ion batteries very significantly. There has been a 20-50% reduction in battery price over the last decade.

Several BESS have been installed worldwide aimed at frequency support applications and for improving system reliability and operational flexibility. The installed capacity of BESS is expected to reach G\W worldwide by the end of 2017.

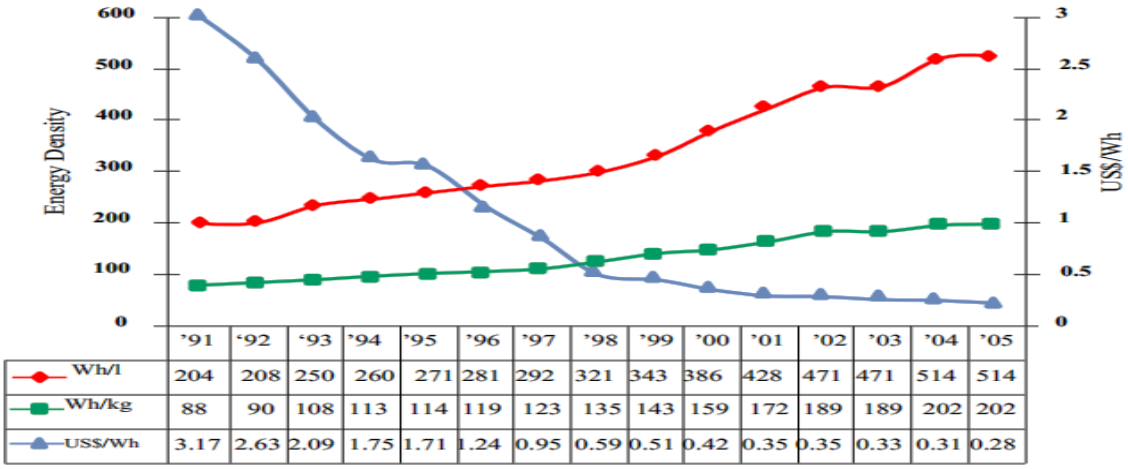

	'91	'92	'93	'94	'95	'96	'97	'98	'99	'00	'01	'02	'03	'04	'05
Wh/l	204	208	250	260	271	281	292	321	343	386	428	471	471	514	514
Wh/kg	88	90	108	113	114	119	123	135	143	159	172	189	189	202	202
US$/Wh	3.17	2.63	2.09	1.75	1.71	1.24	0.95	0.59	0.51	0.42	0.35	0.35	0.33	0.31	0.28

Figure 1-4 Li-ion pricing and energy density over periods [24]

Several BESS models have been put forward in recent times. The basic idea is to combine battery storage with a DC-DC converter and connect this to the DC side of a VSC. The battery model used in this BESS is given in [25], having a similar functionality to that in [26], [27]. The DC-DC converter, which controls active power flow by controlling its switching, is a Cúk converter. The VSC controls the reactive power flow on its AC side to regulate voltage.

1.3 Thesis Outline

This thesis contains four chapters. Chapter 2 discusses synchronous generator modeling of different orders, exciters, and turbine-governor systems. Chapter 3 includes a description of the Static Var Compensator (SVC), the Static Compensator (STATCOM), and a general description of equipment used in Siirtoverkkomalli. It goes on to discuss the impact of FACTS device implementation in Siirtoverkkomalli to alleviate a number of operational problems arising in the network owing to short-circuit faults and increased power transfers between areas. Chapter 4 addresses the topic of BESS, including the battery, the DC-DC converter, the VSC and PWM control. It concludes with an assessment of the BESS in stabilizing the Siirtoverkkomalli network. This includes cases of faults on the DC side of BESS.

2 Small signal modeling of synchronous generator-Single machine connected to an infinite bus

2.1 Introduction

In large interconnected power systems, spontaneous system oscillations at very low frequencies are the norm rather than the exception. For synchronous machine's stability analysis at small perturbations scale, a transfer function block diagram of a single machine infinite-bus system has been extensively used [28] [9] [29] [30] [31]. An extended transfer function block diagram of synchronous generators based on the classical concepts was put forwarded in [32] [33] and used to assess and evaluate further the generator's dynamic performance.

A synchronous generator comprises the field winding and the armature winding. The former is excited by an external source of direct current through the exciter (described in section *2.5*). When the rotor is driven by a turbine, a rotating magnetic field is produced in the air gap, producing an alternating set of voltages across the stator's three -phase terminal. Active power can be transferred when a load is connected to the generator terminal, with a frequency which is a function of the amount of the connected load and the turbine-governor system, if one is available.

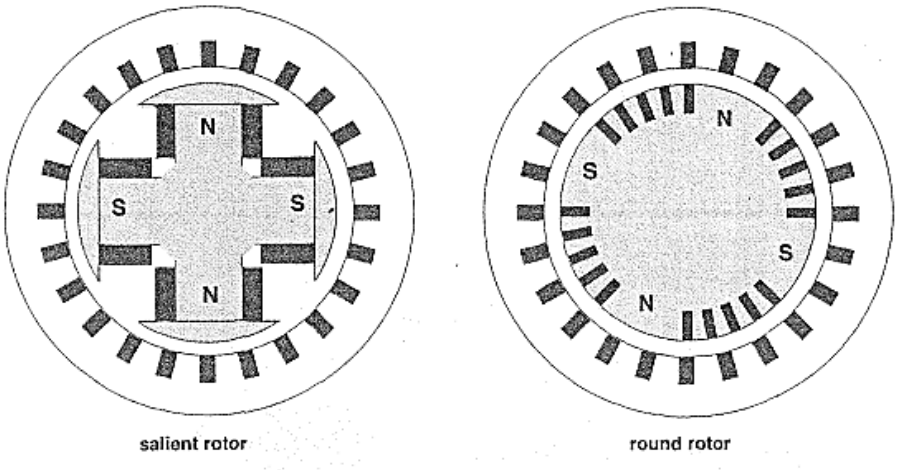

Figure 2-1 Cross sections of salient and cylindrical four pole machines [34]

Salient-pole construction is mostly used in low-speed applications such as hydro generators and cylindrical or round-rotor construction is favored in high speed applications, such as steam generators [34].

2.2 Synchronous machine modeling

For system stability analysis, the basic consideration is that the three-phase synchronous generator has two synchronously rotating fields, one DC-excited field on the rotor together with amortisseur windings, mechanically rotated. The other is an AC-excited stator circuit which takes the form of a three-phase armature winding, with each phase displaced from each other by 120 electrical degrees. The current in the amortisseur coils are assumed to flow in two sets of closed circuits: one along the *d*-axis and other along the *q*-axis [9] [29].

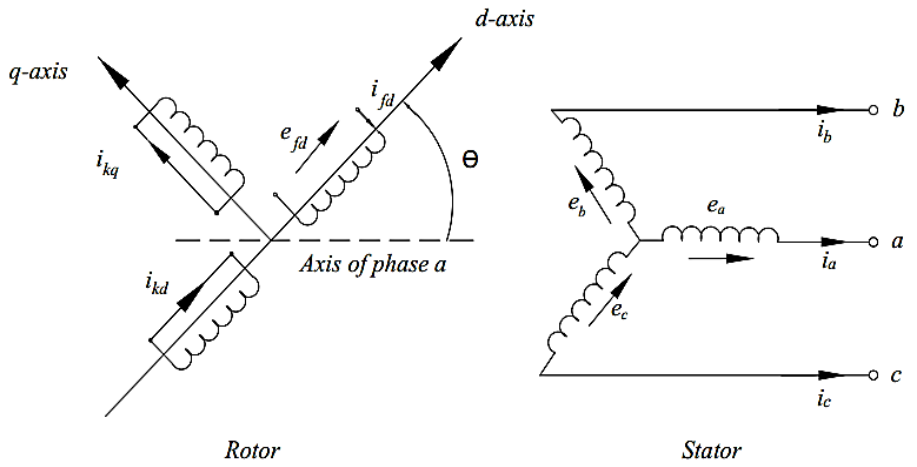

Figure 2-2 Rotor and stator circuit of synchronous machine

2.2.1 Phasor and mathematical representation of a synchronous machine

The electrical characteristic of a three-phase synchronous machine can be described by an equivalent two-phase frame-of-reference, expressed in *d* and *q* axis coordinates. Since the inertia of a synchronous machine prevents instant changes of flux linkage, it is convenient to separates its study into steady-state, transient, sub-transient conditions [9]. An example of a synchronous machine phasor diagram in the *d*-*q* axis for steady state operation is shown in *Figure 2-3* [28].

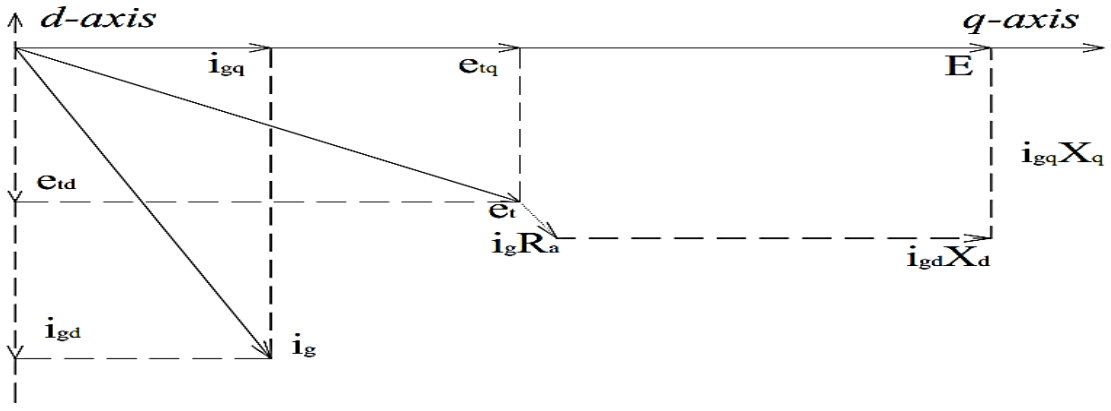

Figure 2-3 Phasor representation of a synchronous machine under steady-state operation

From *Figure 2-3*, each phasor quantity can be represented in terms of its *d* and *q* axis components,

$$\overrightarrow{i_g} = i_{gd} + ji_{gq} \tag{2-1}$$

$$\overrightarrow{e_t} = e_{td} + je_{tq} \tag{2-2}$$

The algebraic equations of the synchronous machine, according to *Figure 2-3*, are as follows:

$$e_{td} = X_q i_{gq} + R_a i_{gd} \tag{2-3}$$

$$e_{tq} = E_f - X_d i_{gd} + R_a i_{gq} \tag{2-4}$$

On the other hand, the algebraic equations for the synchronous machine model, under transient conditions, shown by the phasor diagram in *Figure 2-4*, can be written as follows:

$$E_d^{'} - e_{td} = R_a i_{gd} - X_q^{'} i_{gq} \tag{2-5}$$

$$E_q^{'} - e_{tq} = R_a i_{gq} + X_d^{'} i_{gd} \tag{2-6}$$

The corresponding differential equation can be written as follows:

$$\frac{dE_d^{'}}{dt} = \frac{1}{\tau_{qo}^{'}}\left[i_{gq}\ (X_q - X_q^{'}) - E_d^{'} \right] \tag{2-7}$$

$$\frac{dE_q^{'}}{dt} = \frac{1}{\tau_{do}^{'}}\left[E_{fd} - i_{gd}\ (X_d - X_d^{'}) - E_q^{'} \right] \tag{2-8}$$

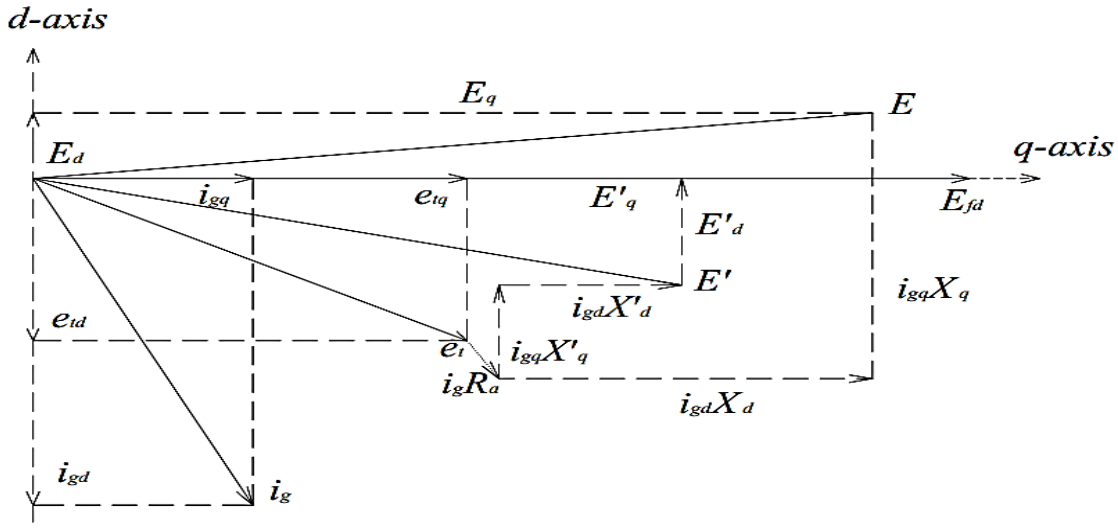

Figure 2-4 Phasor representation of synchronous machine during the transient operating state

The sub-transient equations can be derived by extension of the transient equations:

$$E_d^{"} - e_{td} = R_a i_{gd} - X_q^{"} i_{gq} \tag{2-9}$$

$$E_q^{"} - e_{tq} = R_a i_{gq} + X_d^{"} i_{gd} \tag{2-10}$$

$$\frac{dE_d^{"}}{dt} = \frac{1}{\tau_{qo}^{"}}\left[i_{gq}\left(X_q^{'} - X_q^{"}\right) - E_d^{"} \right] \tag{2-11}$$

$$\frac{dE_q^{"}}{dt} = \frac{1}{\tau_{do}^{"}}\left[E_q^{'} - i_{gd}\left(X_d^{'} - X_d^{"}\right) - E_q^{"} \right] + \frac{dE_q^{'}}{dt} \tag{2-12}$$

The equations of active and reactive powers are:

$$S = P + jQ = \overline{e_t}\,\overline{i_g}^{*} \tag{2-13}$$

$$S = (e_{td} i_{gd} + e_{tq} i_{gq}) + j\,(e_{tq} i_{gd} - e_{td} i_{gq}) \tag{2-14}$$

Dynamic equations of motion:

The power system responds to a disturbance by deviating its operating frequency away from the nominal frequency; each generator experiences an accelerating or a decelerating torque as a result of the imbalance between electrical toque and mechanical torque. This phenomenon can be described by the so-called *swing equation*, presented as follows:

$$\frac{d\Delta\omega}{dt} = \frac{1}{2H}[P_m - P_e - D\Delta\omega] \tag{2-15}$$

$$\frac{d\delta}{dt} = \omega_o \Delta\omega \tag{2-16}$$

2.3 Mathematical formulation of the system under study

The test system to be used for the mathematical model being developed, corresponds to a synchronous machine connected to an infinite bus through a purely inductive transmission line, as shown in *Figure 2-5*.

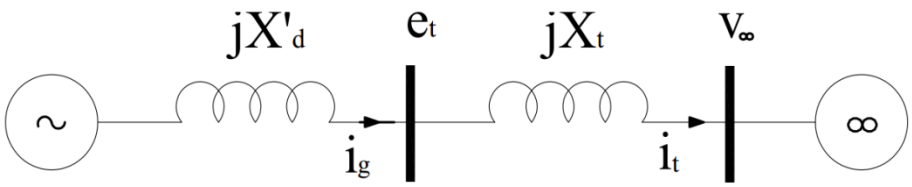

Figure 2-5 One Machine Infinite System under study

The modeling complexity of the synchronous machine to be used in system stability studies, should be commensurate with the nature of the study. The small signal model is developed from first principles, using the synchronous generator's non-linear differential and algebraic equations. For small-disturbance rotor-angle stability analysis, an accurate representation of the field circuit as well as the rotor damper circuits is of paramount importance [35]. Several transfer function models, arising from the dynamic equations, are established for the salient-pole synchronous generator with varying degrees of rotor winding representation [36] [37]. It should be remember that the complexity of the models goes hand in hand with their accuracy.

Model 1

This model comprises the effect of the generator main *field winding* and one damper winding in the *d-axis* and one in the *q-axis*.

Model 2

The damper winding in the *d-axis* rotor circuit is removed from Model 1 to construct Model 2. Hence $E_d^{''}$ is replaced by $E_d^{'}$ and $X_d^{''}$ is replaced by $X_d^{'}$.

Model 3

All damper windings in Model 1 and Model 2 are neglected. Hence, only the effect of the field winding exists, i.e. $X_d^{''} = E_d^{''} = X_d^{'} = E_d^{'} = 0$.

2.4 Representation of the system model

Linearization of the dynamic equations, with the detail presented in *Appendix A* yields the following transfer function, in S domain, shown in *Figure 2-6*:

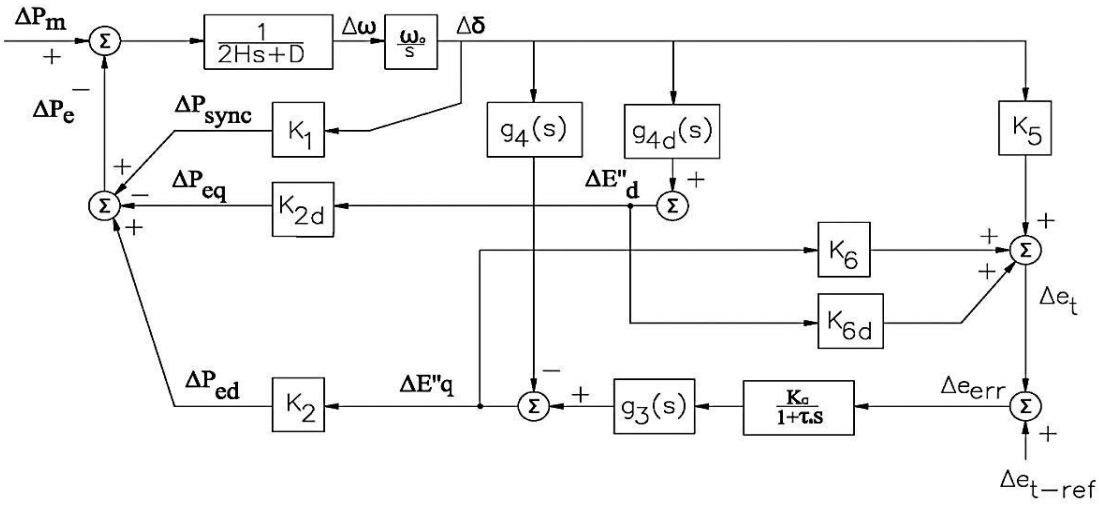

Figure 2-6 Detail block diagram of the synchronous generator

Model 1

The phasor diagram of the system under study can be drawn as shown in *Figure 2-7*:

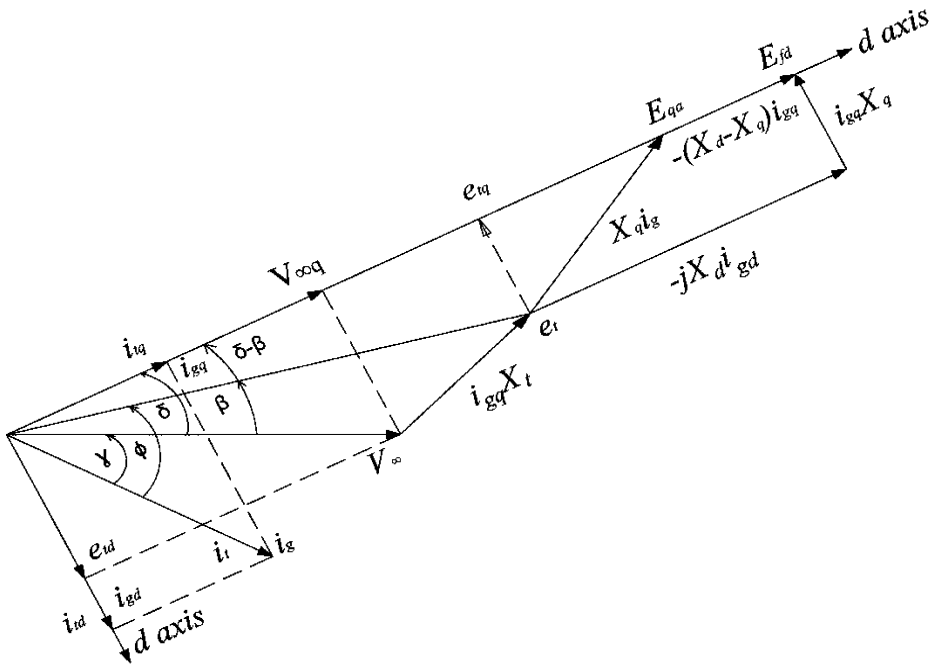

Figure 2-7 Vector diagram of a synchronous generator

From the vector diagram, taking the generator rotor position as the reference vector is:

$$\Delta V_{\infty q} = V_\infty \, Cos\,\delta \tag{2-17}$$

$$\Delta V_{\infty d} = V_\infty \, Sin\,\delta \tag{2-18}$$

For small variations,

$$\Delta V_{\infty q} = -V_{\infty o} Sin\,\delta_0 = -V_{\infty do}\Delta\delta \tag{2-19}$$

$$\Delta V_{\infty d} = V_{\infty o} \, Cos\,\delta_0 \, \Delta\delta = V_{\infty qo}\Delta\delta \tag{2-20}$$

From *Figure 2-7*,

$$\overrightarrow{i_g} = \overrightarrow{i_t} \tag{2-21}$$

Separating into real and imaginary parts, (2-21) can be written as follows,

$$i_{gd} = i_{td} \tag{2-22}$$

$$i_{gq} = i_{tq} \tag{2-23}$$

For small variations,

$$\Delta i_{gd} = \Delta i_{td} \tag{2-24}$$

$$\Delta i_{gq} = \Delta i_{tq} \tag{2-25}$$

Alternatively, (2-21) can be re-written as follows,

$$\overrightarrow{i_g} = \frac{\vec{e}_t - \vec{V}_\infty}{jX_t} \tag{2-26}$$

Separating into real and imaginary parts,

$$e_{tq} = i_{gd} X_t + V_{\infty q} \tag{2-27}$$

$$e_{td} = V_{\infty d} - i_{gq} X_t \tag{2-28}$$

Substituting the stator voltage equation (2-10) into (2-27) yields,

$$E_q^{"} - X_d^{"} i_{gd} = i_{gd} X_t + V_{\infty q}$$

$$i_{gd} = \frac{E_q^{"} - V_{\infty q}}{(X_d^{"} + X_t)} \tag{2-29}$$

Substituting the stator voltage equation (2-9) into (2-28) yields,

$$E_d^{"} + X_q^{"} i_{gq} = i_{gq} X_t + V_{\infty d}$$

$$i_{gq} = \frac{V_{\infty d} - E_d^{"}}{(X_q^{"} + X_t)} \tag{2-30}$$

D-axis Flux Linkage Voltage Equation

Transient voltage equation

Transforming the transient voltage equation (2-6) into the S domain, and for small variations,

$$\left(1 + \tau_{do}^{'} s\right) \Delta E_q^{'} = \Delta E_{fd} - \Delta i_{gd} \ (X_d - X_d^{'}) \tag{2-31}$$

Re-arranging (2-31) by making use of (2-29) gives,

$$\Delta E_q^{'} = \frac{1}{\left(1+\tau_{do}^{'} s\right)} \left(\Delta E_{fd} - C_1 \Delta E_q^{''} - C_2 \Delta\delta\right) \tag{2-32}$$

Sub-transient Voltage Equation

Transforming the transient voltage equation (2-12) into the S domain, and for small variations,

$$\left(1+\tau_{do}^{''} s\right) \Delta E^{'}{}_q = C_3 \Delta E_{fd} - C_4 \Delta i_{gd} + C_5 \Delta E_q^{'}$$

Re-arranging (2-31), by making use of (2-29) and (2-32) gives,

$$\Delta E_q^{''} = g_3(s) \Delta E_{fd} - g_4(s) \Delta\delta \tag{2-33}$$

Q-axis Flux Linkage Voltage Equation

Transforming the transient voltage equation (2-11) into the S domain and for small variations,

$$\left(1+\tau_{do}^{''} s\right) \Delta E^{'}{}_d =_{\cdot} (X_d - X_d^{''}) \Delta i_{gq} \tag{2-34}$$

Re-arranging (2-33) by making use of (2-30)

$$\Delta E_d^{''} = g_{4d}(s) \Delta\delta \tag{2-35}$$

Generator Terminal Voltage Equation

From the phasor representation of the synchronous generator, the generator terminal voltage equation in (2-2) in terms of *d* and *q* axis components, we have,

$$e_t^2 = e_{td}^2 + e_{tq}^2 \tag{2-36}$$

Applying a small perturbation,

$$\Delta e_t = \frac{e_{tdo}}{e_{to}} \Delta e_{td} + \frac{e_{tqo}}{e_{to}} \Delta e_{tq} \tag{2-37}$$

Substituting (2-29) into (2-10) gives,

$$\Delta e_{tq} = \frac{x_t}{\Delta_d^{"}} \Delta E_q^{"} - \frac{X_d^{"} V_{\infty do}}{\Delta_d^{"}} \Delta\delta \tag{2-38}$$

Substituting (2-30) into (2-9) gives,

$$\Delta e_{td} = \frac{x_t}{\Delta_q^{"}} \Delta E_d^{"} + \frac{X_q^{"} V_{\infty qo}}{\Delta_q^{"}} \Delta\delta \tag{2-39}$$

Re-arranging (2-37) and by making use of (2-38) and (2-39), we have,

$$\Delta e_t = K_5 \Delta\delta + K_6 \Delta E_q^{"} + K_{6d} \Delta E_d^{"} \tag{2-40}$$

Electrical power equation

The synchronous generator active power in equation (2-14) can be expressed as,

$$P_e = e_{td} i_{gd} + e_{tq} i_{gq} \tag{2-41}$$

or $$P_e = V_{\infty d} i_{td} + V_{\infty q} i_{tq} \tag{2-42}$$

For small perturbations, the electrical power coming out of the generator:

$$\Delta P_e = V_{\infty do} \Delta i_{td} + \Delta V_{\infty d} i_{tdo} + V_{\infty qo} \Delta i_{tq} + \Delta V_{\infty q} i_{tqo} \tag{2-43}$$

Re-arranging (2-24) and making use of (2-30) and (2-19), we have:

$$\Delta i_{td} = \Delta i_{gd} = \frac{\Delta E_q^{"} + V_{\infty do} \Delta\delta}{(X_d^{"} + X_t)}$$

$$\Delta i_{td} = \frac{1}{\Delta_d^{"}} \Delta E_q^{"} + \frac{V_{\infty do}}{\Delta_d^{"}} \Delta\delta \tag{2-44}$$

Re-arranging (2-25) and making use of (2-30) and (2-20), we have:

$$\Delta i_{tq} = \Delta i_{gq} = \frac{V_{\infty qo} \Delta\delta - \Delta E_d^{"}}{(X_q^{"} + X_t)}$$

$$\Delta i_{tq} = \frac{V_{\infty qo}}{\Delta_q^{"}} \Delta\delta - \frac{1}{\Delta_q^{"}} \Delta E_d^{"} \tag{2-45}$$

Re-arranging (2-43) and making use of (2-44) and (2-45), gives,

$$\Delta P_e = K_1 \Delta\delta + K_2 \Delta E_q^{"} - K_{2d} \Delta E_d^{"} \tag{2-46}$$

$$\Delta P_e = \Delta P_{sync} + \Delta P_{ed} - \Delta P_{eq} \tag{2-47}$$

Swing equation

Transforming the swing equation (2-15) and (2-16) into S domain, for small variations,

$$\Delta\omega = \frac{1}{2Hs}[\Delta P_m - \Delta P_e - D\Delta\omega] \tag{2-48}$$

$$\Delta\delta = \frac{\omega_o}{s}\Delta\omega \tag{2-49}$$

The transfer-function block diagram model of the synchronous generator system for Model 1 is shown in *Figure 2-8*. This is derived by combining the equations (2-33), (2-35), (2-40), (2-46), (2-47), (2-48) and (2-49).

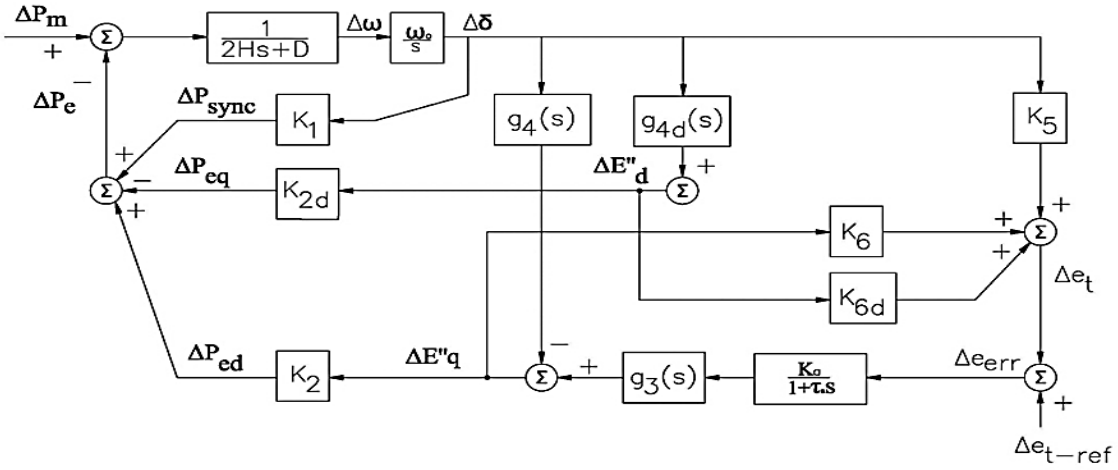

Figure 2-8 Detailed block diagram of the synchronous generator with Model 1

Model 2

The electrical power equation is:

$$\Delta P_e = K_1 \Delta\delta + K_2 \Delta E_q^{'} - K_{2d} \Delta E_d^{"} \tag{2-50}$$

The generator terminal voltage equation is:

$$\Delta e_t = K_5 \Delta\delta + K_6 \Delta E_q^{'} + K_{6d} \Delta E_d^{"} \tag{2-51}$$

D-axis flux linkage voltage equation is:

$$\Delta E_q^{'} = g_3(s)\Delta E_{fd} - g_4(s)\Delta\delta \tag{2-52}$$

The transfer-function block diagram of the synchronous generator system for Model 2 is shown in *Figure 2-9*. This results are from the abstraction of equations (2-35), (2-48), (2-49), (2-50), (2-51) and (2-52).

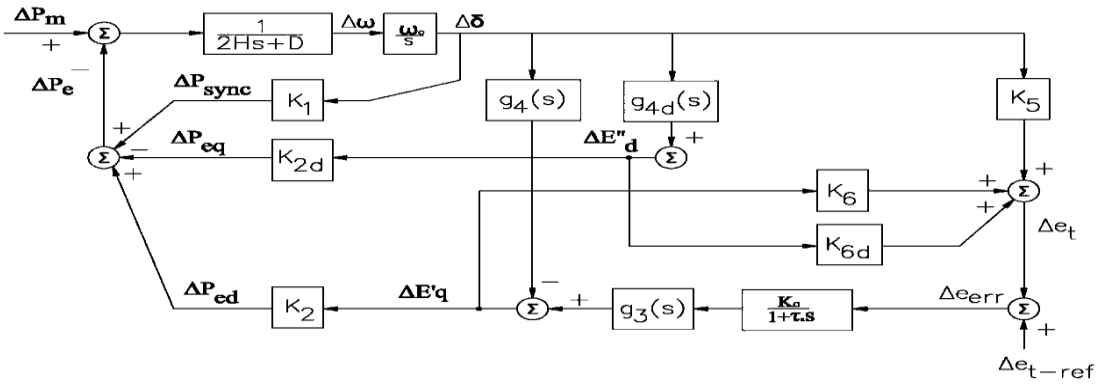

Figure 2-9 Detailed block diagram of the synchronous generator with Model 2

Model 3

The electrical power equation is:

$$\Delta P_e = K_1\Delta\delta + K_2\Delta E_q^{'} \tag{2-53}$$

The generator terminal voltage equation is:

$$\Delta e_t = K_5\Delta\delta + K_6\Delta E_q^{'} \tag{2-54}$$

The transfer-function block diagram of the synchronous generator system for Model 2 is shown in *Figure 2-10*. This results are from the abstraction of equations (2-48), (2-49), (2-52), (2-53) and (2-54).

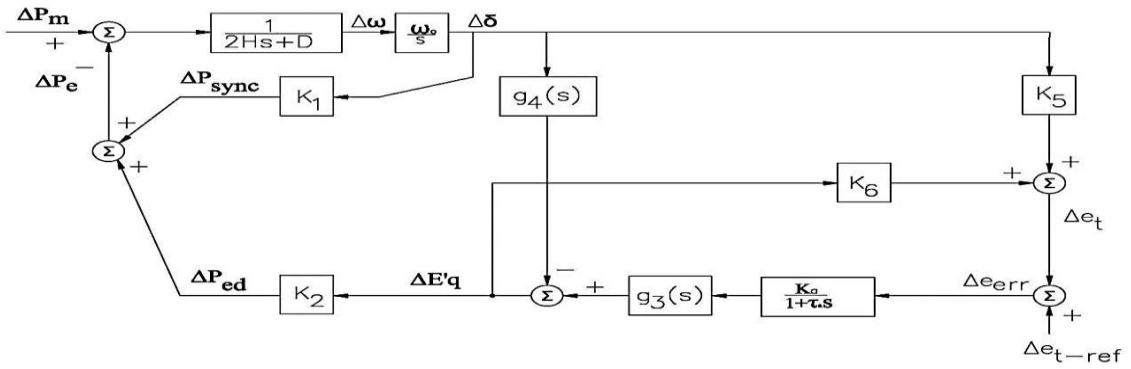

Figure 2-10 Detailed block diagram of the synchronous generator with Model 3

2.5 Excitation system

The excitation system supplies direct current to the synchronous machine. The AC excitation system comprises an alternator with either a stationary or a rotating rectifier to produce the necessary DC value. The control functions of the exciter allow controlling the voltage and reactive power of synchronous machine within specified limits. The type ST-static excitation system transforms voltage and current (in compound systems) using either a controlled or a non-controlled rectifier.

IEEE type exciter AC5A for steam based generation and ST2A type for hydro based generation are popular choices in these kinds of studies. The no-load compensation option is not used in this model.

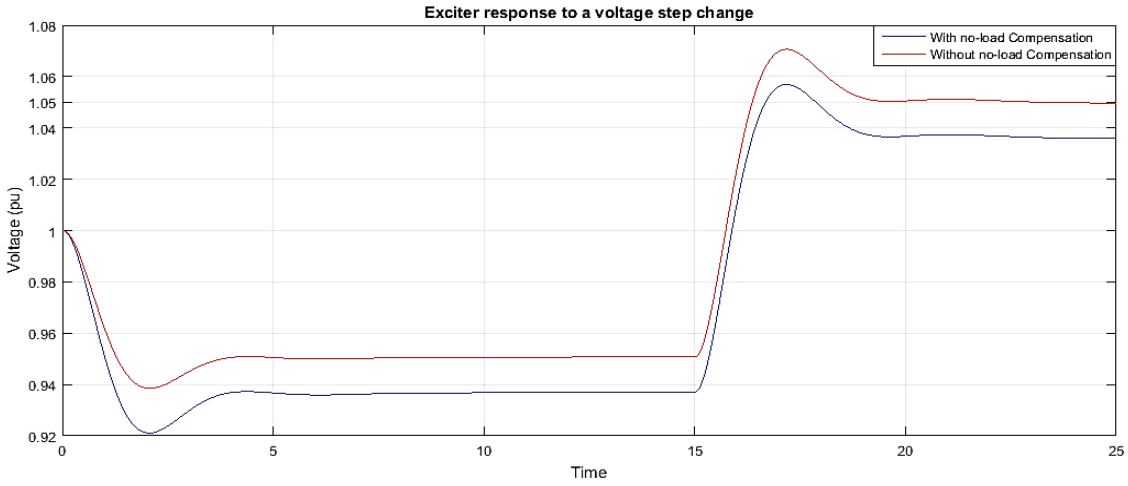

Figure 2-11 Exciter response at step changes with and without no-load compenssation

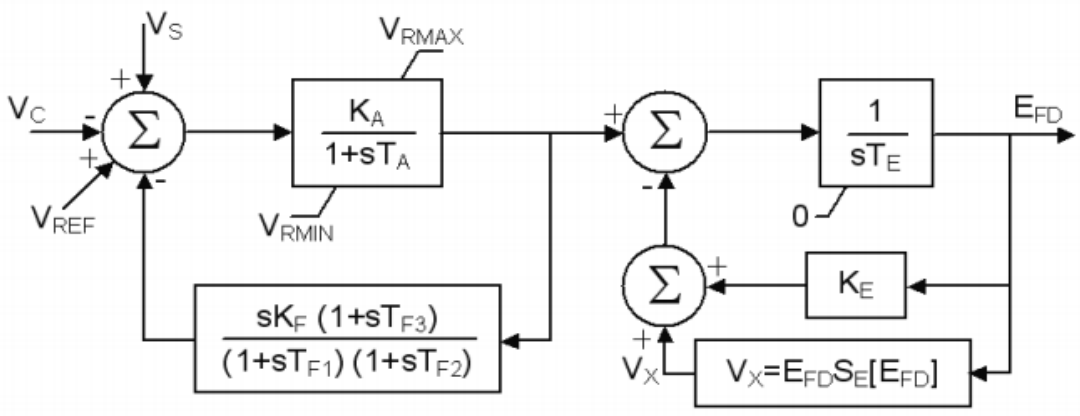

Figure 2-12 Type AC5A-Simplified rotating rectifier excitation system representation [38]

The block diagram of the type ST2A exciters, mostly used with hydro based generators, is shown below,

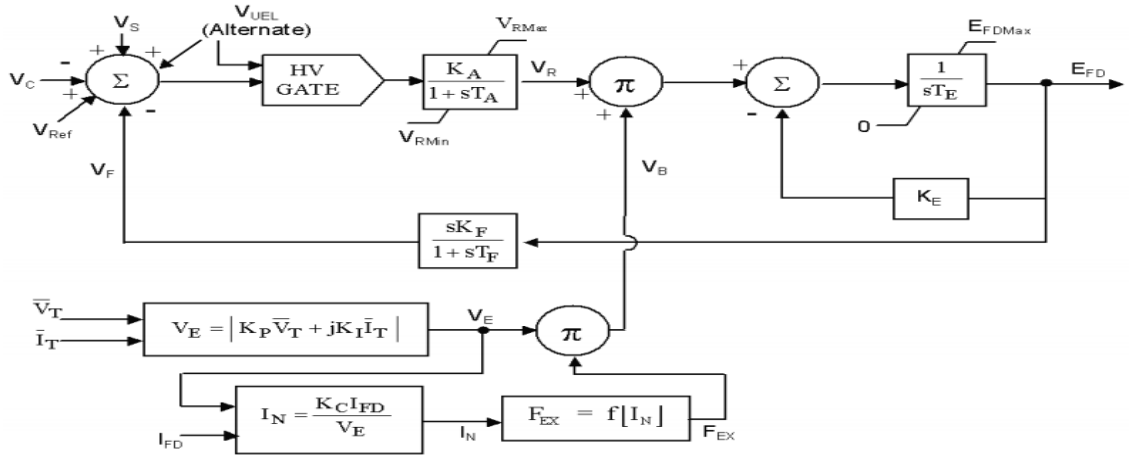

Figure 2-13 Type ST2A-Compound-source rectifier exciter [38]

2.6 Turbine-Governor System

The prime mover function includes the varying prime mover's output, automatically regulated by turbine-generator speed control, hence, the frequency and active power are also controlled in the face of the load variations. The governor parameter controls the set-point which is also known as speed-reference. The speed governor receives a signal input and actuates the governor controlled gates which in turn regulates the water input into the turbine. This has the effect to regulate power and frequency through suitable control mechanisms [9], [39], [40], [41], [42], [43], [44].

The functional relationship between the generator, the turbine and the governing system, is shown below for a conventional generating unit.

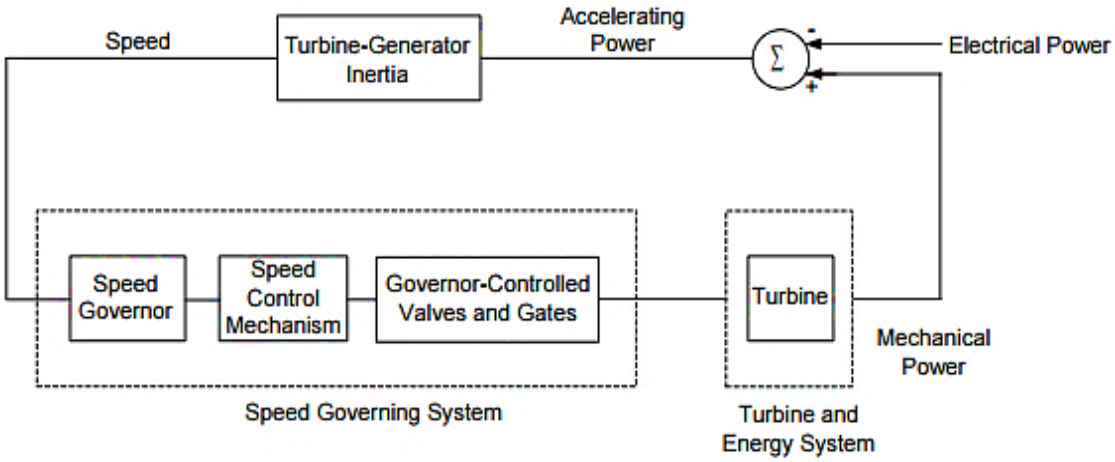

Figure 2-14 Turbine, governor system, and generator functional relationships [45]

The speed sensing device is usually a flyball assembly for mechanical-hydraulic governors and a frequency transducer for electro-hydraulic governors [46].The main disadvantages of the flyball assembly (Watt centrifugal governor) are the presence of dead-bands and a relatively low accuracy while in electro-hydraulic governors the turbine rotor speed is measured electronically with high accuracy [9], [43] [44] [45].

A linear turbine model is suitable for studying small-signal performances i.e. small displacements. Transfer function representations for hydraulic turbines for signal stability studies have been widely studied [45]. They are not adequate for studying and analyzing large variations in output power and frequency [40]. The real gate opening is the change of position from fully closed to fully open, being equal to 1 p.u. This is known as turbine gain [47].

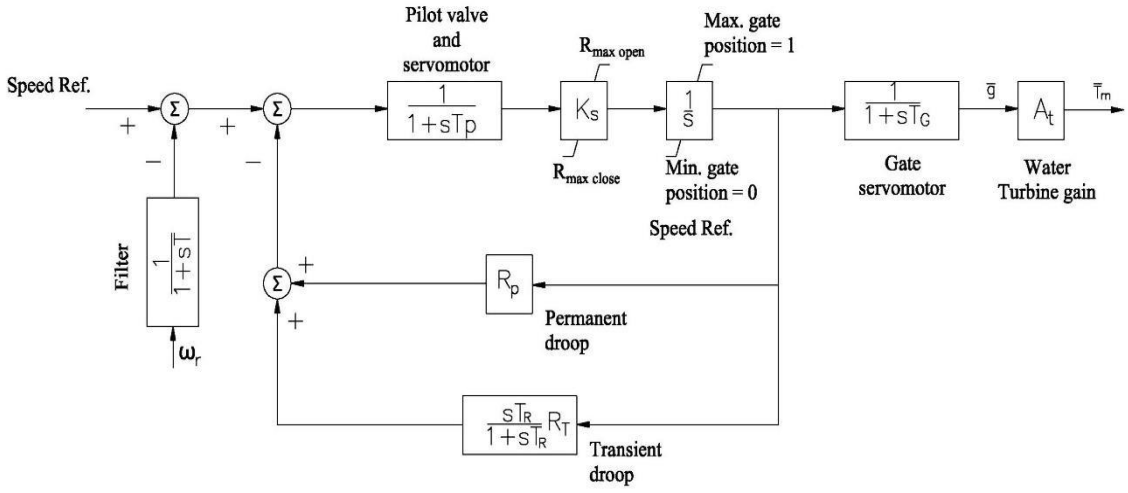

Figure 2-15 Modified governor model for hydraulic turbine with filter and water turbine [9]

2.7 Load description

A three-phase dynamic load representation is used in the Siirtoverkkomalli power network. The Three-Phase Dynamic Load block corresponds to a three-phase, three-wire dynamic load whose active power P and reactive power Q vary as function of positive-sequence voltage considering a balanced system [48]. If the terminal voltage is lower than a minimum specified value then the load impedance is kept constant. When the terminal voltage is greater than the minimum specified value, the active power P and reactive power Q of the load vary as follows [48]:

$$P(\mathrm{s}) = P_0 \left(\frac{V}{V_0}\right)^{n_\mathrm{p}} . \left(\frac{1+T_{p1}s}{1+T_{p2}s}\right) \tag{3-1}$$

$$Q(\mathrm{s}) = Q_0 \left(\frac{V}{V_0}\right)^{n_q} . \left(\frac{1+T_{q1}s}{1+T_{q2}s}\right) \tag{3-2}$$

where,

V_0 = initial positive sequence voltage.

P_0 and Q_0 =initial active and reactive powers at the initial voltage V_0.

V = positive-sequence voltage.

n_p and n_q =exponents (usually between 1 and 3) controlling the nature of the load.

T_{p1} and T_{p2} =time constants controlling the dynamics of the active power P.

T_{q1} and T_{q2} =time constants controlling the dynamics of the reactive power Q.

The mathematical modeling of the synchronous generator, the turbine-governor system, the exciter, and the load model is broadly discussed throughout this chapter. The 5th and 6th order machine models and the equipment discussed in this chapter were used to implement the equivalent Siirtoverkkomalli network model. The system was implemented in matlab/simulink environment. The library of Simulink is enhanced with wide range of applications including hydraulics, power electronics, electrical systems, control systems, power systems etc. The model is being built by adding one generator and one load at a time and testing has been done for the system validation. Four types of cases and their results are described in the next 2 chapters.

3 SVC and STATCOM integration into an equivalent grid model, dynamic analysis.

Reactive power compensation is a mandatory operational requirement to smooth out the transmission system electrical characteristics undergoing load changing conditions. The ultimate purpose of this reactive power compensation is to increases steady-state transmittable power while maintaining a healthy voltage profile along the line. A shunt-connected device with an inductive behavior will ameliorate over-voltages during light load conditions and a shunt-connected device with capacitive behavior will increase voltage levels under heavily loaded conditions.

3.1 Static Var Compensator (SVC)

Static Var Compensator (SVC) is a shunt connected variable reactance which regulates voltage at the connection point by controlling the amount of reactive power to be injected or absorbed from the system. SVC generates reactive power when the system voltage is low (capacitive) and absorbs reactive power when the system voltage is high (inductive).

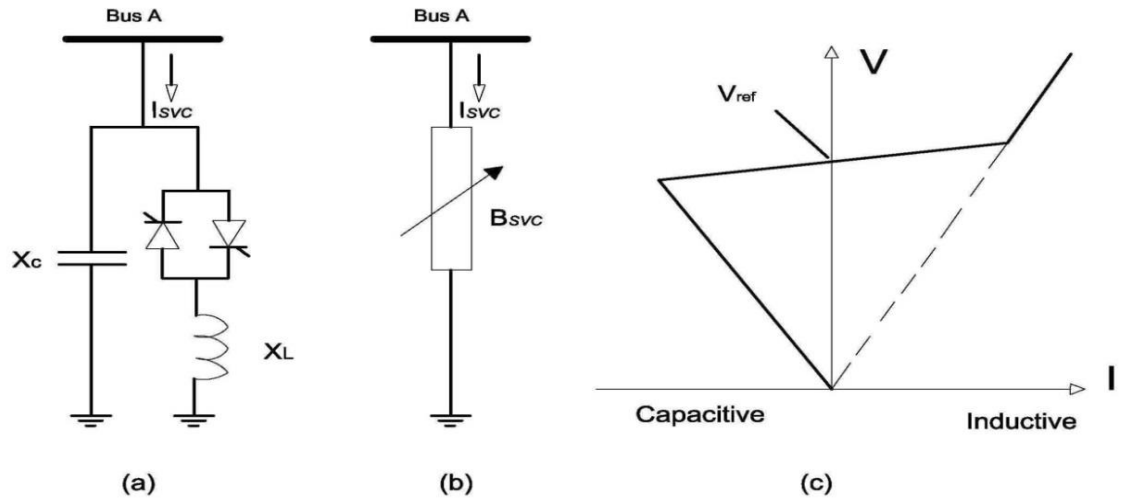

Figure 3-1 (a) SVC, fixed capacitor and TCR type (b) SVC, variable suceptance model (c) SVC V-I characteristics

SVCs can be operated in two different modes:

- In voltage regulation mode , the voltage is regulated within the rated limits
- In var control mode , the SVC susceptance is kept constant

Voltage regulation mode allows the SVC to adjust the device within the minimum and maximum susceptance limits of the capacitor bank and the reactor, in order to achieve its desired voltage output. One of the drawbacks of the SVC is that since the SVC is dependent on the voltage at the connection point, the SVC can worsen the system's operation if the voltage at the connection point is too low.

3.2 Static Synchronous Compensator (STATCOM)

The Static Synchronous Compensator (STATCOM) is a shunt-connected device for reactive power compensation. The STATCOM regulates system voltage by generating or consuming reactive power. The STATCOM has similar characteristics to the rotating synchronous condenser but it provide/absorbs reactive power at a faster rate because it has practically no inertia.

The main components of the STATCOM are a voltage source converter (VSC) with a DC capacitor and a connecting transformer between the VSC and the system. The basic principles of the STATCOM's operation are depicted below:

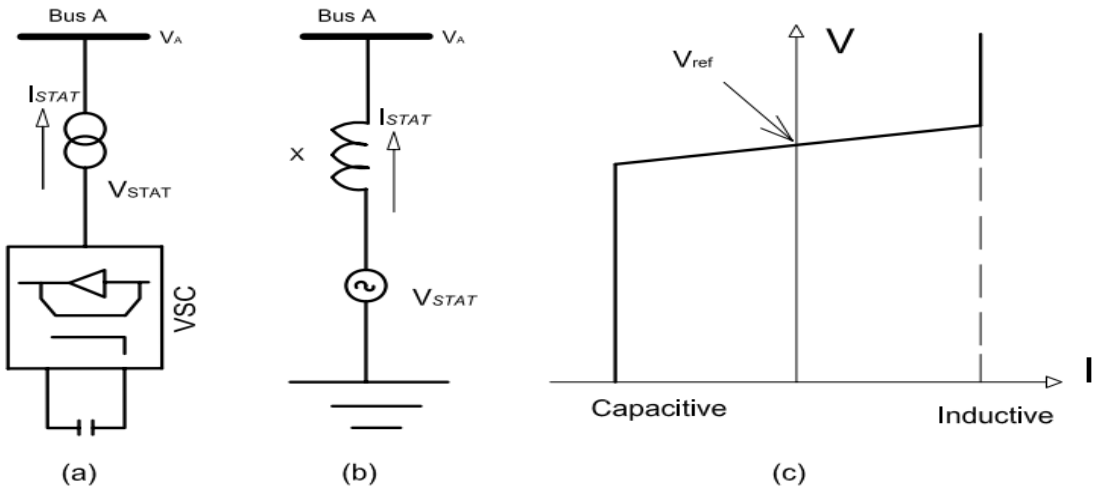

Figure 3-2 (a) STATCOM basic configuration (b) STATCOM equivalent circuit model (c) STATCOM V-I characteristics

If $V_A > V_{STAT}$ then Q_{STAT} becomes positive and the STATCOM absorbs reactive power and if $V_A < V_{STAT}$ then Q_{STAT} becomes negative and the STATCOM generates reactive power.

The ability to provide more reactive power by the STATCOM during a short-circuit fault in its vicinity is one major advantage that it has got over the SVC of comparable rating. This feature is due to the fact that the capacitive power generated by the SVC is proportional to the square of the system voltage (constant susceptance) whereas for the STATCOM, this is independent from the actual voltage at its connection point.

Hence, the STATCOM is able to provide a more effective support than an SVC of the same rating. Alternatively, a STATCOM can provide the same support as an SVC of a higher rating. This makes the STATCOM a more popular choice than the SVC in terms of its smaller footprint. However, the former is still more expensive.

3.3 Equivalent Siirtoverkkomalli

An equivalent transmission grid model termed ‘’Siirtoverkkomalli’’ by Fingrid Oyj has been singled out for study. This network reflects to a large extent the actual operation of Fingrid Oyj. The main focus was on assessing the power transfers between areas, network stability, and reactive power compensation to stabilize the system during post-fault operations. Three types of FACTS devices have been studied in connection with the Siirtoverkkomalli installation.

This equivalent grid model consists of 11 synchronous generators and 4 equivalent synchronous generators in the neighboring Nordic-32 system. The load scenario used in this thesis is the low-load case. The generators and associated parameters are given in *Appendix B*. The generator 5^{th} order model and governor system (6^{th} order model) for constant torque has been chosen.

Hydro and Steam turbine governor models are used in this model. The electrical part of the machines in the North area of Siirtoverkkomalli and the North area of Nordic-32 are represented by 5th-order state-space models where the turbine and governor systems are used for mechanical torque operation. For the South and Central areas of Siirtoverkkomalli and Nordic-32, the electrical parts of the 11 machines are represented by 6^{th} order models and the machines are operated with constant torque.

The following cases have been studied; a) **Three-phase-to-ground** fault at Kemijokisuu (NW); b) **loss of line** between Rovaniemi (N)- Bus_Nordic_N ; c) **increased electrical length by 100%** between Kemijokisuu (NW)- Bus_Nordic_N for the cases below:

1. Case-1: Zero flow case
2. Case-2: 1100MW South- Bus_Nordic_N export case (unstable case) and stabilization with SVC and STATCOM
3. Case-3: 1250MW South- Bus_Nordic_N export case (unstable case) and stabilization with SVC and STATCOM

The fault clearance time is 100ms for all of the test cases.

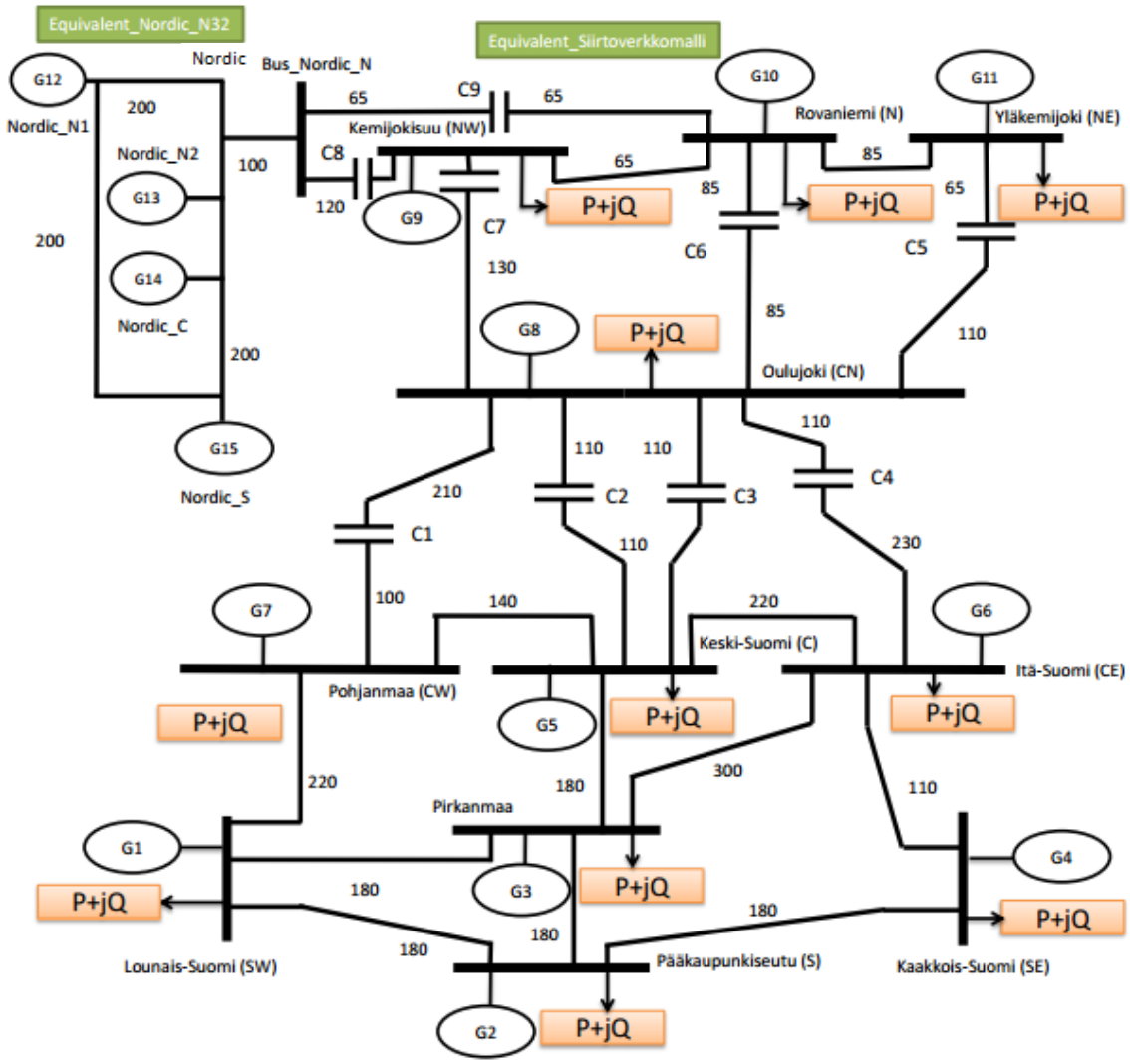

Figure 3-3 Siirtoverkkomalli and Nordic-32 equivalent (length is in km)

3.4 Case-1: Zero power flow case

Zero power flow study (almost zero power flows throughout the bus) is a case when demand has been met solely by local generators. A three-phase-ground fault has been applied at Oulujoki (CN) and the ensuing voltage and frequency behaviors are shown in *Figure 3-4* and *Figure 3-5*, corresponding to nodes Lounais-Suomi (SW), Oulujoki (CN), Kemijokisuu (NW), and Nordic_N1.

It can be seen from these results that the system is stable after the three-phase-fault has been removed. Since the system is stable there is no need for any compensation devices to be installed.

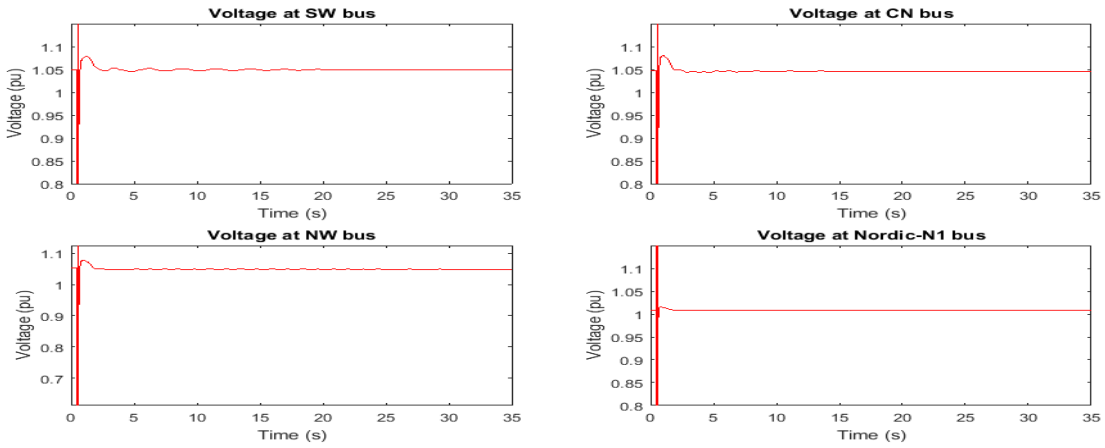

Figure 3-4 Voltage at 400kV buses undergoing a 3-phase-to-ground fault (zero flow)

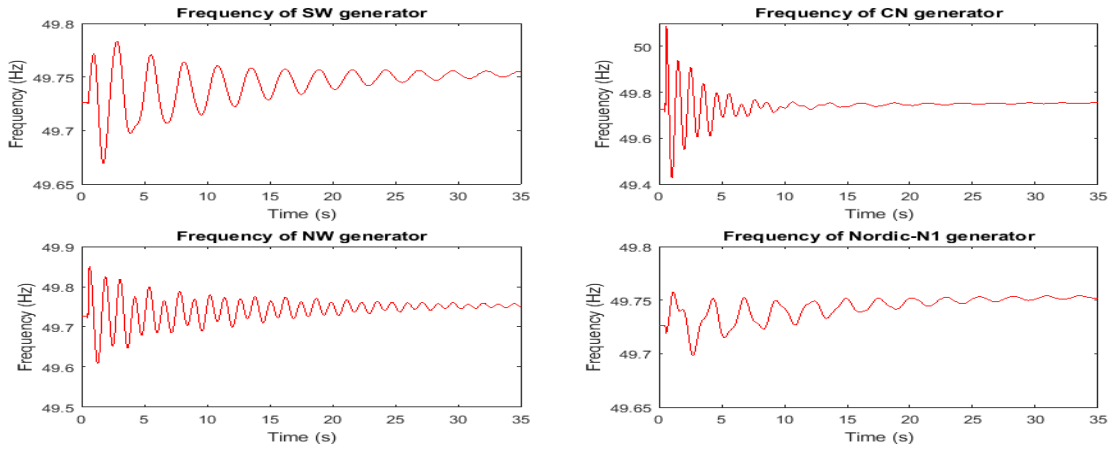

Figure 3-5 Frequency of generators undergoing a 3-phase-ground fault (zero flow)

It may be argued that zero power flows is closed to the ideal case in terms of economy and stability of the network point of view. However, in practice zero power flows are very difficult to achieve since the production of the power generation plants are affected by the type of fuel that they use and their transportation.

3.5 Case-2: 1100MW South- Bus_Nordic_N export case (unstable case) and stabilization with SVC and STATCOM

It has been observed that in the case of 1100MW export from the South to the Bus_Nordic_N, the system is unstable under the following conditions: a) 3-phase-to-ground fault b) Loss of line c) Increases electrical length. Reactive power compensation by means of shunt connected FACTS devices is capable of stabilizing the system. Three types of options have been considered:

1) SVC
2) SVC with higher rating
3) STATCOM with the same rating as the SVC

3.5.1 Unstable case

Increasing amounts of active power have been exported from the south side to the north side, to identify points of unstable operation, including three-phase faults, increased electrical lengths of transmission lines and loss of transmission lines.

The system is stable and with a fault applied at 0.5s. The system voltage and frequency starts to oscillate and at 30s of simulation time, the system becomes unstable, as shown in *Figure 3-6* and *Figure 3-7*.

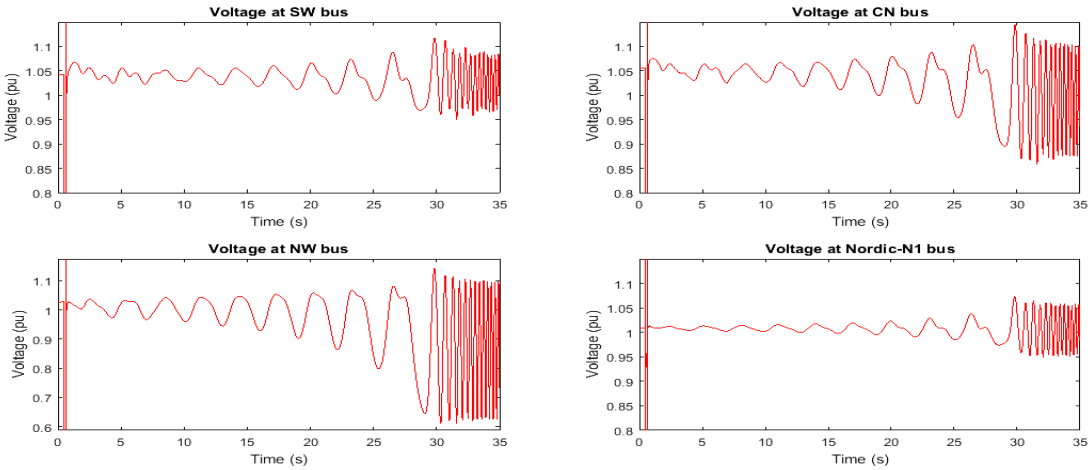

Figure 3-6 Voltage at 400kV buses undergoing a 3-phase-to-ground fault (unstable)

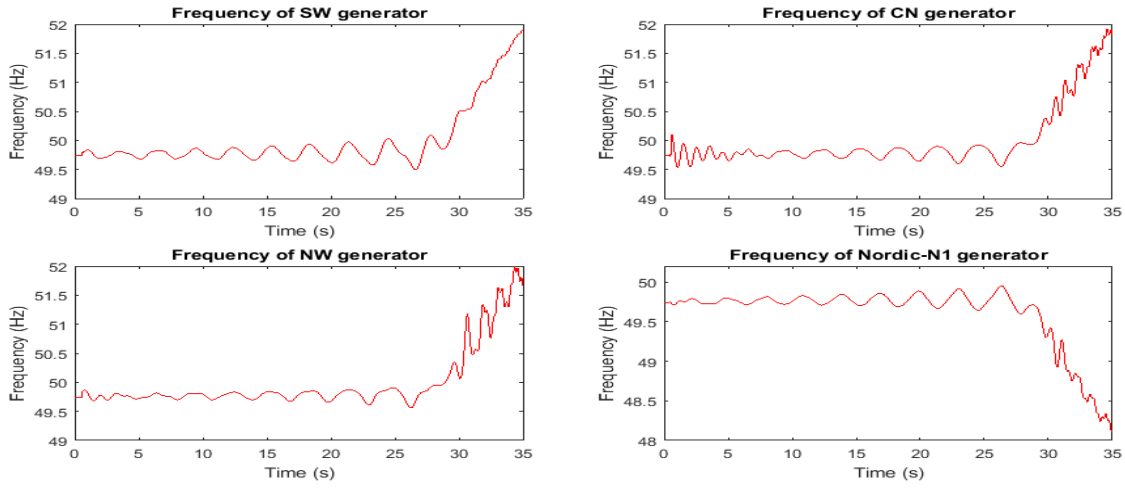

Figure 3-7 Frequency of generators undergoing a 3-phase-to-ground fault (unstable)

It is summarized that once the system becomes unstable, reactive power support is needed to stabilize it.

3.5.2 Stabilization with SVC and STATCOM

To enable stabilization of the system, a 285MVA STATCOM, a 285MVAr SVC and a 293MVAr SVC have been used to assess the impact on the network voltage and frequency stability during the post-fault operation.

It is observed that both the SVC and STATCOM stabilize the voltage and frequency of the network. It is further observed, from *Figure 3-9* that the STATCOM does not induces large oscillations unlike the SVC. Moreover it is also observed in *Figure 3-10* that the SVC with a similar rating to the STATCOM cannot provide similar support to the network voltage. In order to have similar kind of reactive power support and contribution to the system, as in the case of the STATCOM, the rating of the SVC must be higher.

The reactive power support provided by the STATCOM and the SVC are shown in *Figure 3-12*. It is observed that the STATCOM yields more reactive power support during the fault than the similar and higher rated SVC than the STATCOM.

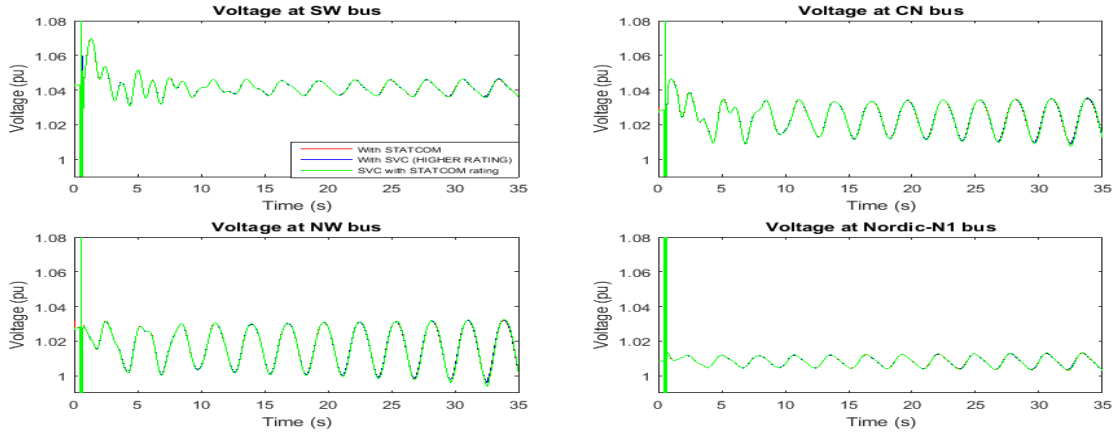

Figure 3-8 Voltage at 400kV buses undergoing a 3-phase-to-ground fault with (SVC-285MVar (green), SVC-293MVAr (blue) and STATCOM-285MVA (red))

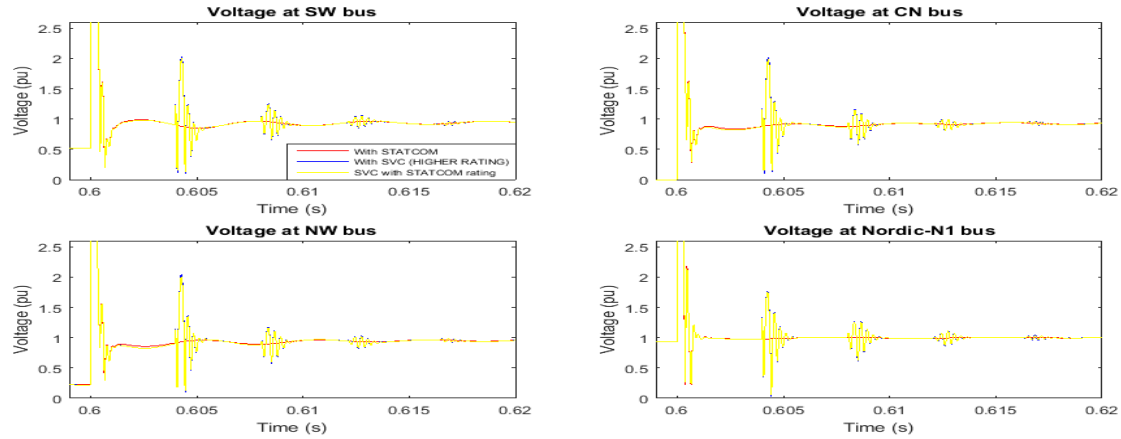

Figure 3-9 Voltage at 400kV buses (right after the fault) with SVC (yellow and blue) and STATCOM (red)

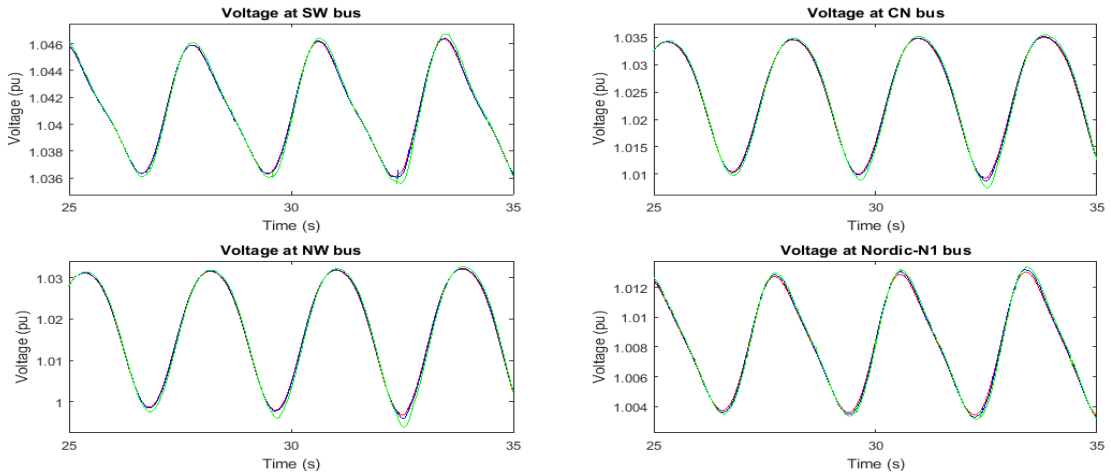

Figure 3-10 Voltage at 400kV buses (last 10s simulation) with SVC-285MVar (green), SVC-293MVAr (blue) and STATCOM-285MVA (red)

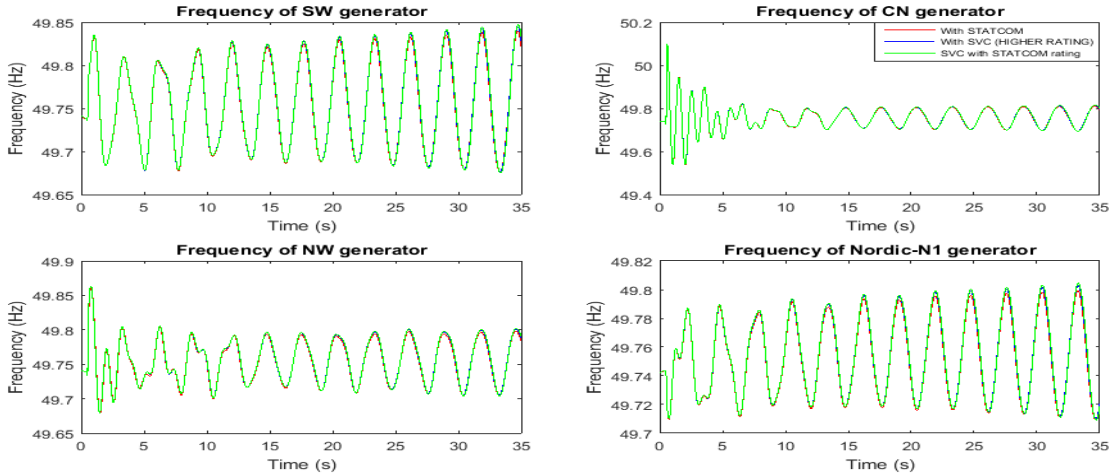

Figure 3-11 Frequency of generators undergoing a 3-phase-to-ground fault (With SVC-285MVar (green), SVC-293MVAr (blue) and STATCOM-285MVA (red))

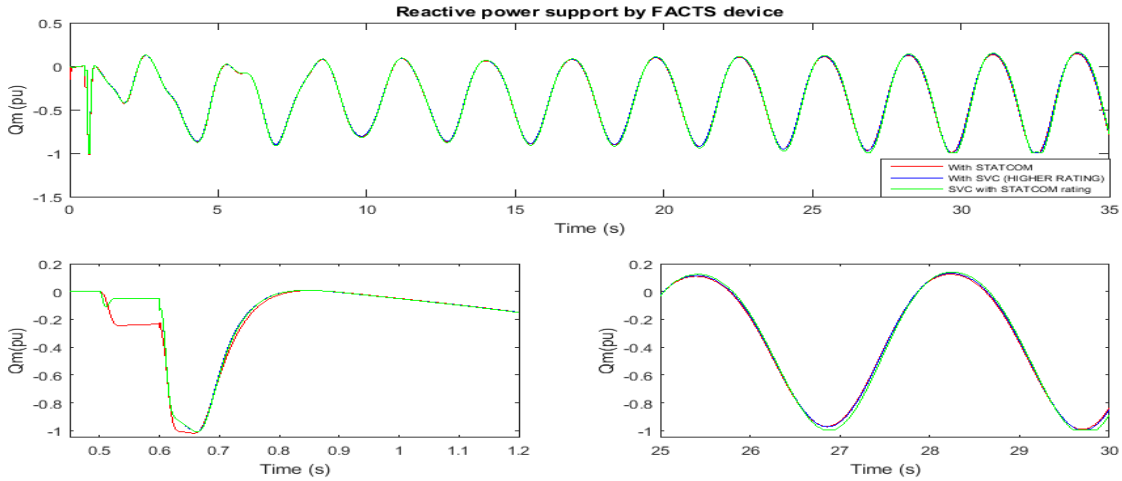

Figure 3-12 Reactive power support by SVC and STATCOM

3.6 Case-3: 1250MW South-North export case (Unstable case) and stabilization with SVC and STATCOM

A higher amount of active power transfer was studied to assess better the impact of the distinct type of FACTS equipment being represented in this study. The results are shown below. The SVC and STATCOM are connected into the same location as in the previous study.

3.6.1 Unstable Case

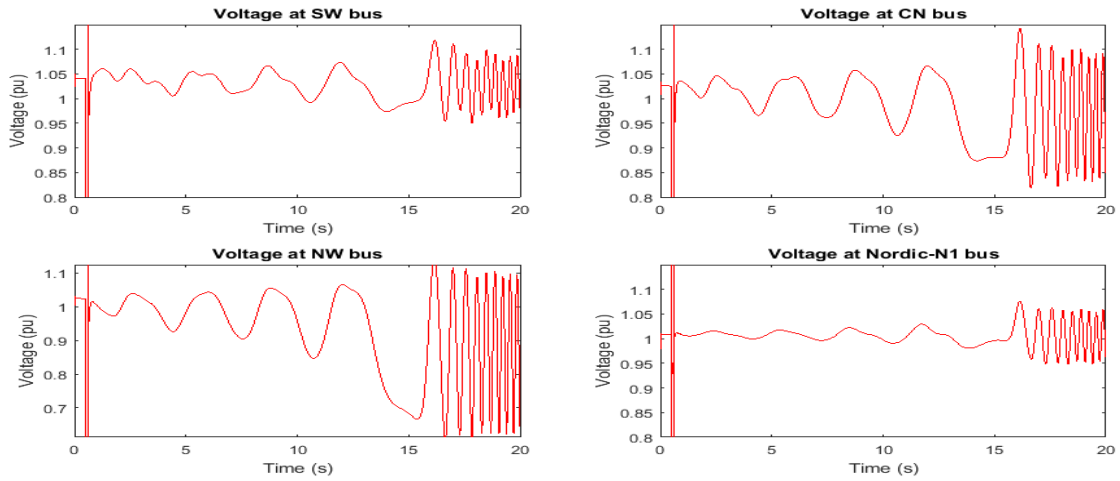

Figure 3-13 Voltage at 400kV buses undergoing a 3-phase-to-ground fault (unstable)

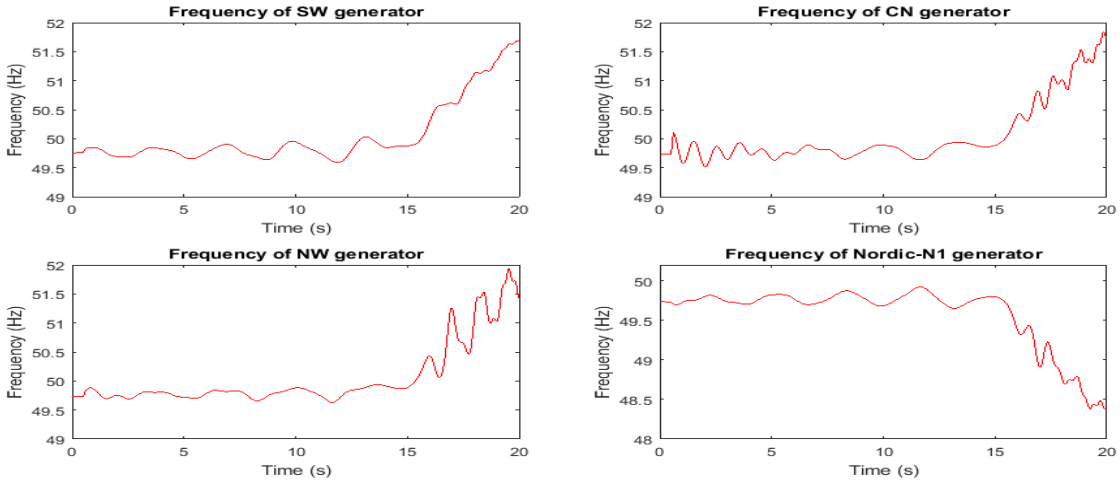

Figure 3-14 Frequency of generators undergoing a 3-phase-to-ground fault (unstable)

As expected, when 1250MW are exported, the network becomes unstable faster when 1100MW are exported.

3.6.2 Stabilization with SVC and STATCOM

For the 1250MW export case, a 510MVA STATCOM, a 510MVAr SVC and a 550MVAr SVC are used to stabilize the system during the post fault operation. Large fluctuations are visible in *Figure 3-16* with the SVC as in the 1100MW case, and very little fluctuations for the case of the STATCOM. It is observed that the SVC with the same rating as the STATCOM is not able to stabilize the system, as shown in *Figure 3-17.*

Its also seen from *Figure 3-19,* that the STATCOM provides more reactive power support during the fault than the SVC of similar or higher rating than the STATCOM.

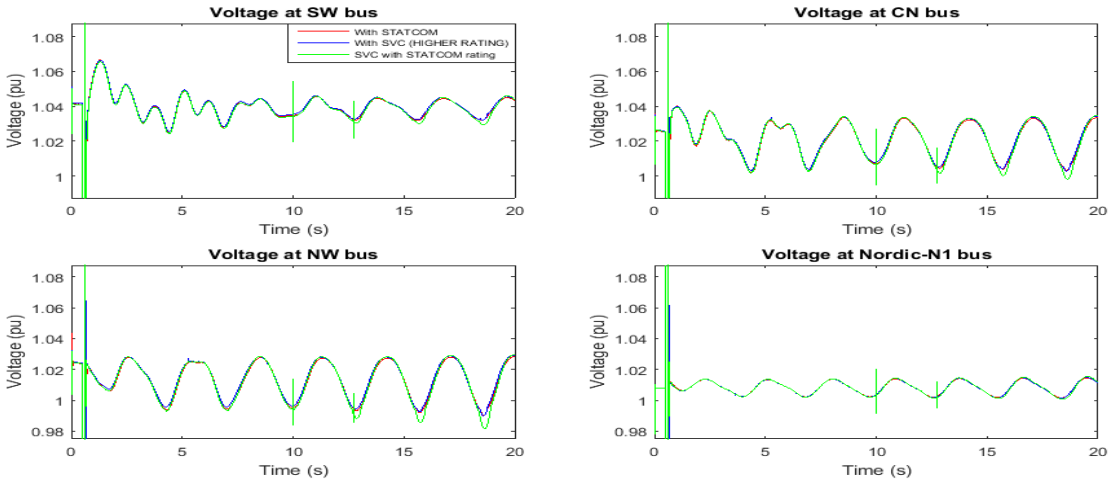

Figure 3-15 Voltage at 400kV buses undergoing a 3-phase-to-ground fault with (SVC-510MVar (green), SVC-550MVAr (blue) and STATCOM-510MVA (red))

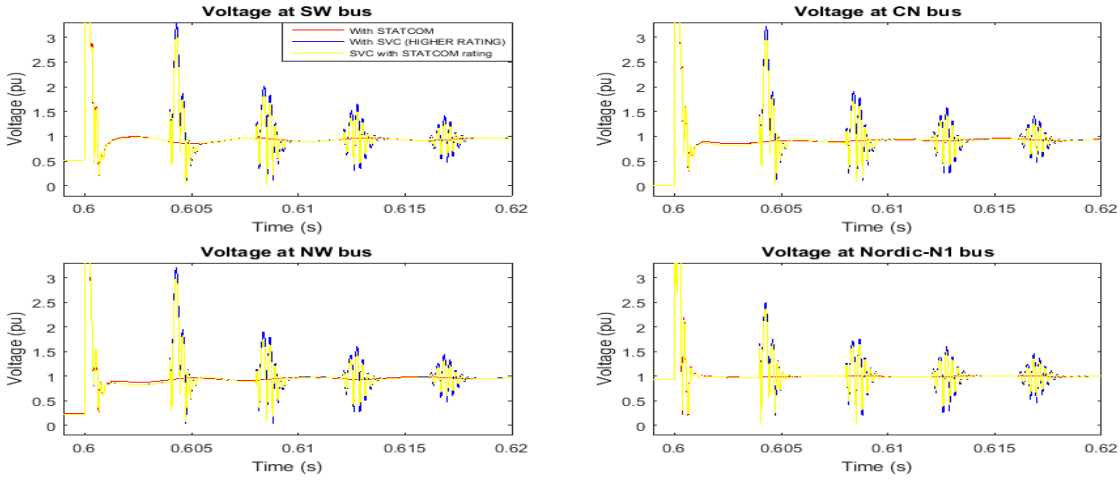

Figure 3-16 Voltage at 400kV buses (right after the fault) with SVC (yellow and blue) and STATCOM (red)

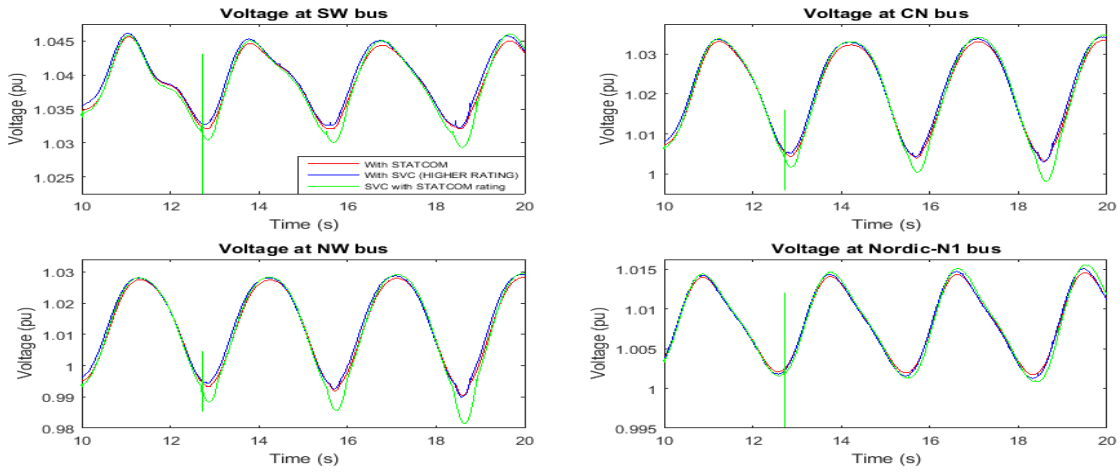

Figure 3-17 Voltage at 400kV buses (last 10s simulation) with SVC-510MVar (green), SVC-550MVAr (blue) and STATCOM-510MVA (red)

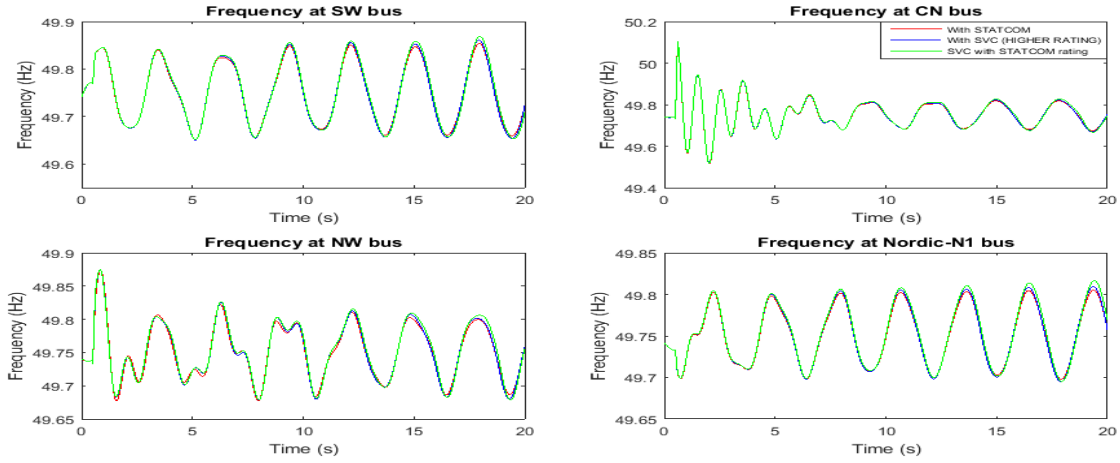

Figure 3-18 Frequency of generators undergoing a 3-phase-to-ground fault (With SVC-510MVar (green), SVC-550MVAr (blue) and STATCOM-510MVA (red))

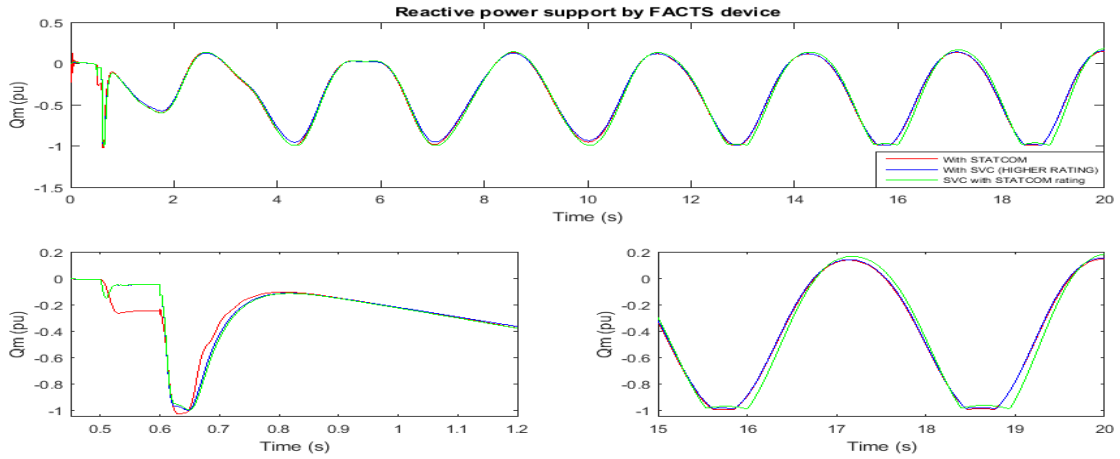

Figure 3-19 Reactive power support by SVC and STATCOM

4 Battery Energy Storage System, components details, and impact on the equivalent network model

4.1 Electrochemical Batteries and their characteristics

Continuous improvement in the battery technology invented by Alessandro Volta in 1800, have made it possible to see the battery being use today in practically all areas of human activity. In general, electrical energy storage requires storing the energy in any other form different from electrical energy. The battery stores the energy by transforming electrical energy into chemical energy where chemical compounds acts as the storage medium and the reverse process works when current is drawn from the battery to supply power to a connected load. Based on this two way operational characteristic process, two different types of battery are described in [49], [50]:

a) Primary batteries where chemical energy is transformed into electrical energy only once with the reverse process not being an available option.
b) Secondary batteries where chemical reactions are reversible and the battery can be charged /discharged repeatedly over many cycles.

Secondary batteries are widely used in industrial and in automobile applications because of their rechargeable characteristics.

4.1.1 Basic components of Cells and Batteries

A battery comprises one or more cells (i.e., basic electrochemical unit), where a cell consists of three main components-

a) The negative electrode or anode is oxidized by supplying (during discharge reaction) electrons to an external circuit or oxidizing by absorbing (during charge reaction) electrons from the external circuit. The anode is usually made of metal or a metal compound with very few electrons in the valance shell.
b) The positive electrode or cathode is oxidized by supplying (during charge reaction) electrons to an external circuit or oxidizing by absorbing (during discharge reaction) electrons from an external circuit.
c) The electrolyte is an ionic conductor which provides a conductive medium between the positive and negative electrodes for the transfer of charges as ions. The electrolyte is water or a solvent with dissolved salts, or an alkaline solution, or an acidic solution.

Batteries and capacitors both stores energy but they exhibit key differences in the way in which they store the energy and their time responses. The capacitor stores energy in the electric field setup between two plates, limited by the maximum amount of voltage that they can handle. This premise also applies to super capacitors [51]. The battery charges and discharges energy through associated chemical reactions in the electrolyte, which generates a nearly constant voltage by changing the charge.

The capacitor charges and discharges at a very fast rate compared to the battery. A cross section view of a Lithium-ion battery is shown in *Figure 4-1* [52].

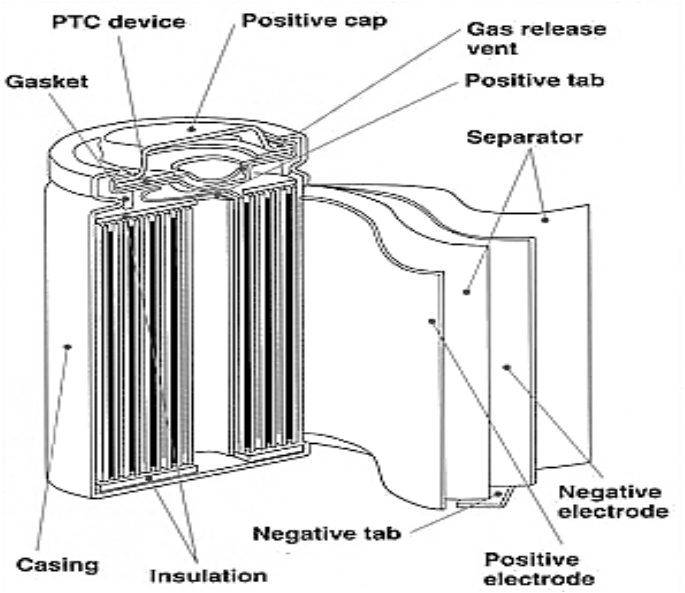

Figure 4-1 Cross section of a lithium-ion cylindrical cell

4.1.2 Cells operation during a charging/discharging cycle

The cell operation during discharge is shown in the *Figure 4-2*.The negative electrode or anode supplies (during discharge reaction) electrons to the cathode through the external circuit and is oxidized during electrochemical reaction [53] [54].

Negative electrode: anodic reaction (oxidation, loss of electron)

$$LiC_6 \rightarrow Li^+ + e^- + C_6$$

Positive electrode: cathodic reaction (reduction, gain of electron)

$$Li^+ + e^- + MO_2 \rightarrow LiMO_2$$

Overall reaction (discharge): $LiC_6 + MO_2 \rightarrow C_6 + LiMO_2$

Reverse flow of current is seen during the recharge process and opposite phenomenon in chemical reaction happens.

Negative electrode: anodic reaction (oxidation, loss of electron)

$$Li^+ + e^- + C_6 \rightarrow LiC_6$$

Positive electrode: cathodic reaction (reduction, gain of electron)

$$LiMO_2 \rightarrow Li^+ + e^- + MO_2$$

Overall reaction (discharge): $C_6 + LiMO_2 \rightarrow LiC_6 + MO_2$

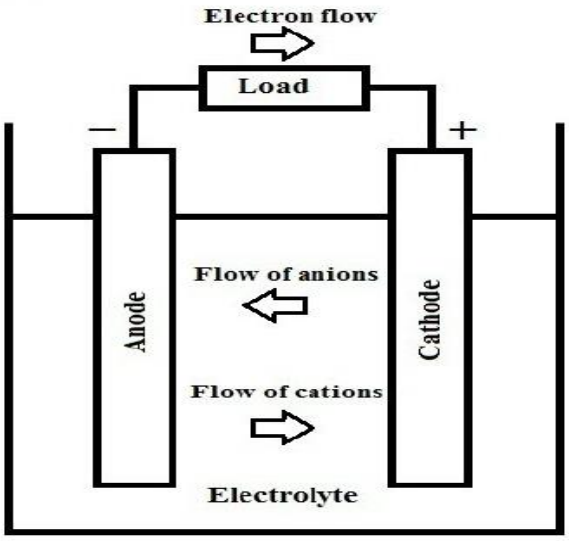

Figure 4-2 Electrochemical operation of a cell (discharge)

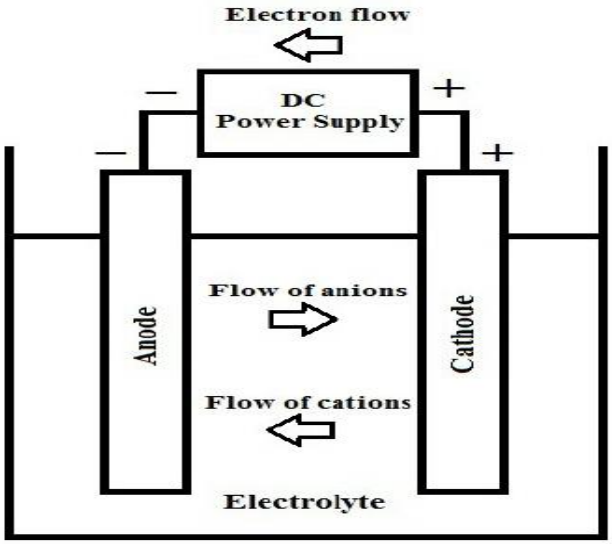

Figure 4-3 Electrochemical operation of a cell (charge)

4.1.3 State of Charge (%)

The state of charge (SOC) is the existing battery capacity as a percentage of the maximum capacity. This definition brings the idea of battery aging as the capacity is deteriorating over period of time. There are several techniques described to determine the SOC status in [55] [56] [57].The most commonly used method for SOC calculation is the use of integration of the current supplied/drawn to determine the change in battery capacity over time.

Accurate determination of SOC prevents safe and efficient operation and avoid under or over charging conditions.

Open circuit voltage (OCV) is one of the many methods for determining SOC. In lead-acid battery, OCV and SOC have linear relationship discussed in [58] whereas in lithium-ion the linear relationship does not exist [59].

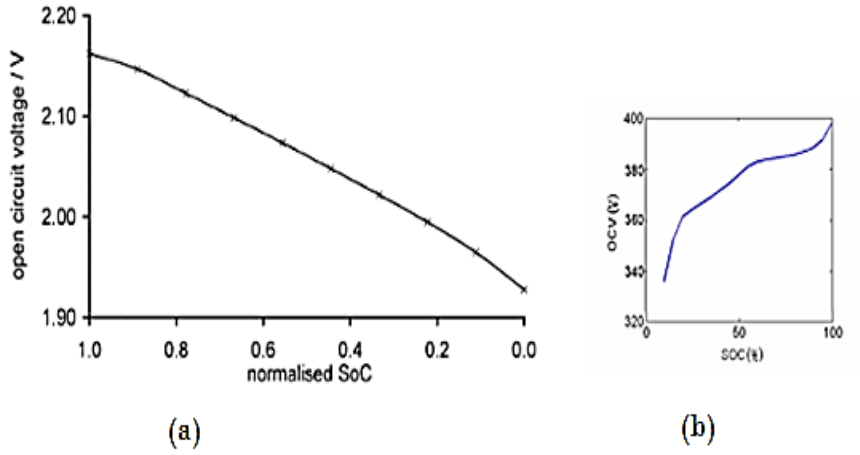

Figure 4-4 Relationship between SOC and OCV, (a) lead-acid, (b) Li-ion

4.1.4 Open circuit voltage

Open circuit voltage (OCV) refers to the voltage at battery terminal at no load condition. The accurate measurement is not possible since self-discharge phenomenon is happening even during no-load period. The parameters that affect the OCV are depth-of discharge (DOD), status-of-health (SOH), battery temperature, SOC [54] [58] [59]. OCV for a rough estimation of SOC is shown in *Figure 4-5*.

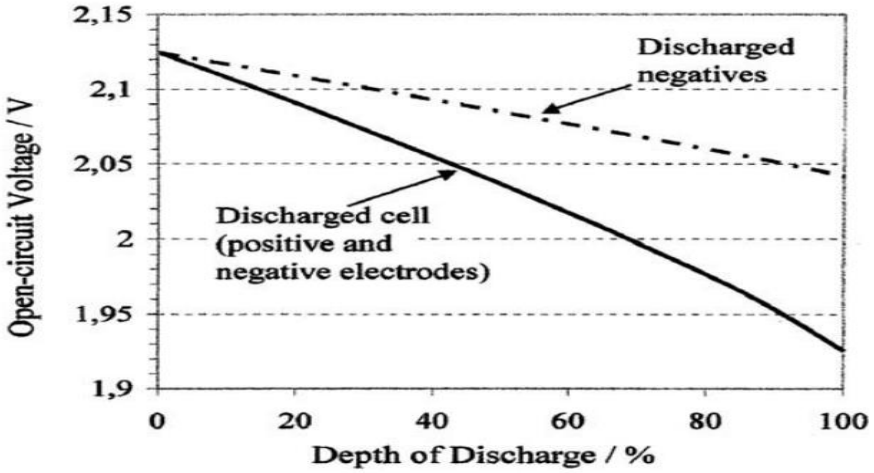

Figure 4-5 Open circuit voltage vs. depth of discharge (DOD)of lead-acidbatteries

In the above figure, the continuous line indicates the relation when both electrodes are discharged and the broken line represents the relation when only the negative electrode is discharged [50].

4.1.5 Operating voltage

An important parameter for battery system is the voltage at which it operates during recharge and discharge to supply electrical energy and power. Open circuit voltage is determined by the thermodynamics of chemical reaction between the components in the electrodes during the supply of ions in the electrolyte and electrons in the external circuit [60].

The concept of energy quality is analogous to heat quality and it was well observed that high temperature heat has higher quality. Also the high voltage energy has higher quality than the low voltage energy. From the power vs. voltage relationship, the electrical power P is directly related to the square of the voltage and the resistance by,

$$P = E^2 / R \tag{4-1}$$

Because of the square relationship between power and voltage, high voltage energy is superior to low voltage energy. When the current is drawn from the battery, due to the current dependent impedances at the electrode/electrolyte interfaces, the value of ionic impedances may increase with output current. This will result drop in the output voltage as well heat generation. The discharge rate of battery (C-Rate) will affect not only the output voltage but also the charge delivered which can be seen in *Figure 4-6* , so C-Rate drops as the battery discharged [60].

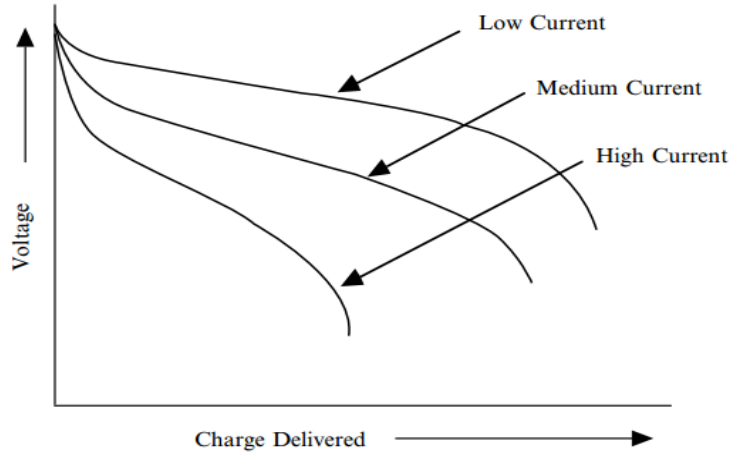

Figure 4-6 The influence of the current density upon the discharge curve

4.1.6 Capacity

The capacity of battery is defined as the electrical charge in units of Ah that can be drawn from the battery and when the battery sis discharged at constant current, its capacity is given by [50]-

$$C_{Ah} = \int_0^t I(t)\,\mathrm{dt} \tag{4-2}$$

The energy contained in an electrochemical system is the integral of the voltage multiplied by the charge capacity [60], i.e., the amount of charge available is -

$$Energy = \int Edq \tag{4-3}$$

Where E is the output voltage which varies with stat of charge, kinetic parameters, as well as amount of electronic charge it can supply to the external circuit. Hence, it is essential to know the maximum theoretically available capacity of the battery i,e amount of electrical charge that can be stored in the battery at a certain time.

4.1.7 Self-discharging

Self-discharge refers to the gradual decrease in available battery capacity over time during open circuit condition. There are several reason of self-discharging-

a) Gradual reduction of the oxidation state in the positive electrode [50].
b) By oxidizable or reducible substances in the electrolyte when they reach the positive or negative electrode [50].
c) Impurities react with constituents in the electrodes or the electrolyte to reduce available capacity over time [60].
d) Self-discharge is also temperature dependent [61].

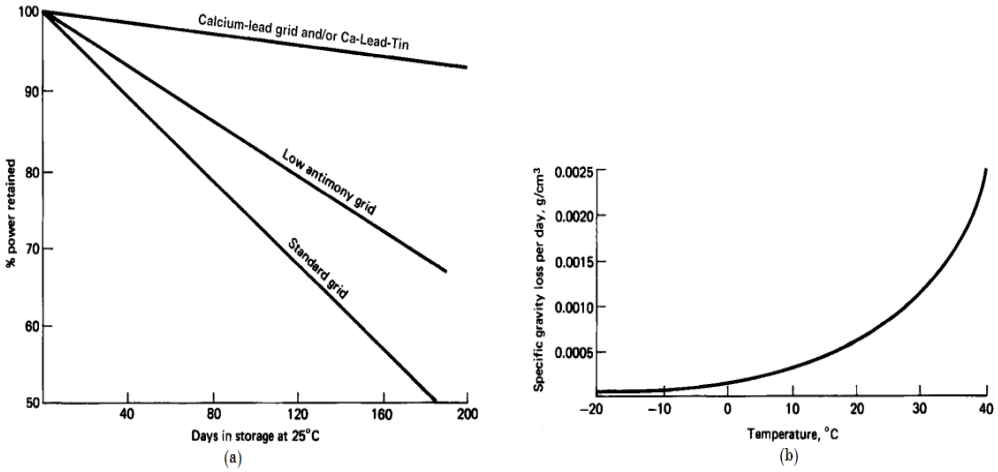

Figure 4-7 (a) Capacity retention during stand or storage at 25℃ [62],(b) Loss of specific gravity per day with temperature of a new, fully charged lead-acid battery with 6% antimonial lead grids [63].

4.1.8 Equivalent internal impedance

Based on the dynamic characteristics and the battery working principles, various equivalent circuit models are widely used and proposed by researchers through the use of resistor, capacitor and voltage source to form a circuit environment [64] [65].

The design and selection of battery depends on several factors including optimized system performance [66] [67], predicting battery runtime and I-V performance [68], predicting battery runtime at different load profiles [69] and improving battery efficiency performance [70]. Dynamic characteristics analysis involves resistor (R) and capacitor (C) in parallel pairs represents transients.

The number of RC pairs depends on matching the frequency response of the equivalent circuit model with the battery impedance spectra within the desired range. In *Figure 4-8* R_o causes voltage drop at battery terminal.

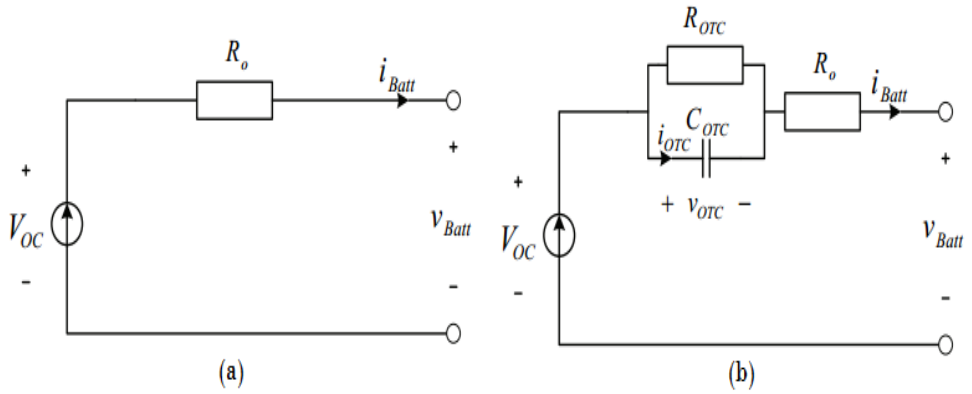

Figure 4-8 (a) Schematic diagram of the Rint model (most basic model) (b) Schematic diagram for the Thevenin model [71]

4.1.9 Li-ion Batteries

Lithium-ion (Li-ion) batteries are the composition of cells that employ lithium intercalation compounds as the positive and negative materials and when the battery is cycled, lithium ions (Li^+) exchange between the positive and negative electrodes [72]. The higher energy density of Li-ion is the key differentiate characteristics compared to the conventional sealed nickel–cadmium (Ni–Cd), nickel-metal hydride (Ni-MH), and valve-regulated lead acid (VRLA) battery systems. Also with this advanced benefit, the cost of battery is going down since the beginning of Li-ion battery production.

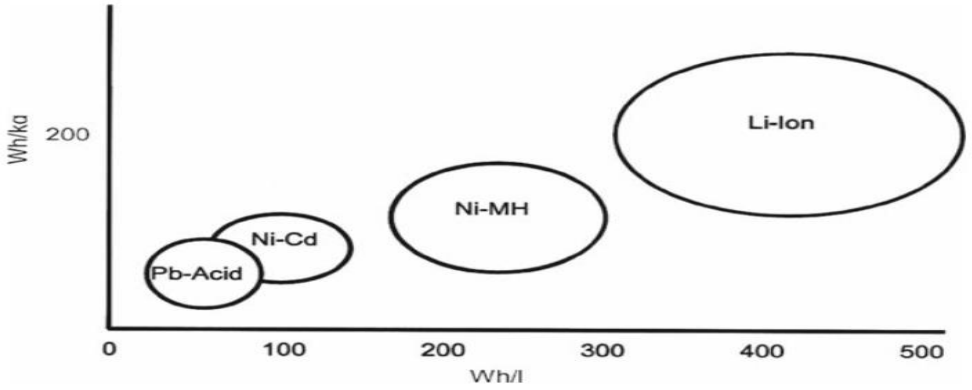

Figure 4-9 Energy density (Wh/l) and specific energy (Wh/kg) for the major small-sealed rechargeable battery systems [73]

The major advantages and disadvantages of Li-ion relative to other battery types is summarized in [72] [73]which is given in ***Table 1***.

Table 1 *Advantages and Disadvantages of Li-ion Batteries*

Advantages	Disadvantages
• Chemistry with the highest energy (Wh/g) and lightest weight (Wh/kg) • High energy efficiency • Good high-rate capability • Long cycle life • Broad temperature range of operation • No memory effect • Long shelf life • Low self-discharge rate	• Relatively expensive • Thermal runaway concerns • Not tolerant of overcharge and over-discharge • Capacity loss or thermal runaway when overcharged • Cylindrical designs typically offer lower power density than NiCd or NiMH • Need for protective circuitry

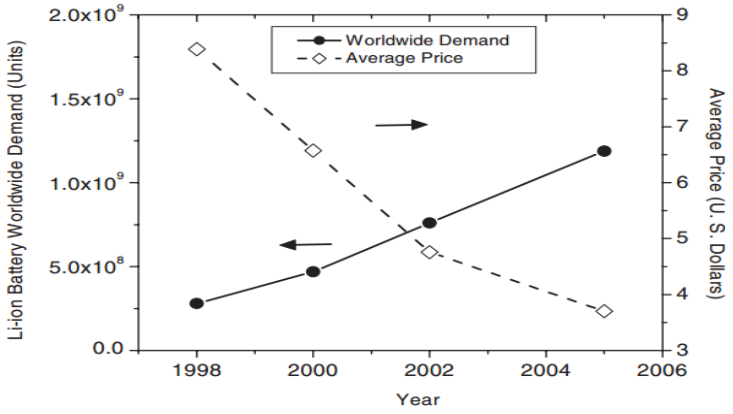

Figure 4-10 Worldwide demand and average price for Li-ion batteries [74] [75]

Electrode and cell reaction in a Li-ion cell is discussed in section 4.1.2.

4.1.10 Battery model details (Simulink)

The battery block used in matlab/simulink is the most common generic model of rechargeable batteries shown in *Figure 4-11* [76]. The temperature effect on the battery behavior is ignored and model parameters for the battery charging and discharging is given below [76]-

Discharge Model ($i^* > 0$)

$$f_2(it, i^*, i) = E_o - K \cdot \frac{Q}{Q - it} \cdot i^* - K \cdot \frac{Q}{Q - it} \cdot it + A \cdot exp(-B \cdot it) \tag{4-4}$$

Charge Model ($i^* < 0$)

$$f_2(it, i^*, i) = E_o - K \cdot \frac{Q}{it + 0.1Q} \cdot i^* - K \cdot \frac{Q}{Q - it} \cdot it + A \cdot exp(-B \cdot it) \tag{4-5}$$

where,

E_{Batt} = Nonlinear voltage (V)
E_0 = Constant voltage (V)
Exp(s) = Exponential zone dynamics (V)
Sel(s) = Represents the battery mode. Sel(s) = 0 during battery discharge, Sel(s) = 1 during battery charging.
K = Polarization constant (Ah^{-1}) or Polarization resistance (Ohms)
i* = Low frequency current dynamics (A)
i = Battery current (A)
it = Extracted capacity (Ah)
Q = Maximum battery capacity (Ah)
A = Exponential voltage (V)
B = Exponential capacity $(Ah)^{-1}$

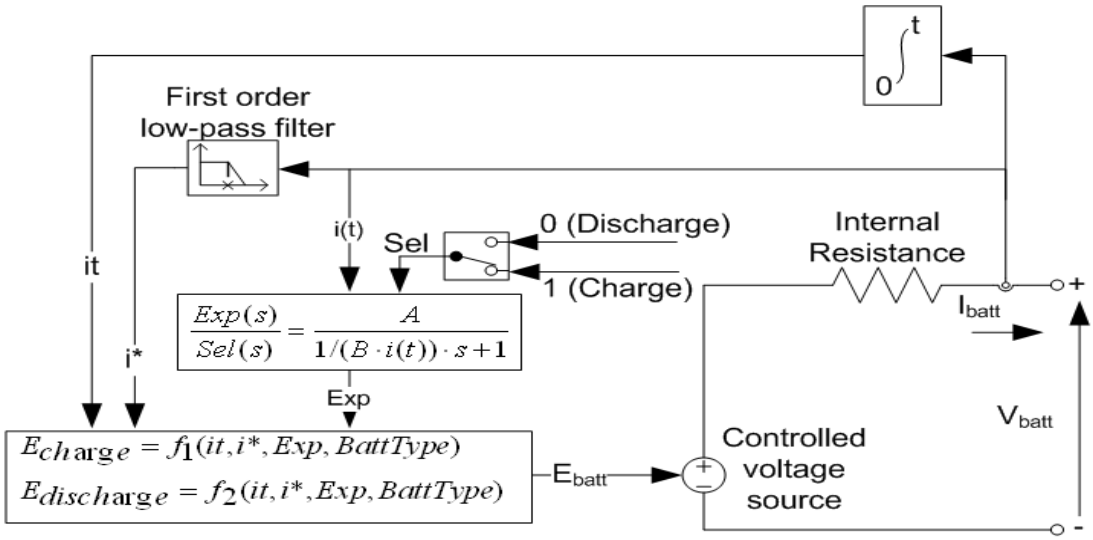

Figure 4-11 Equivalent circuit of the battery

The equivalent circuit parameter varies based on the discharge characteristics. A typical discharge characteristic is shown in *Figure 4-12* [77], [25].

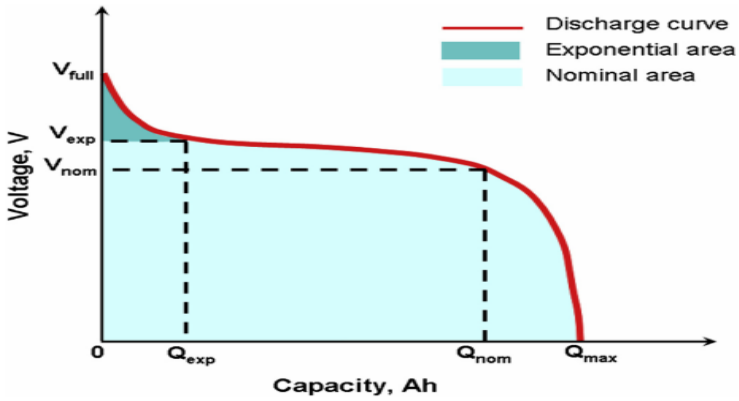

Figure 4-12 Typical discharge characteristic of Li-ion battery

First section represents the exponential voltage drop when the battery is fully charged. Next section represents the charge that will be extracted from the battery before it reaches to the nominal value. Once the voltage reaches the nominal limit, battery starts to discharge, voltage starts to drop rapidly. Duration and amplitude of each section will depends on the battery type and capacity and other variable conditions. When the battery current flows in the reverse direction, i.e. negative current flows in the battery, the battery will recharge according to following characteristics [76]-

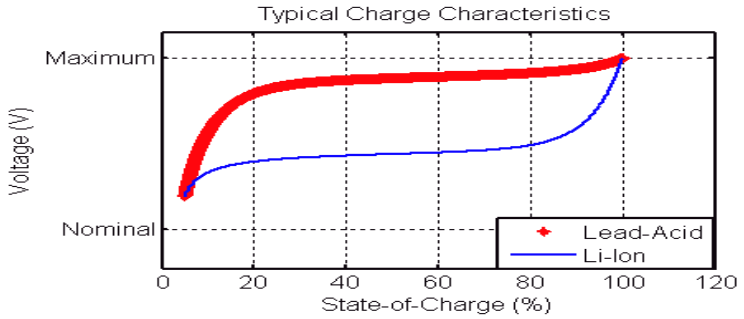

Figure 4-13 Typical charge characteristic of Li-ion battery

4.2 Power Converter

Power converter is considered to be the most essential part of the Battery energy storage system (BESS). The BESS system comprises two converters; the DC-DC converter which controls active power flow between the battery and grid and a pulse width modulated (PWM) inverter which controls the reactive power injection to stabilize the system voltage.

4.2.1 DC-DC Converter

The DC-DC converter's purpose is to supply the desired voltage at its terminal and regulating the DC voltage against the load and line variations, to protect the supplied system and input source from the electro-magnetic interference (EMI). The average output voltage is achieved by changing the pulse width to control the switching. One of the methods to control the output voltage is by switching at constant frequency. Pulse width is changing by comparing the reference value over a saw-tooth wave shown in *Figure 4-14* . When the switch is on, is termed as δ [78], [79]. The output is 0 and 1depending on the reference value compare to the instantaneous value of sawtooth,

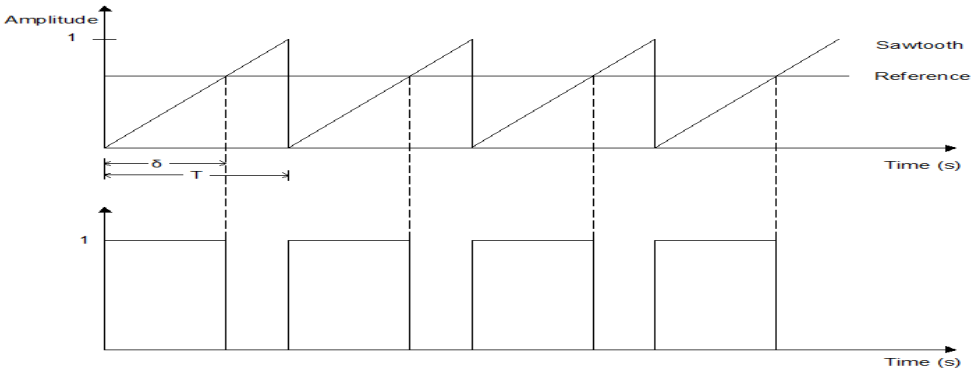

Figure 4-14 Pulse width modulator comparator signals

4.2.2 Cúk Converter

Cúk converter performs the DC-DC conversion similar to the buck-boost converter; increase or decrease the magnitude of the output DC voltage and it can also provide the negative polarity output voltage with respect to the input voltage. The capacitor C_2 stores and transfers the energy from the input to output. Voltage across C_2 is larger than V_1 and V_2.

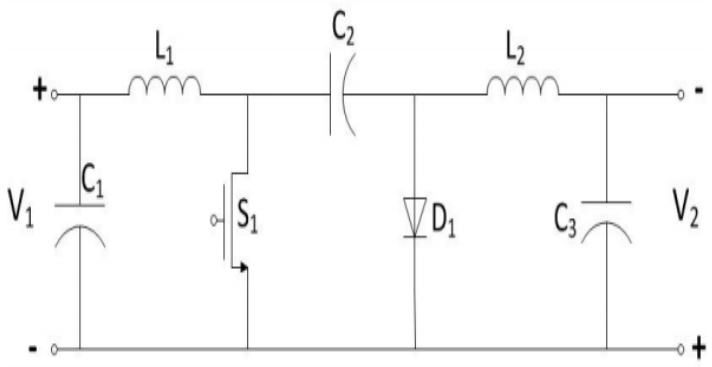

Figure 4-15 Unidirectional Cúk converter [80]

The main benefits of the Cúk converter is that it allows to flow the power flows in both directions and this dual option of Cúk converter is very important for battery energy storage system (BESS).

4.2.3 PWM in Single phase Voltage Source Inverter

The Voltage source inverter is divided into three different general categories, **Pulse-width-modulated inverters**, **Square-wave inverters, Single-phase inverters with voltage cancellation**. Several techniques have been developed for full bridge VSI, among which unipolar and bipolar is most popular.

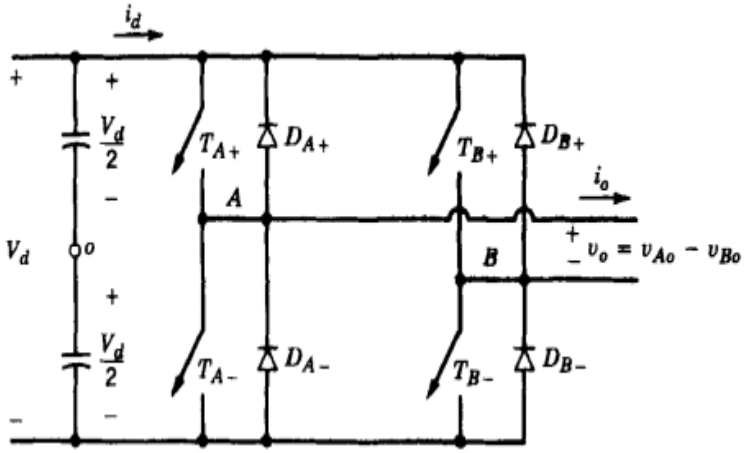

Figure 4-16 Single-phase full-bridge inverter. [78]

Full bridge converter has the benefit of providing twice the maximum output voltage that of half bridge rectifier. Hence the output current and switch current is one half those for a half bridge rectifier.

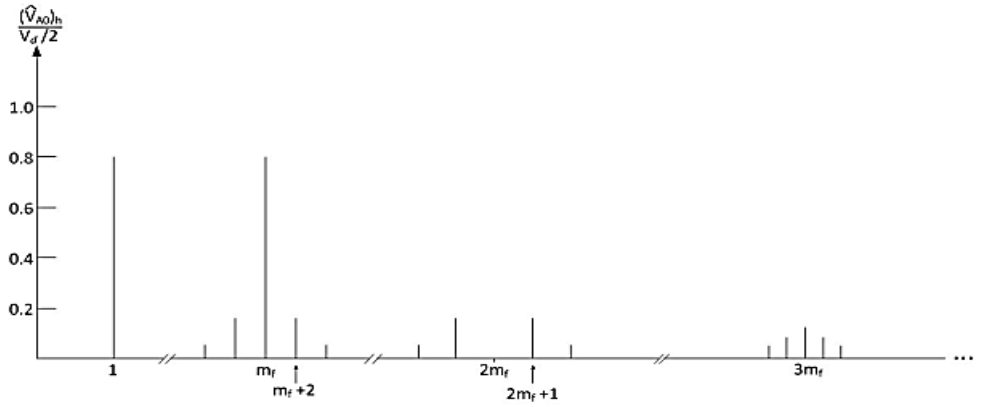

Figure 4-17 Bipolar switching (single phase): Harmonics of f1 (ma = 0.8, mf= 15) [78]

Unipolar has a very crucial benefit over bipolar is that, the harmonics in the AC output voltage of unipolar PWM technique will appear around twice the normalized carrier frequency and its multiples and this allows using of small filtering components to obtain higher quality voltage and current waveform. Harmonics of unipolar and bipolar switching can be seen in *Figure 4-17* and *Figure 4-18*.

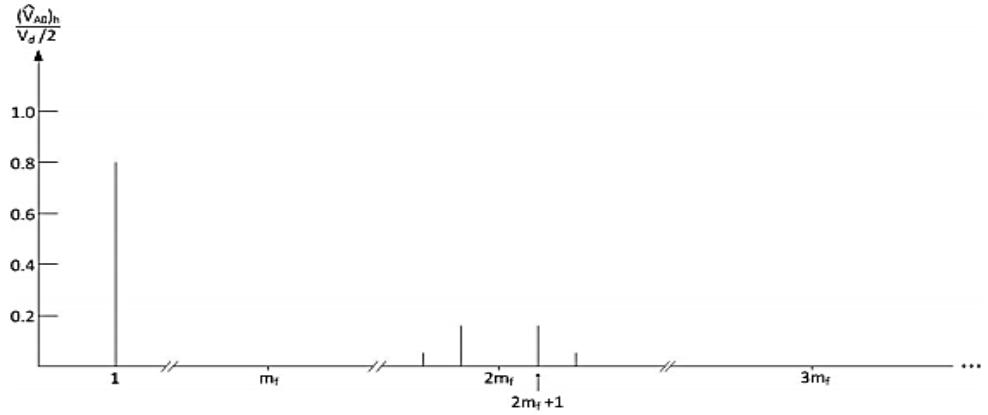

Figure 4-18 Unipolar switching(single phase): Harmonics off1 (ma = 0.8, mf= 15) [78].

4.2.4 PWM in Three phase Voltage Source Inverter

A voltage source converter (VSI) generates the AC voltage at its output from the DC voltage. Even though it is refereed as an inverter, it also has the capability of power transfer in both directions. With a VSI, the magnitude, phase angle and the frequency of the output voltage can be controlled [14].

For the low power application, single phase inverter is preferred whereas medium and high power application requires three phase inverter. Three-level inverter offer better sinusoidal waveform than two-level inverter as the output voltage can be formed with more voltage levels, this result less total harmonic distortion (THD).

Also, as the multiple stages in output voltage are possible, this reduces the dv/dt stress, thus reduces Electromagnetic compatibility (EMC) problem can be solved. The switching frequency is lower in 3-level converter. Hence, switching loss is lower. Three phase, two-level and three-level converter and spectrums are shown in *Figure 4-19* and *Figure 4-21*.

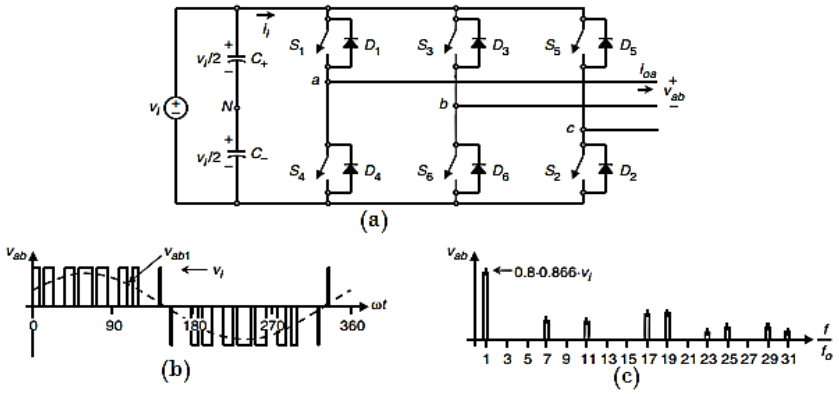

Figure 4-19 Three-phase,2-level (Six-switch) voltage source inverter (mf = 9, ma = 0.8): (a) power topology; (b) ACoutput voltage; and (c) ACoutput voltage spectrum [81].

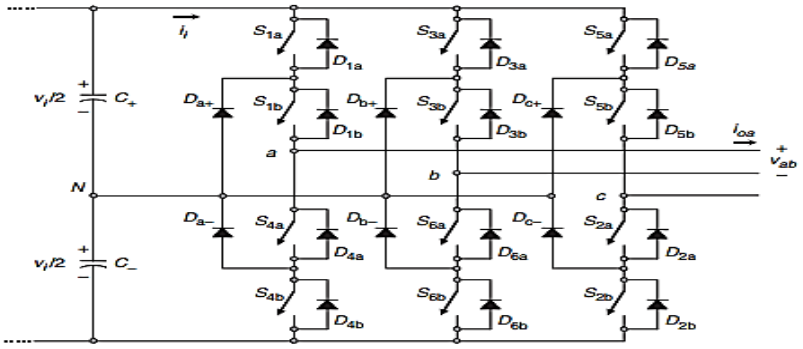

Figure 4-20 Three-phase three-level VSI topology [81].

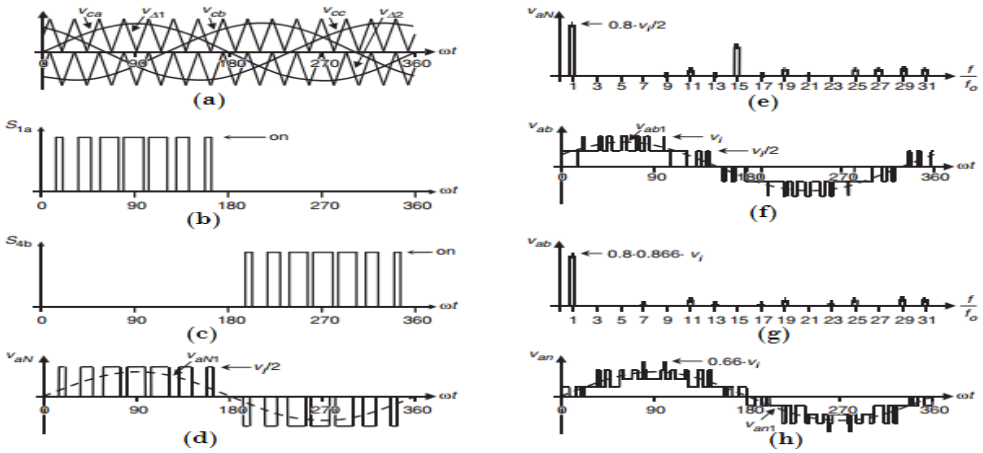

Figure 4-21 Three-level VSI topology. Relevant waveforms using a SPWM (mf = 15, ma = 0.8): (a) modulating and carrier signals; (b) switchS1a status; (c) switch S4b status; (d) inverter phase a voltage; (e) inverter phase a voltage spectrum; (f) load line voltage; (g) load line voltage spectrum;and (h) load phase a voltage [81].

4.2.5 48 Pulse Converter Operation

Three-phase VSI used in the BESS model is a 48 pulse converter. The 48 pulse comprises four identical 12-pulse GTOs converter with four transformers; two having +7.5 degrees phase shift from each other and two having -7.5 degrees phase shift. More information can be found in [14] [82] [83].

4.3 Battery Energy Storage System

Since the emerging of renewable energy, their impulsiveness creates the necessity of storage system. Considering several types of existing energy storage system, battery storage system is becoming more desirable because of their energy storage capability for long duration; downward trend of battery prices. The battery energy storage system with the STATCOM has emerged as promising near-term technologies in power applications [22] [84]. MW-level battery energy storage system integration with traditional power system is running for decades and operational experience is rather encouraging from the existing installations, as in Chilean power grid, West Virginia and Ohio [85], California [86]. Having beneficial outcome, the BESS integration is growing more and more. The issues relating to the frequency support and the voltage control has been deeply discussed and simulated results have been shown in [80]. The stability support is worth studying which will add more value to the BESS integration into the grid.

4.3.1 BESS working principles

The BESS in Smart grid concepts have put a greater value and it requires much more attention than before. The BESS model used in this work includes a Li-ion battery pack, Cúk type DC-DC converter, an x-level VSC, and interfacing transformer point to connect with the grid. The basic structure of BESS is shown in *Figure 4-22*.

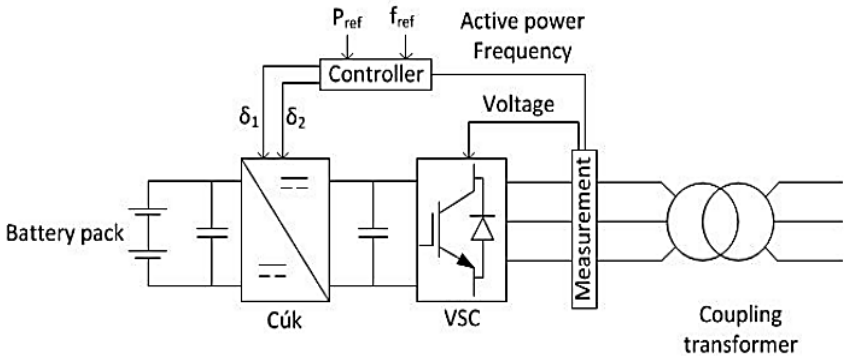

Figure 4-22 Battery Energy Storage System

Typically a STATCOM injects/draws reactive power into/from the system depending on the voltage level of the converter terminal and grid voltage. The main purpose of this VSC is to control the AC voltage [14] [87]. The VSC model with BESS implementation is based on the existing VSC matlab/similink model (power_statcom_gto48p).In a VSC model, phase angle between the converter and system voltage is used to control a STATCOM.

However, in BESS model, the DC voltage is controlled by the Cúk converter. Hence, active and reactive power is controlled by the BESS, for more detail information about this model read [88] .

Active power flow between the storage system and the grid is controlled by the duty cycles of the DC-DC converter. The switch S1 controls the power drawn from the battery into the grid and switch S2 controls the power injection into the battery.

The control systems of Cúk converter is split into three major stages. In first stage operating mode is determined on the error calculation between the actual frequency and the target value, with the impact of BESS proportional to the error.

In second stage, target output voltage is calculated based on the changes in the frequency according to the following relationship-

$$V_{out} = V_{int} + k(f_{ref} - f_{actual}) \tag{4-6}$$

Where f_{ref} and f_{actual} are target frequency and actual frequency respectively. Based on the difference of actual and target frequency, k takes positive or negative value to control duty cycle δ_1 and δ_2.

In third stage, duty cycle is calculated which are then transformed into PWM signal and the value of δ is calculated by this equation with n=1 or 2

$$\delta_n = \frac{v_{out,n}}{v_{batt} + v_{out,n}} \tag{4-7}$$

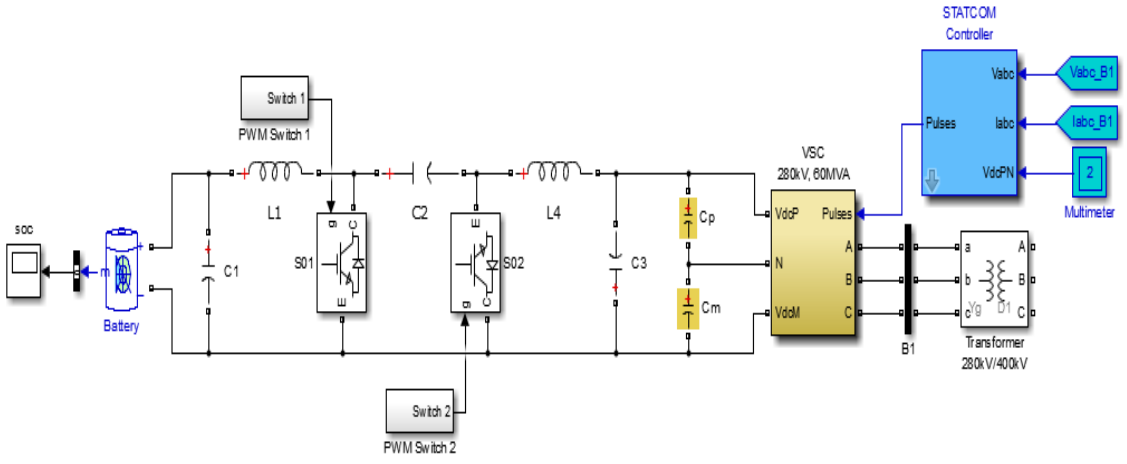

Figure 4-23 BESS model connection diagram in matlab/simulink

The above BESS model includes three distinctive parts-

a) Battery pack for energy storage
b) Cúk converter for active power control to/from the grid
c) VSC for reactive power control

Parameters of the DC-DC converter is as follows-

C1= 3000 µF C2=500 µF C3=1500 µF

L1= 28 mH L2=25 mH

A detail descriptions and working principles of the BESS model used in this testing are mentioned by Jan [80].

4.4 Siirtoverkkomalli Equivalent Network

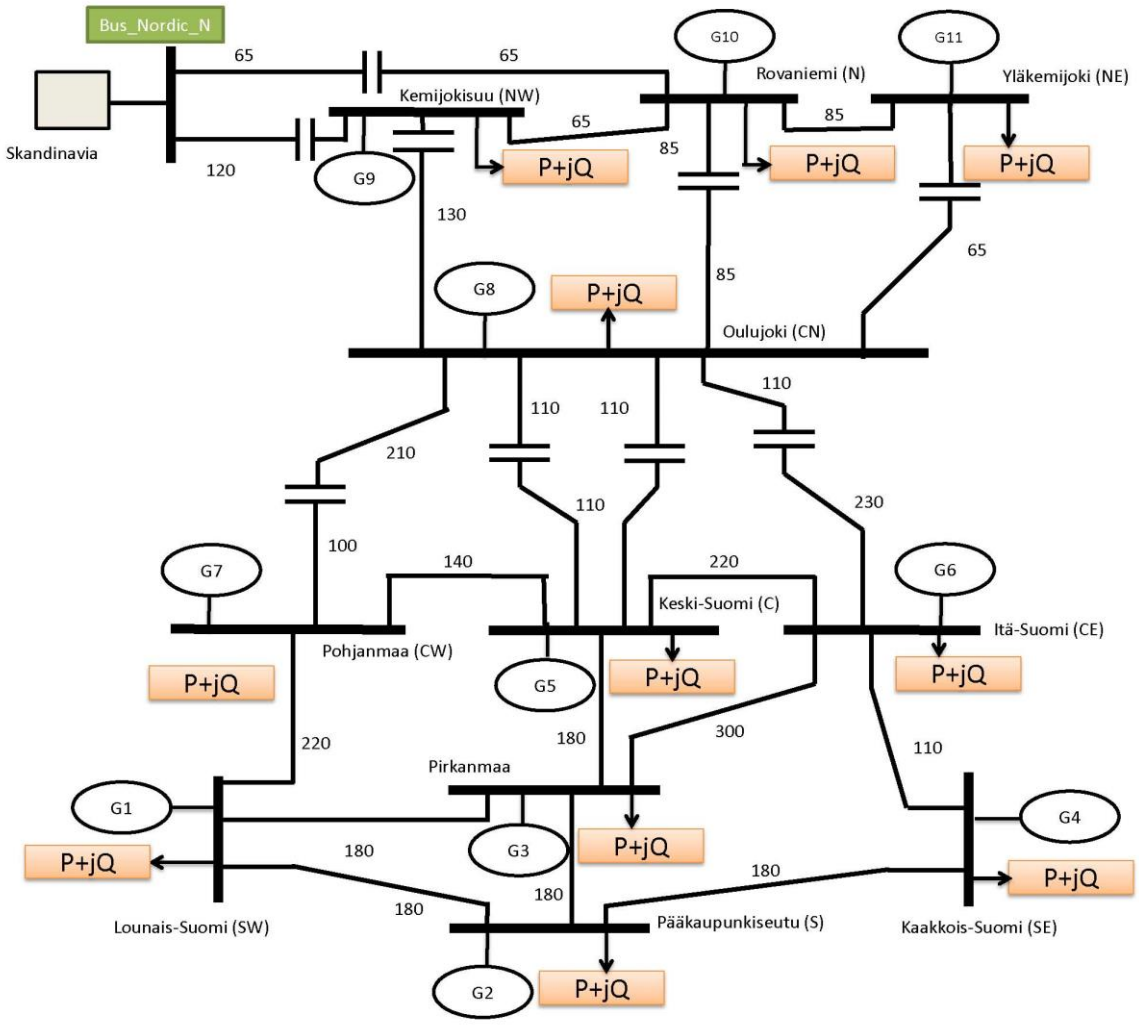

Figure 4-24 Siirtoverkkomalli equivalent model (length is in km)

This network is a reduced equivalent of the network in *Figure 3-3*. Due to the long simulation times required for the full Siirtoverkkomalli and Nordic-32 in discrete mode in simulink, a smaller network was found more amenable to use in this part of the research.

4.5 Simulation Results

To assess the applicability of the BESS in system stability analysis, an unstable condition was identified for the export case in the network of *Figure 4-24*. This was followed by an application of the BESS to stabilize the network after the fault. Similar types of fault conditions are applied in the testing network as it was in the case for the SVC/STATCOM application i.e., three-phase-to-ground fault, increasing electrical the length of the line and loss of line.

4.5.1 Unstable case

The equivalent network in *Figure 4-24* becomes unstable during the 500MW power exporting for the testing conditions stated in *section 3.3*.

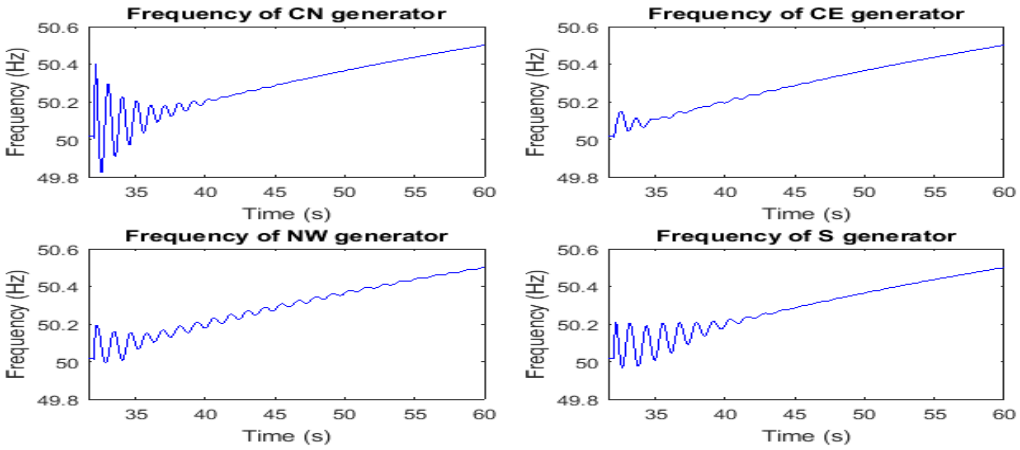

Figure 4-25 Frequency of generators undergoing a 3-phase-to-ground fault

It can be observed from the above graphs that, after the occurrence of the fault, the frequency keeps an upwards trend hence, the system becomes unstable. Quite clearly the system is not stable during the fault while exporting 500MW power and subjected to a three-phase-to-ground fault. Hence, additional supports need to be added to the system to stabilize it. This is achieved by connecting a BESS into the system and assessing the overall system for stability. However, the system voltage does not seem to be affected by the fault.

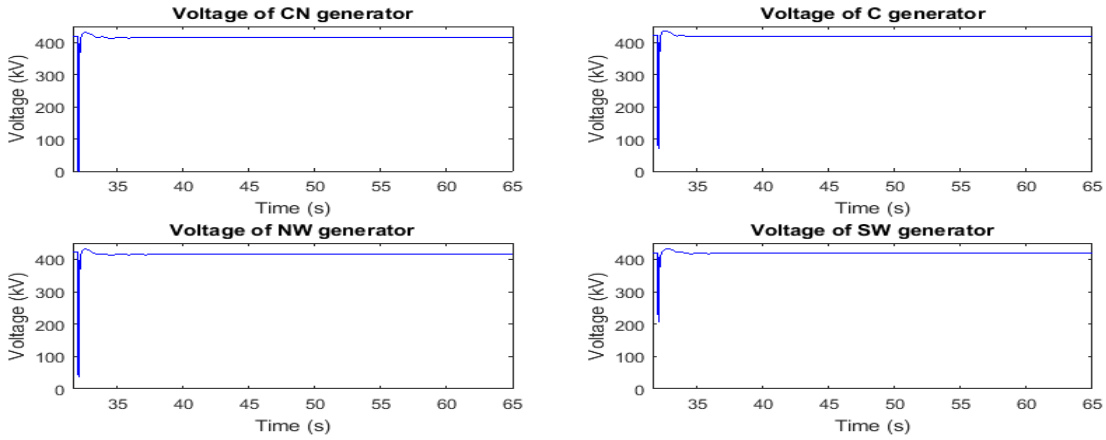

Figure 4-26 AC Voltage at 400kV bus undergoing a 3-phase-to-ground fault

4.5.2 Stabilization with Battery Energy Storage System

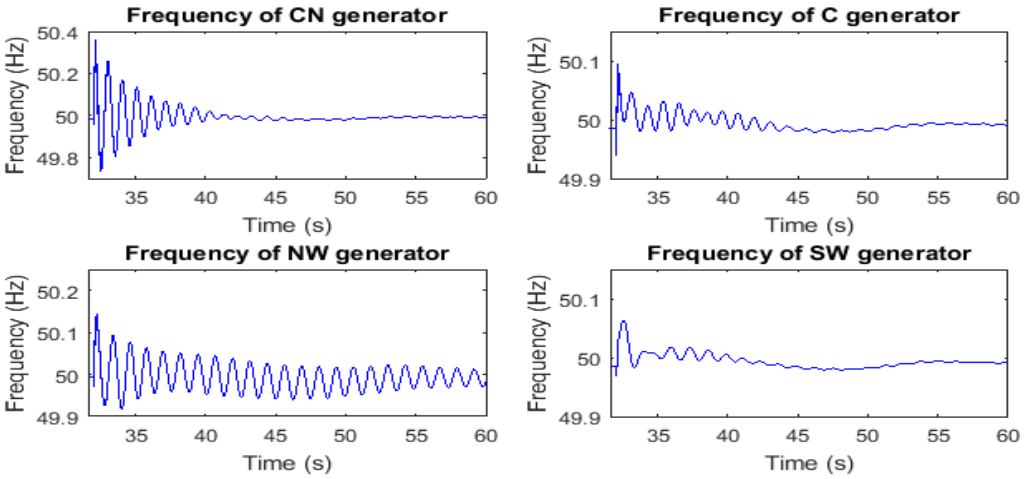

Figure 4-27 Frequency of generators undergoing a 3-phase-to-ground fault with a BESS

Since the system is unstable, the BESS is connected into the network to support and stabilize the system. It can be observed from *Figure 4-27* that the frequency becomes stable after the fault has been removed, when the BESS is connected.

The active power supported by the BESS is 60MW. Since the frequency after the fault is higher than 50Hz, the BESS will consume power and get charged. The battery model was designed in such a way that, the battery emulates the action of a motor function when the system frequency is higher than the nominal frequency, consuming power from the network and a generator function in the case when the system frequency is lower than nominal, supplying power to the network. The reactive power supported by the BESS is 50MVAR.

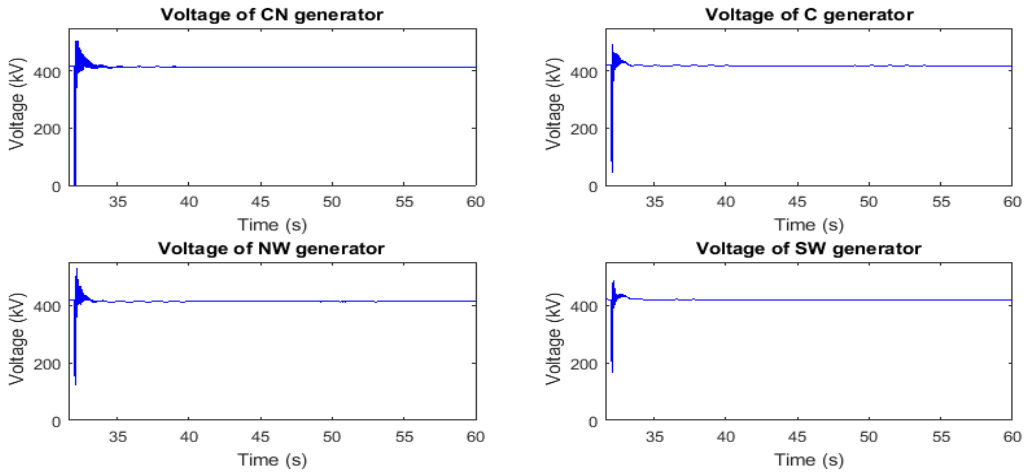

Figure 4-28 AC voltage at 400kV bus undergoing a 3-phase-to-ground fault

The Cúk converter output voltage is nearly constant after the fault at a value of 14kV and the AC voltage at inverters output terminal is 300kV.

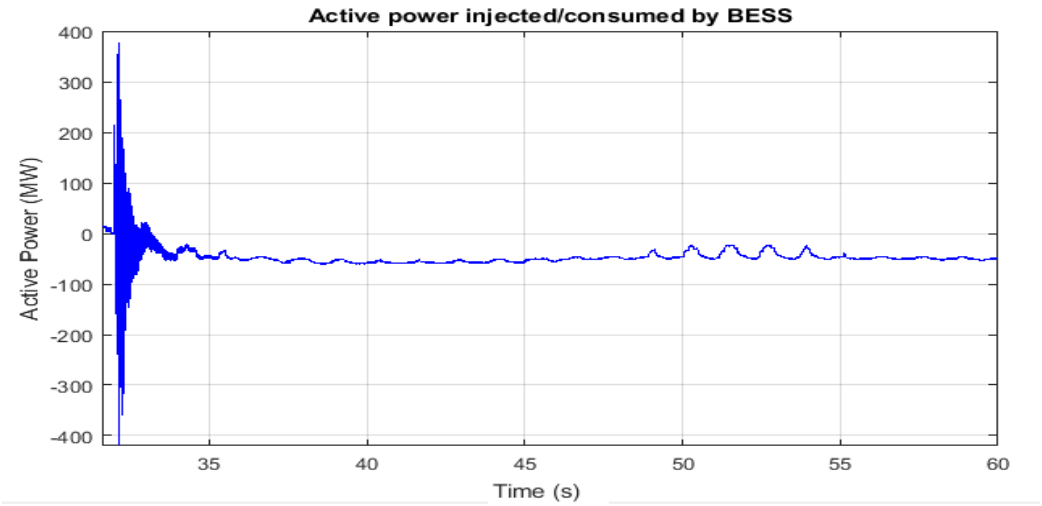

Figure 4-29 Active power supported by battery energy storage system (BESS)

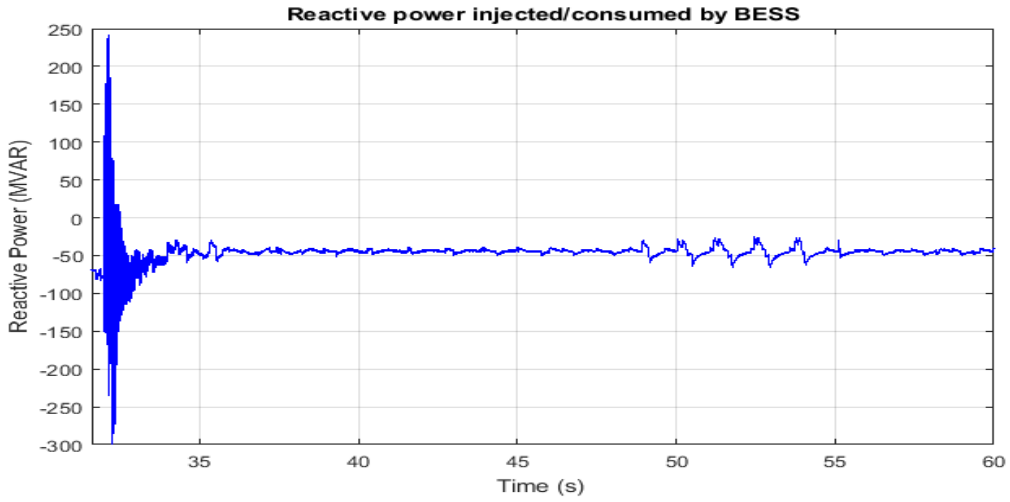

Figure 4-30 Reactive power supported by battery energy storage system (BESS)

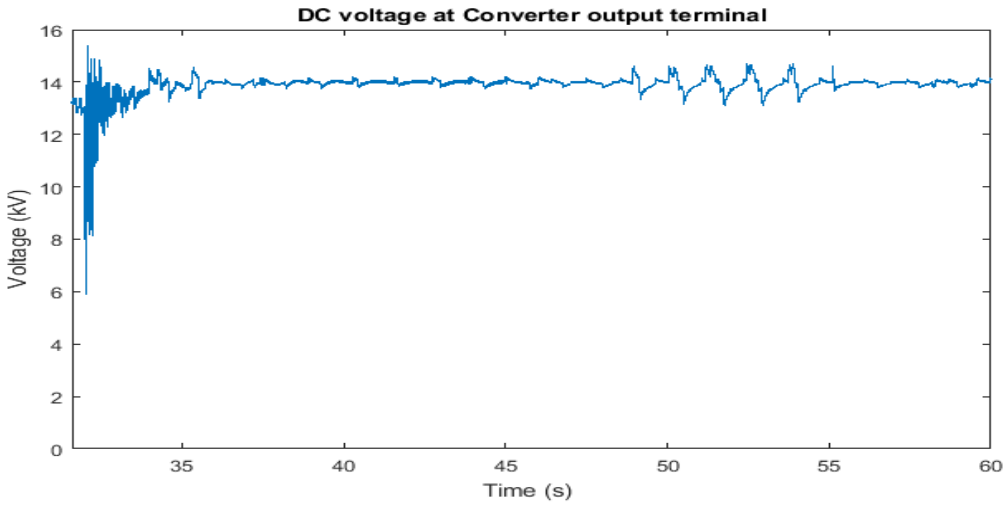

Figure 4-31 Cúk converter's output DC voltage undergoing a 3-phase-to-ground fault

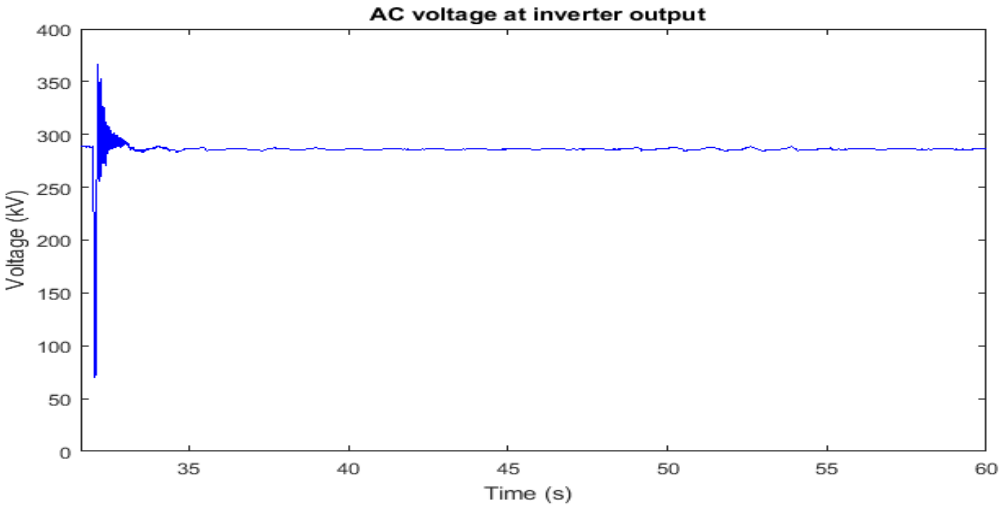

Figure 4-32 AC voltage at inverter output terminal

4.5.3 Faults on the DC side of the BESS (positive-pole-to-ground)

Further to analysis of the fault on the AC network, the issue of faults on the DC side has also been investigated for instance; one-pole-to-ground fault on the DC side of the BESS for 100ms, to assess its impact on the network. The schematic diagram corresponding to this faulted condition is shown in *Figure 4-33*. Small fluctuations are visible in the graphs due to high sample time in the model.

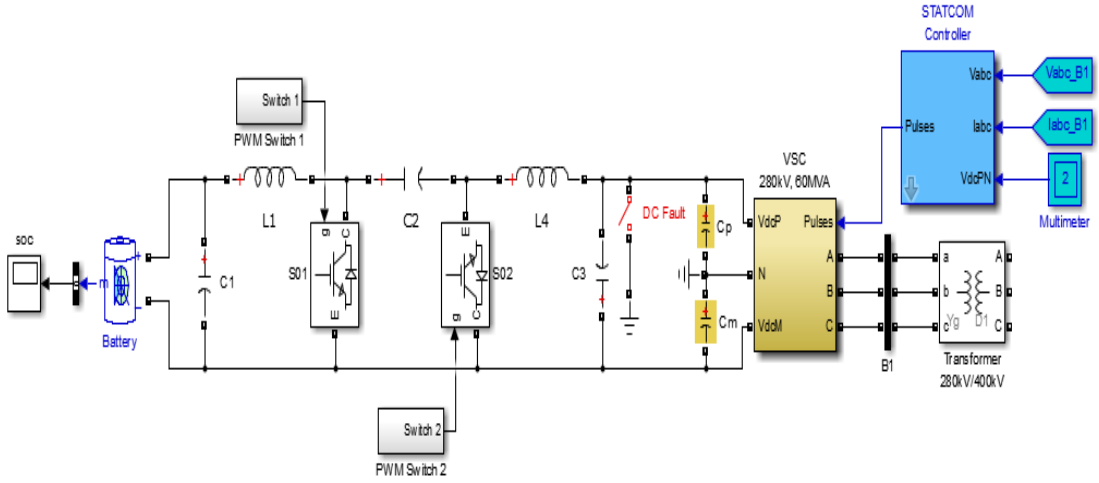

Figure 4-33 Positive-pole-to-ground fault on DC side of BESS

It can be observed from the figure that the fault on the DC side of BESS does not raise any instability issues in the network. The synchronous generators frequencies are not affected by this type of fault on the DC side. Also, the dip in the Cúk converter output voltage during the fault is 42% compared to the 57% during the fault in the AC network. The voltages at the 400kV buses and at the inverter output voltage are not affected by the DC fault. A small amount of active power and 50-80MVAR reactive power is supplied by the BESS into the network.

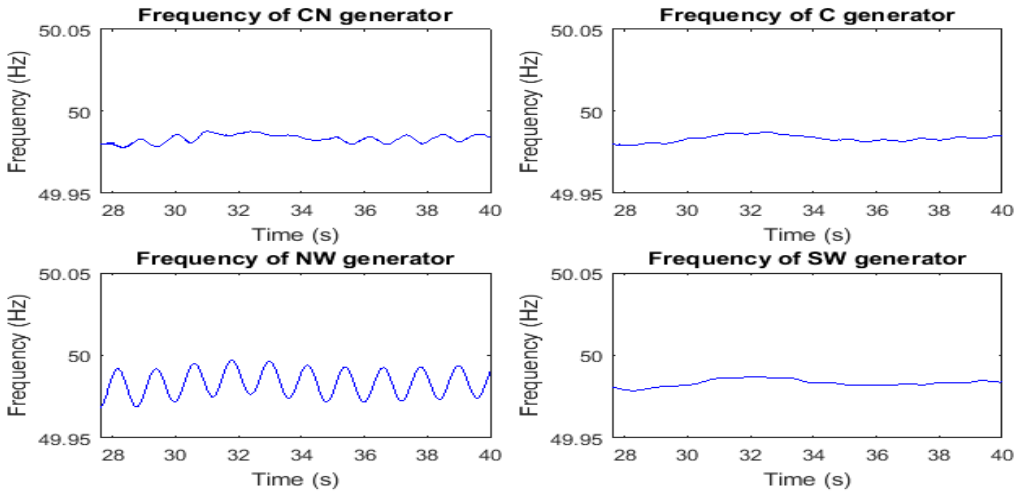

Figure 4-34 Frequency of synchronous generators undergoing one-pole-to-ground fault on DC side of the BESS

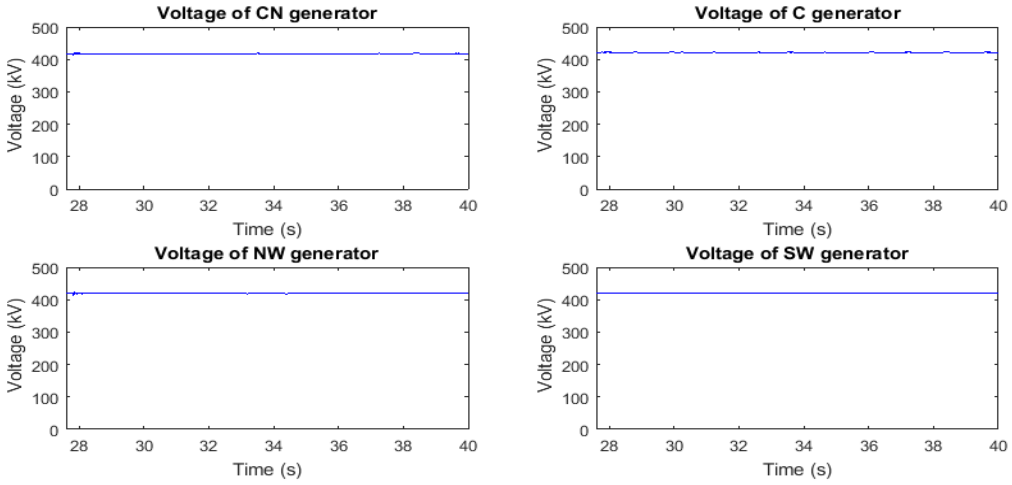

Figure 4-35 AC Voltage at 400kV bus undergoing one-pole-to-ground fault on DC side

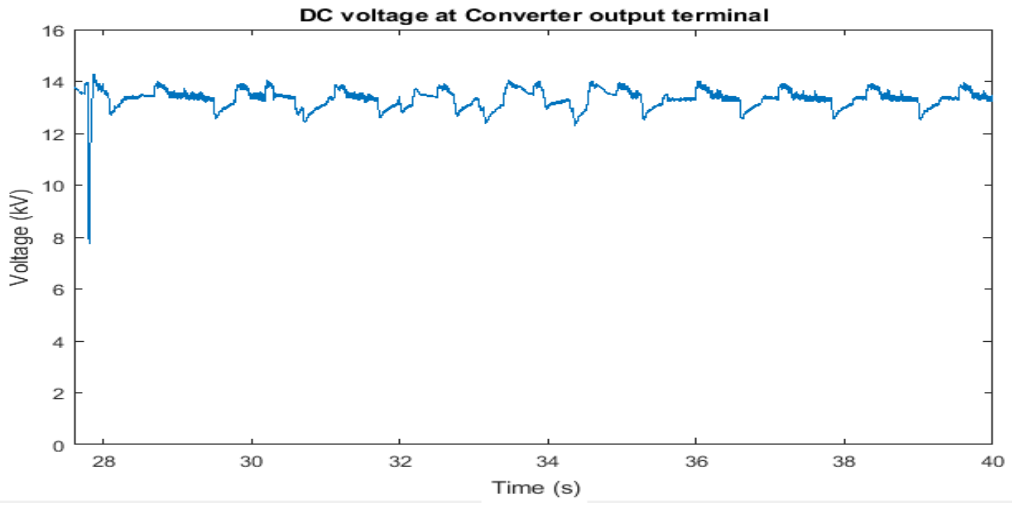

Figure 4-36 Cúk converter output DC voltage undergoing one-pole-to-ground fault on DC side

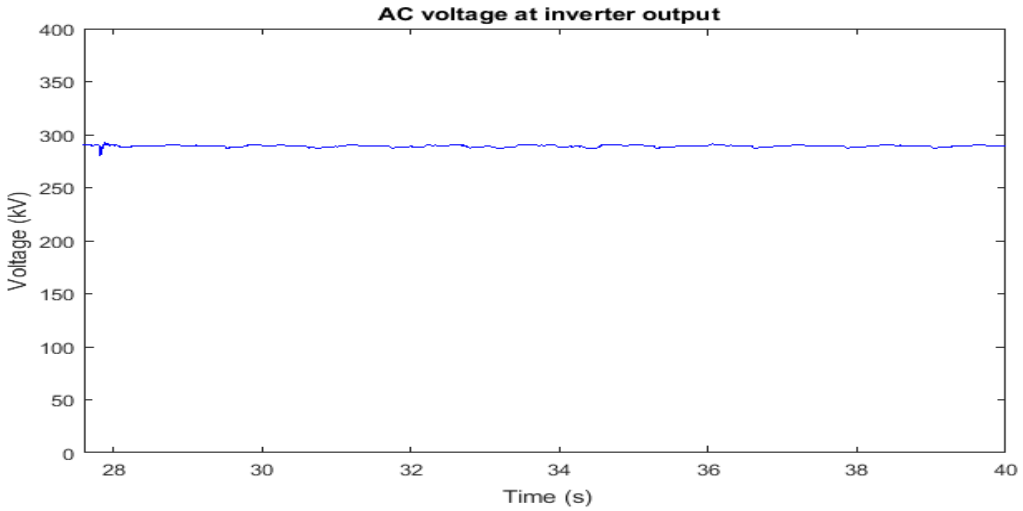

Figure 4-37 AC voltage at inverter output undergoing one-pole-to-ground fault on DC side of the BESS

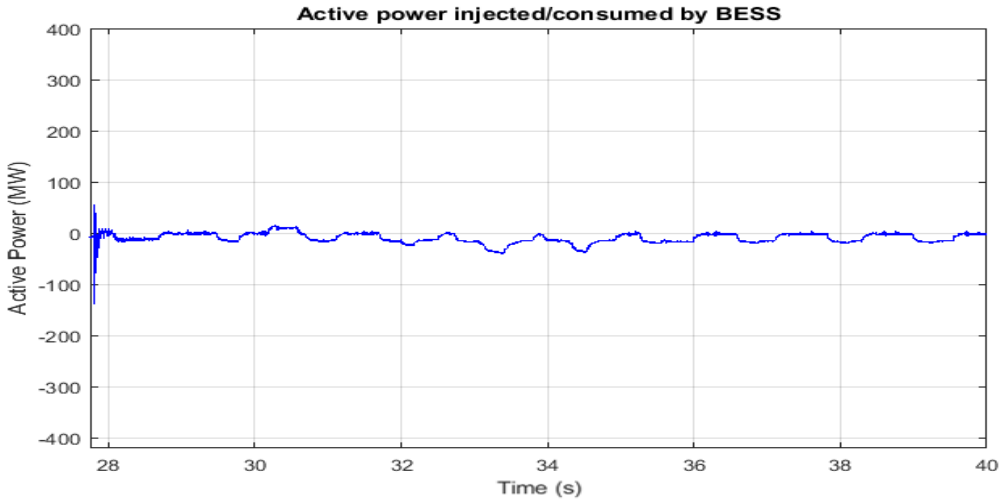

Figure 4-38 Active power of BESS undergoing one-pole-to-ground fault on DC side of the BESS

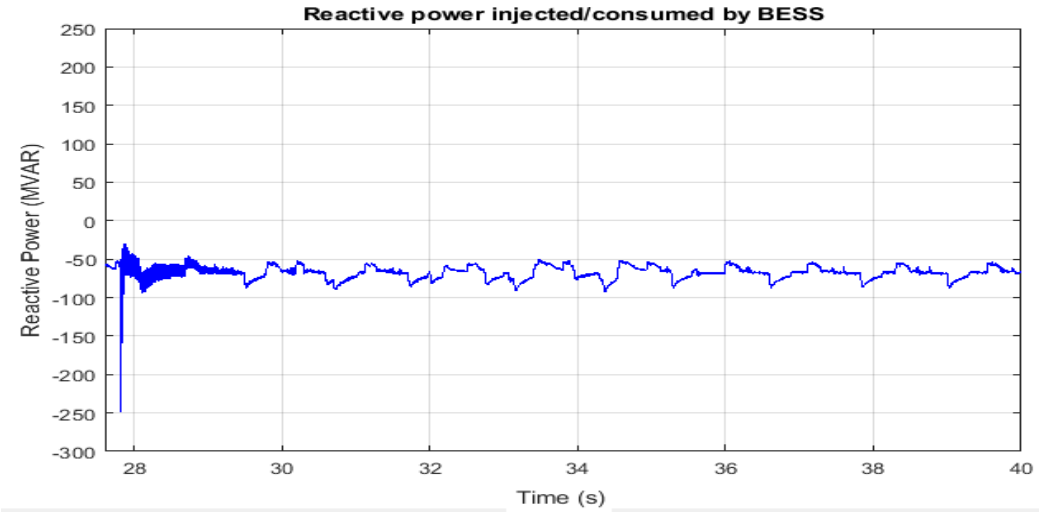

Figure 4-39 Reactive power of BESS undergoing one-pole-to-ground fault on DC side of the BESS

4.5.4 Faults on the DC side of the BESS (pole-to-pole)

A pole-to-pole fault was applied on the DC side of the BESS and its impact on the AC network was assessed. It can be observed that the system frequency is greatly affected by this type of fault and the frequency starts keep an upwards trend clearly indicating a sign of instability. However, the system voltage does not seem to be affected by the fault. To keep the voltage at its nominal value, the reactive power drawn by the battery is rather high compare to one-pole-to-ground fault.

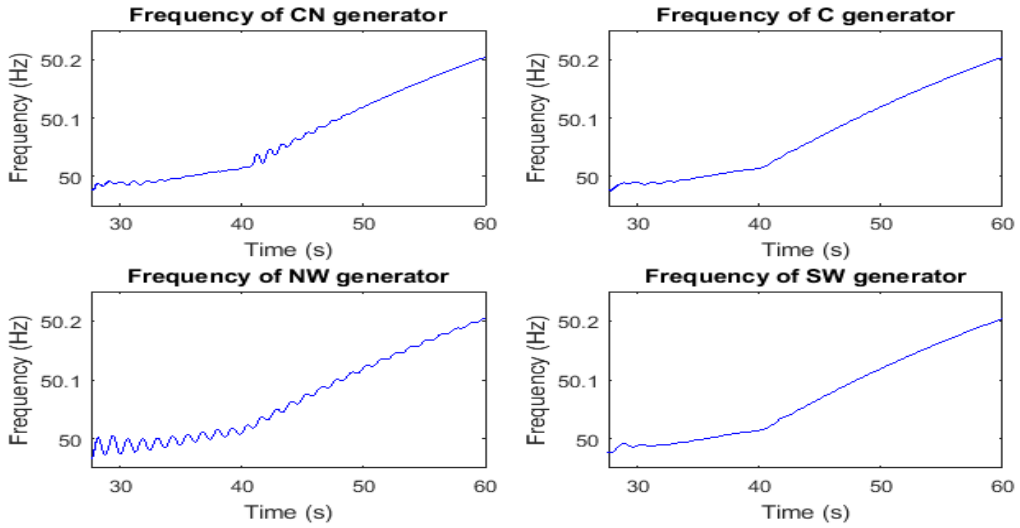

Figure 4-40 Frequency of synchronous generators undergoing a pole-to-pole fault on DC side of the BESS

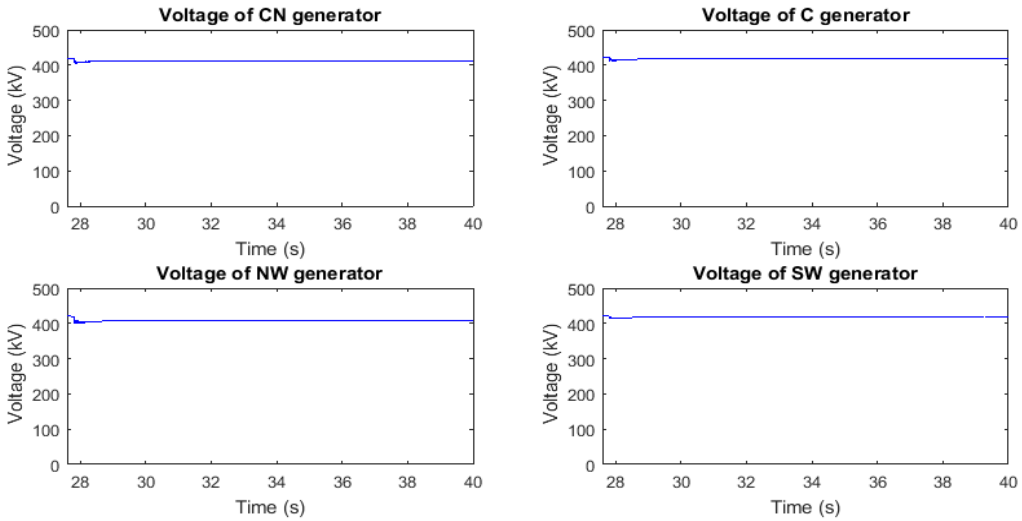

Figure 4-41 Voltages of 400kV bus undergoing a pole-to-pole fault on DC side of the the BESS

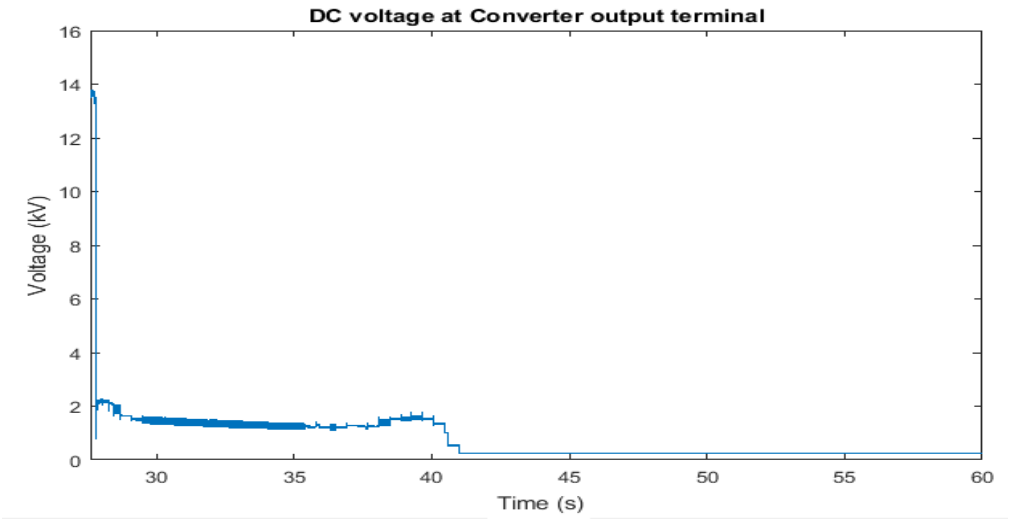

Figure 4-42 Cúk converter output DC voltage undergoing a pole-to-pole fault on DC side

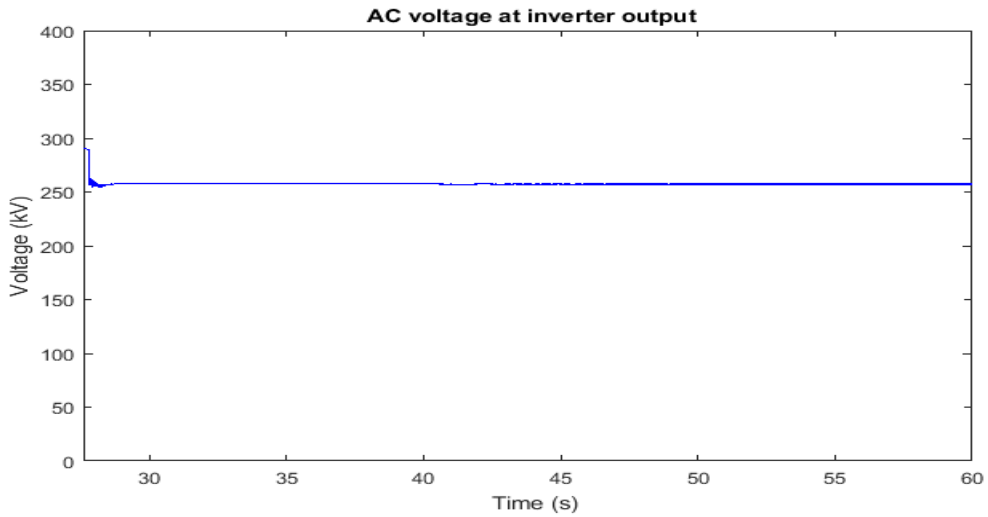

Figure 4-43 AC voltage (rms)at inverter output undergoing a pole-to-pole fault on DC side

The DC voltage at the Cúk converter output is not stable anymore. It starts to decrease right after the occurrence of fault, at around 2kV and it eventually drops to nearly zero. The system becomes unstable since the BESS fails to isolate the impact of pole-to-pole DC fault.

Active power of the BESS is controlled by the Cúk converter output voltage. As the converter is not designed with the dc fault reverse blocking capability, active and reactive power exchange between the dc side and ac grid, undergoing a pole-to-pole fault, is not zero. Since the converter voltage drops near to zero at the fault period, the active power drawn by the BESS is rather small, but never becomes zero, as shown in *Figure 4-44*. The large amount of reactive power is drawn by the BESS during the dc fault, shown in *Figure 4-45*.

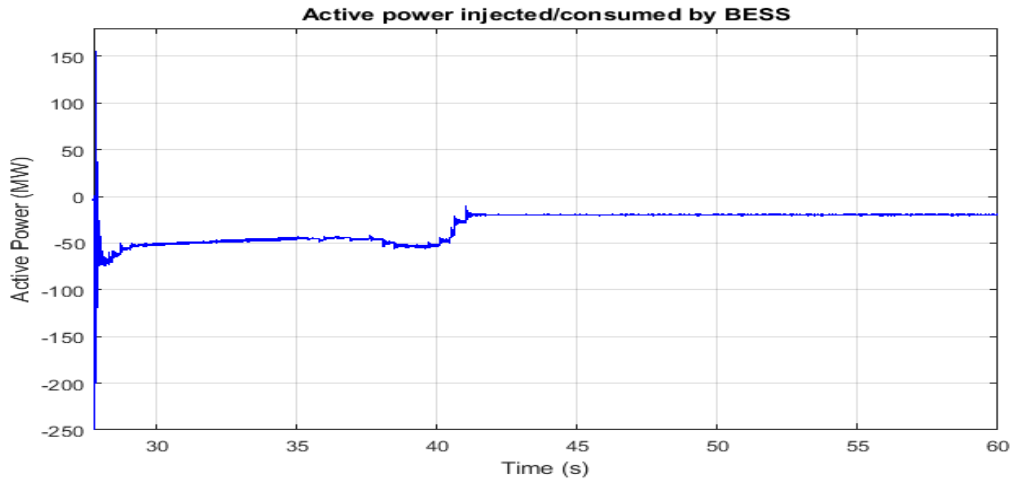

Figure 4-44 Active of BESS undergoing a pole-to-pole fault on DC side of BESS

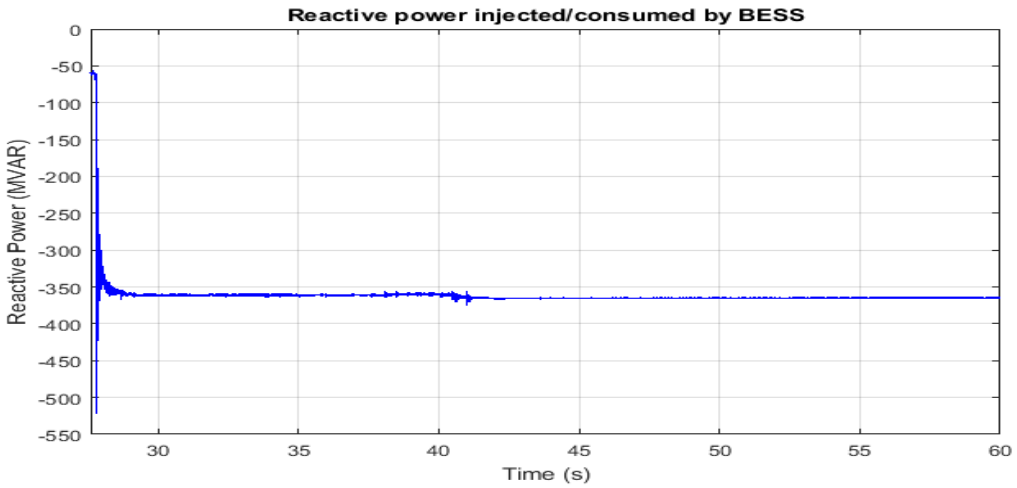

Figure 4-45 Reactive of BESS under line-line fault on DC side of BESS

5 Summary

Major objectives and simulation results is summarized in this chapter. In latter part, recommendation for further possible development has also been discussed in concise form.

5.1 Conclusion

The main objective of this thesis was to investigate what is the maximum available power that can be exported from one end of Siirtoverkkomalli to the other, without incurring stability issues, including faulted conditions in the network. This proved to be a steep learning curve in the use of the software package. The unstable situations were well understood after extensive simulation studies and the integration of SVC and STATCOM was employed to provide system reliability and stability enhancement to Siirtoverkkomalli. The results show very significant stability improvements in power exporting capabilities, with the capacity of FACTS devices being strongly related to the amount of power exporting.

The latter part of the thesis concentrates on the use of BESS in Siirtoverkkomalli to ameliorate further the instabilities experienced by the system. It was observed that the BESS stabilizes the network under faulted conditions, which justifies the integration of this technology into the network. When the system frequency is higher than the nominal frequency, the battery draws power to maintain the system frequency at about nominal value and battery charges. Conversely, when the system frequency is lower than the nominal frequency, the battery injects power into the system to maintain the system frequency at about nominal value and battery discharges.

After extensive simulation studies of the export cases, it has been observed that the STATCOM plays better performance compared to the similar rated or higher rated SVC in case of frequency and voltage instability at post fault operation. On the other hand, the BESS provides frequency stability support at post fault condition; a new application of the BESS in the power system.

5.2 Recommendations for future work

Upon the investigation of several cases with the FACTS devices in Siirtoverkkomalli network, the future possible recommendation on the present work may be summarized, as given below:

An analytical method was not considered for optimizing the SVC/STATCOM location using optimization techniques to find the optimal placement in the network could be one of the improvements that can be carried out in the future. This would yield more accurate studies and conclusions.

No attempt was made to optimize the controller of the BESS in this thesis. It is expected to have better results in battery charging/discharging control during the faults period. Better control techniques can prevent the battery from sharp charging/discharging during the faults.

Carrying out an economic assessment of BESS over traditional the FACTS devices like SVC, STATCOM is another future work area. This can justify the prospect of installing BESS in this power system.

The line-to-line fault in the dc side of the BESS causes the system to go unstable. Since the purpose of the BESS is to improve the system stability, BESS should be available in the system when it is needed. Hence faults in the dc side should be isolated quickly to ensure the integrity of the network. Therefore, the fault tolerance of the DC side could be other possible area of further study.

6 References

[1] IEA. (2015) www.iea.org. [Online]. https://www.iea.org/publications/freepublications/publication/KeyWorld_Statistics_2015.pdf

[2] (2015) The IEA Photovoltaic Power Systems Programme. [Online]. http://www.iea-pvps.org/index.php?id=trends0

[3] (2013) The IEA Photovoltaic Power Systems Programme. [Online]. http://www.iea.org/publications/freepublications/publication/technology-roadmap-wind-energy---2013-edition.html

[4] Andrei Ter-Gazarian, *Energy Storage for Power Systems*, 2nd ed. Trowbridge, Wiltshire : Redwood Books, 2011.

[5] Sandia National Laboratories. (2013) www.sandia.gov. [Online]. http://www.sandia.gov/ess/publications/SAND2013-5131.pdf

[6] International Electrotechnical Commision and Fraunhofer Institut für Solare Energiesysteme. (2011) http://www.iec.ch/. [Online]. http://www.iec.ch/whitepaper/pdf/iecWP-energystorage-LR-en.pdf

[7] U.S energy Information Administration. (2016, Feb) www.eia.gov. [Online]. https://www.eia.gov/tools/faqs/faq.cfm?id=74&t=11

[8] Kris De Decker. http://www.lowtechmagazine.com/. [Online]. http://www.lowtechmagazine.com/2015/05/sustainability-off-grid-solar-power.html

[9] P. Kundur, *Power system stability and control*. New York: McGraw-Hill , Inc, 1993.

[10] ABB AB FACTS. www.abb.com. [Online]. https://library.e.abb.com/public/75362d2c1aa7f86783257e0c00478a6f/SVC%20A02-0100.pdf

[11] CIGRE Working Group 38.05 T. Petersson, *Analysis and Optimization of SVC Use in Transmission Systems*. Paris, France: CIGRE, 1993.

[12] Carson W. Taylor, *Power System Voltage Stability*.: McGraw-Hill Ryerson, 1994.

[13] "FACTS Applications," *IEEE/PES Special Publication TP-116-0*, 1996.

[14] Narain G. Hingorani and Laszlo Gyugyi, *Understanding FACTS: Concepts and Technology of Flexible AC Transmission Systems*. New York, USA: Wiley-IEEE Press, 1999.

[15] Yoshihiko Sumi et al., "New Static Var Control Using Force-Commutated Inverters," *IEEE Transactions on Power Apparatus and Systems* , vol. PAS-100, no. 9, pp. 4216 - 4224, Sep 1981.

[16] Nannery P.R., Mattern K.E., Gubernick J. Edwards C.W., "Advanced static VAR generator employing GTO thyristors," *IEEE Trans. Power Deliv.*, vol. 3, no. 4, pp. 1622-1627, 1988.

[17] Hatziadonui C.J. and Chalkiadakis F.E, "A 12-pulse static synchronous compensator for the distribution system employing the 3-level GTO-inverter," *IEEE Trans. Power Deliv.*, vol. 12, no. 4, pp. 1830-1835, 1997.

[18] XU L. TANG Y., "A new converter topology for advanced static VAR compensation in high power applications," *IEEE Industry Applications Society Annual Meeting, Conf. Record*, vol. 2, pp. 947-953, 2-8 October 1993.

[19] Gernhardt M., Stacey E. et al. Schauder C., "Development of a + 100 MVAR static condenser for voltage control of transmission systems," *IEEE Trans. Power Deliv.*, vol. 10, no. 3, pp. 1486-1496, 1995.

[20] Matsuno K., Hasegawa T. et.al. Mori S., "Development of a large static VAR generator using self-commutated inverters for improving power system stability," *IEEE Trans. Power Syst.*, , vol. 8, no. 1, pp. 371-377, 1993.

[21] Tsai Z.-Y. Wang L., "Dynamic stability enhancement of nuclear power plants of Taiwan power system using STATCON," *IEEE Power Engineering Society WM*, vol. 1, pp. 604-609, 1999.

[22] S. Eckroad, "FACTS with energy storage: conceptual design study," EPRI, Palo Alto, Calif, EPRI Report TR-111093, 1999.

[23] S.O., A.K.Barnes, and J.C.Balda Geurin, "Smart grid applications of selected energy storage technologies," *Innovative Smart Grid Technologies (ISGT), IEEE PES*, 2012.

[24] Battery University. http://batteryuniversity.com/. [Online]. http://batteryuniversity.com/learn/article/battery_statistics

[25] O. and Dessaint, L.-A Tremblay, "Experimental Validation of a Battery Dynamic Model for EV," *Hybrid and Fuel Cell Electric Vehicle Symposium,AVERE, Stavanger*, pp. 1-9, 2009.

[26] C. M. Bingham, D. A. Stone and P. Bentley C. R. Gould, "New Battery Model and State-of-Health Determination Through Subspace Parameter Estimation and State Observer Techniques," *IEEE Transactions On Vehicular Technology*, vol. 58, pp. 3905-3916, 2009.

[27] K. J. Tseng and S. S. Choi S. X. Chen, "Modeling of lithium-ion battery for energy storage system simulation," *Power and Energy Engineering Conference*, pp. 1-4, 2009.

[28] M. Paul Anderson and A. A. Fouad, *Power System Control and Stability*, 2nd ed.: The Iowa State University Press, 1986.

[29] Yao Nan Yu, *Electric Power System Dynamics*. New York: Academic Press Inc., 1983.

[30] Charles Concordia and Demello, F.P., "Concepts of Synchronous Machine Stability as affected by excitation control," *IEEE Transactions on Power Apparatus and Systems*, pp. pp.316 - 329, April 1969.

[31] R.A. Phillips and Heffron, W.G., "Effect of a Modern Amplidyne Voltage Regulator on Underexcited Operation of Large Turbine Generators," *AIEE Transactions*, vol. Vol. 71, pp. pp. 692-697, August 1952.

[32] Hughes. F.M and Saidy, M., "Block diagram transfer function model of a generator including damper windings," *IEE Proceedings on Generation, Transmission and Distribution*, vol. Vol.141, no. Issue. 6, pp. pp.599 - 608, Nov 1994.

[33] Hughes F.M and M. Saidy, "An extended block diagram transfer function model of a synchronous machine," *International Journal of Electrical Power & Energy Systems*, vol. Vol.18, no. Issue.2, pp. pp.139–142, February 1996.

[34] Chee-Mun Ong, *Dynamic Simulations of Electric Machinery: Using MATLAB/SIMULINK*. New Jersey: Prentice Hall, 1997.

[35] IEEE Standards 1110-2002, "IEEE Guide for Synchronous Generator Modeling Practices and Applications in Power System Stability Analyses," pp. 0_1 - 72, 2003.

[36] IEEE Standards 1110-1991, "IEEE Guide for Synchronous Generator Modeling Practices in Stability Analyses," 1991.

[37] IEEE task Force on Definitions and Procedures, "Current Usage & Suggested Practices in Power System Stability Simulations for Synchronous Machines," *Energy Conversion, IEEE Transactions on*, pp. 77 - 93, March 1986.

[38] IEEE standard 421.5-1992, "IEEE Recommended Practice for Excitation System Models for Power System Stability Studies," *IEEE Power & Energy Society*, 2002.

[39] IEEE Working Group Report, "Hydraulic turbine and turbine control models for system dynamic studies," *IEEE Transactions on Power Systems*, vol. 7, no. 1, pp. 167 - 179, 1992.

[40] "IEEE Guide for the Application of Turbine Governing Systems for Hydroelectric," *IEEE Std 1207-2004*, pp. 0_1 - 121, 2004.

[41] J. Machowski, Bialek J. , and Bumby D.J. , *Power System Dynamics: Stability and Control*, 2nd ed.: John Wiley & Sons, Ltd., 2008.

[42] Murty, M.S.R., and M.V. Hariharan, "Analysis and Improvement of the Stability of a Hydro-Turbine Generating Unit With Long Penstock," *IEEE Transactions on Power Apparatus and Systems*, vol. PAS-103, no. 2, pp. 360 - 367, 1984.

[43] Ramey D. G. and W. Skooglund John , "Detailed Hydrogovernor Representation for System Stability Studies," *IEEE Transactions on Power Apparatus and Systems*, vol. PAS-89, no. 1, pp. 106 - 112, 1970.

[44] Report IEEE Committee, "Dynamic Models for Steam and Hydro Turbines in Power System Studies," *IEEE Transactions on Power Apparatus and Systems*, vol. PAS-92, no. 6, pp. 1904 - 1915, 1973.

[45] Koritarov Vladimir et al., "Review of Existing Hydroelectric," Decision and Information Sciences, Argonne National Laboratory,Siemens PTI, 2013.

[46] D. Vu Hoa and Agee J. C. , "WECC Tutorial on Speed Governors," WECC Control Work Group, 1998.

[47] J. M. Undrill and J. L. Woodward, "Nonlinear Hydro Governing Model and Improved Calculation for Determining Temporary Droop," *IEEE Transactions on Power Apparatus and Systems* , vol. PAS-86, no. 4, pp. 443 - 453, April 1967.

[48] Mathworks. [Online]. http://se.mathworks.com/help/physmod/sps/powersys/ref/threephasedynamicload.html

[49] Gates Energy Products, "Rechargeable Cells and Batteries ," in *Rechargeable Batteries Applications Handbook*.: Newnes, 1997, ch. 2, p. 9.

[50] D. Berndt, "Electrochemical Energy Storage," in *Battery Technology Handbook*.: CRC Press , 2003, ch. 1.

[51] L. Gauchía Babé, "Nonlinear dynamic per-unit models for electrochemical energy systems : application to a hardware-in-the-loop hybrid simulation," Universidad Carlos III de Madrid, Madrid, Spain, PhD thesis 2009.

[52] Battery University. (2016, May) [Online]. http://batteryuniversity.com/learn/article/types_of_battery_cells

[53] David Linden, "Basic Concepts," in *Hanbook of Batteries*, David Linden and Thomas B. Reddy, Eds.: McGraw-Hill, 2001, ch. 1, pp. 1.7-1.8.

[54] Kwo Young, Caisheng Wang, Yi Wan Le , and Kai Strunz, "Electric Vehicle Battery Technologies," in *Electric Vehicle Integration into Modern Power Networks*, João A. Peças Lopes Rodrigo Garcia-Valle, Ed. New York, 2013, ch. 2, p. 29.

[55] Sabine Piller, Marion Perrin, and Andreas Jossen, "Methods for state-of-charge determination and their applications," *Journal of Power Sources, ELSEVIER*, pp. 113-120, 2001.

[56] Juan Carlos Alvarez Anton , Paulino Jose Garcia Nieto, Esperanza Garcia Gonzalo, and Juan Viera , "A new predictive model for the state-of-charge of a high power lithium-ion cell based on a PSO optimized multivariate adaptive regression splines approach," *IEEE Transactions on Vehicular Technology* , vol. PP, no. 99, pp. 1-12, December 2015.

[57] Xiaosong Hu, Shengbo Li, Huei Peng, and Fengchun Sun, "Robustness analysis of State-of-Charge estimation methods for two types of Li-ion batteries," *Journal of Power Sources, ELSEVIER*, vol. 217, pp. 209–219, November 2012.

[58] B. S. Bhangu , P. Bentley, and D. A. Ston, "Nonlinear Observers for Predicting State-of-Chargeand State-of-Health of Lead-Acid Batteries forHybrid-Electric Vehicles," *IEEE Transactions on Vehicular Technology* , vol. 54, no. 3, pp. 783 - 794, May 2005.

[59] Li Jun , Zhao Fuquan, You Yi , Dong Tingting, and Jin Qiqian, "Analysis on the Influence of Measurement Error on state of charge estimation of LiFePO4 power Battery," *Materials for Renewable Energy & Environment (ICMREE), 2011 International Conference on*, vol. 1, pp. 644 - 649, May 2011.

[60] Robert Huggins, *Advanced Batteries: Materials Science Aspects*. New York: Springer, 2010.

[61] Alvin J. Salkind, Anthony G. Cannone, and Forrest A. Trumbure, "LEAD-ACID BATTERIES," in *Handbook of batteries*, Thomas B. Reddy David Linden, Ed., 2001, ch. 23, p. 23.13.

[62] A. Sabatino, *Maintenance-free Batteries, Heavy Duty Equipment Maintenance*. Lincolnwood: Irving-Cloud Publishing, 1976.

[63] "Special Issue on Lead-Acid Batteries," *J. Power Sources* , vol. 2, no. 1, 1977/1978.

[64] V.H. Johnson, "Battery performance models in ADVISOR," *Journal of Power Sources ELSEVIER*, pp. 321-329, 2002.

[65] Seongjun Lee, Jonghoon Kim, Jaemoon Lee, and B.H. Cho, "State-of-charge and capacity estimation of lithium-ion battery using a new open-circuit voltage versus state-of-charge," *Journal of Power Sources ELSEVIER*, vol. 185, no. 2, pp. 1367–1373, December 2008.

[66] H. L. Chan and D. Sutanto, , "“A new battery model for use with battery energy storage systems and electric vehicles power systems," *IEEE Power Engineering Society Winter Meeting*, pp. 470-475, 2000.

[67] C. J. Zhan et al., "Two electrical models of the lead-acid battery used in a dynamic voltage restorer," *IEE Proc. Generation, Transmission, and Distribution*, vol. 150, no. 2, pp. 175-182, March 2003.

[68] R. Rao, S. Vrudhula, and D. N. Rakhmatov, "Battery modeling for energy-aware system design," *Computer*, vol. 36, no. 12, pp. 77-87, 2003.

[69] M. Pedram and Q. Wu, "Design considerations for battery-powered electronics," *Design Automation Conf*, pp. 861-866, 1999.

[70] C. F. Chiasserini and R. R. Rao, "Energy efficient battery management," *IEEE J. Selected Areas in Communications*, vol. 19, no. 7, pp. 1235-1245, July 2001.

[71] He Hongwen, Xiong Rui, and Fa Jinxin, "Evaluation of Lithium-Ion Battery Equivalent Circuit Models for State of Charge Estimation by an Experimental Approach," *Energies*, vol. 4, no. 4, pp. 582-599, April 2011.

[72] Grant M. Ehrlich, "Lithium-Ion Batteries," in *Handbook of Batteries*, David Linden and Thomas Reddy, Eds., 2001, ch. 35.

[73] Ralph J. Brodd, "Synopsis of the Lithium-Ion Battery Markets," in *Lithium-Ion Batteries, Science and Technologies*, Masaki Yoshio, Ralph J. Brodd, and Akiya Kozawa, Eds.: Springer, 2009, ch. 1, p. 2.

[74] Yano Research Institute Ltd. of Japan, "Studies of the Li-ion Battery Market, year-1999," 2000.

[75] D. MacArthur, G. Blomgren, and R. Powers, "Lithium and Lithium Ion Batteries.'' ," Power Associates , 2000.

[76] Mathworks. (2008) Mathworks. [Online]. http://se.mathworks.com/help/physmod/sps/powersys/ref/battery.html?requestedDomain=se.mathworks.com

[77] O. Tremblay, L.-A. Dessaint, and A.-I. Dekkiche, "A Generic Battery Model for the Dynamic Simulation of Hybrid Electric Vehicles," *IEEE Vehicle Power and Propulsion Conference*, September 2007.

[78] N. Mohan and T. M. Undeland, *Power Electronics: Converters, Applications, and Design*.: Wiley India Pvt. Limited, 2007.

[79] R. W. Erickson and D. Maksimovic, *Fundamentals of Power Electronics*.: Springer, 2001.

[80] Jan Servotte, "The impact of a distributed battery energy storage system on transmission and distribution power grids," Tampere university of technology, Tampere, 2013.

[81] Muhammad H. Rashid, Ed., *Power electronics handbook*, Third Edition ed. USA: Butterworth-Heinemann, 2010.

[82] M. S. El-Moursi and A. M. Sharaf, "Novel controllers for the 48-pulse VSC STATCOM and SSSC for voltage regulation and reactive power compensation," *IEEE Transactions on Power Systems* , vol. 20, no. 4, pp. 1985 - 1997, November 2005.

[83] Ashwin Kumar Sahoo, K. Murugesan, and T. Thygarajan, "Modeling and simulation of 48-pulse VSC based STATCOM using simulink's power system blockset," *2006 India International Conference on Power Electronics*, pp. 303-308, December 2006.

[84] A. Arulampalam, J. B. Ekanayake, and N. Jenkins, "Application study of a STATCOM with energy storage," *IEE Proceedings*, vol. 150, no. 3, pp. 373-384, 2003.

[85] (2015, April) http://aesenergystorage.com/. [Online]. http://aesenergystorage.com/2015/04/27/aes-energy-storage-announces-260-mw-interconnected-global-projects-construction-late-stage-development/

[86] N. W. Miller, R. S. Zrebiec, G. Hunt, and R. W. Deimerico, "Design and commissioning of a 5 MVA, 2.5 MWh battery energy storage system," *Transmission and Distribution Conference, 1996. Proceedings., 1996 IEEE*, 1996.

[87] Vijay K Sood, *HVDC and FACTS Controllers; Applications of Static Converters in Power Systems*. United States of America: Springer, 2004.

[88] Ashwin Kumar Sahoo, K. Murugesan, and T. Thygarajan, "blockset, Modeling and simulation of 48-pulse VSC based STATCOM using simulink's power system," *IEEE, India International Conference on Power Electronics*, pp. 303 - 308, 2006.

[89] Mathworks. [Online]. http://se.mathworks.com/help/physmod/sps/powersys/ref/threephasepisectionline.html

Appendix A.

D-axis Flux Linkage Voltage Equation

Transient voltage equation

Transforming the transient voltage equation (2-6) into the S domain, and for small variations,

$$\left(1+\tau_{do}^{'}s\right)\Delta E_{q}^{'}=\Delta E_{fd}-\Delta i_{gd}\ (X_{d}-X_{d}^{'}) \tag{A-1}$$

Re-arranging (A-1) by making use of (2-29) gives,

$$\Delta E_{q}^{'}=\frac{1}{\left(1+\tau_{do}^{'}s\right)}\ (\Delta E_{fd}-C_{1}\Delta E_{q}^{''}-C_{2}\Delta\delta) \tag{A-2}$$

Where,

$$C_{1}=\frac{(X_{d}-X_{d}^{'})}{\Delta_{d}^{''}} \tag{A-3}$$

$$C_{2}=\frac{(X_{d}-X_{d}^{'})V_{\infty do}}{\Delta_{d}^{''}} \tag{A-4}$$

$$\Delta_{d}^{''}=X_{d}^{''}+X_{t} \tag{A-5}$$

Sub-transient Voltage Equation

Transforming the transient voltage equation (2-12) into the S domain, and for small variations,

$$\left(1+\tau_{do}^{''}s\right)\Delta E^{'}{}_{q}=C_{3}\Delta E_{fd}-C_{4}\Delta i_{gd}+C_{5}\Delta E_{q}^{'} \tag{A-6}$$

Where,

$$C_{3}=\left[\frac{\tau_{do}^{''}}{\tau_{do}^{'}}\right] \tag{A-7}$$

$$C_{4}=\left[\left(X_{d}^{'}-X_{d}^{''}\right)+\frac{\tau_{do}^{''}}{\tau_{do}^{'}}(X_{d}-X_{d}^{'})\right] \tag{A-8}$$

And $C_5 = \left[1 - \frac{\tau''_{do}}{\tau'_{do}}\right]$ (A-9)

Re-arranging (A-6), by making use of (A-2) and (2-29) gives,

$$C_6(s)\Delta E''_q = C_7(s)\Delta E_{fd} - C_8(s)\Delta\delta \tag{A-10}$$

$$C_6(s) = \left[\frac{\Delta_d + \{\tau'_{do}\Delta'_d + \tau''_{do}(\Delta''_d + (X_d - X'_d))\}s + (\tau'_{do}\tau''_{do}\Delta''_d)s^2}{\Delta''_d\left(1 + \tau'_{do}s\right)}\right] \tag{A-11}$$

$$\Delta'_d = X'_d + X_t \tag{A-12}$$

$$\Delta_d = X_d + X_t \tag{A-13}$$

$$C_7(s) = \frac{1 + \tau''_{do}s}{1 + \tau'_{do}s} \tag{A-14}$$

$$C_8(s) = \left[\frac{(X_d - X''_d) + \{\tau'_{do}\left(X'_d - X'_d\right) + \tau''_{do}(X_d - X'_d)\}s}{\Delta''_d\left(1 + \tau'_{do}s\right)}\right]V_{\infty do} \tag{A-15}$$

or,

$$\Delta E''_q = g_3(s)\Delta E_{fd} - g_4(s)\Delta\delta \tag{A-16}$$

Where

$$g_3(s) = \left[\frac{\Delta''_d\left(1 + \tau''_{do}s\right)}{\Delta_d + \{\tau'_{do}\Delta'_d + \tau''_{do}(\Delta''_d + (X_d - X'_d))\}s + (\tau'_{do}\tau''_{do}\Delta''_d)s^2}\right] \tag{A-17}$$

$$g_4(s) = \left[\frac{((X_d - X''_d) + \{\tau'_{do}\left(X'_d - X'_d\right) + \tau''_{do}(X_d - X'_d)\}s)V_{\infty do}}{\Delta_d + \{\tau'_{do}\Delta'_d + \tau''_{do}(\Delta''_d + (X_d - X'_d))\}s + (\tau'_{do}\tau''_{do}\Delta''_d)s^2}\right] \tag{A-18}$$

Q-axis Flux Linkage Voltage Equation

Transforming the transient voltage equation (2-11) into the S domain, and for small variations,

$$\left(1 + \tau''_{do}s\right)\Delta E'_d =. (X_d - X''_d)\Delta i_{gq} \tag{A-19}$$

Re-arranging (A-16) by making use of (2-30)

$$\Delta E_d^{"} = g_{4d}(s)\Delta\delta \tag{A-20}$$

Where,

$$g_{4d}(s) = \frac{K_{4d}}{\left(1+\tau_q^{"}s\right)} \tag{A-21}$$

$$K_{4d=}\frac{(X_q - X_q^{"})V_{\infty qo}}{\Delta_q} \tag{A-22}$$

$$\Delta_q = X_q + X_t \tag{A-23}$$

$$\tau_q^{"} = \frac{\Delta_q^{"}}{\Delta_q}\tau_{qo}^{"} \tag{A-24}$$

$$\Delta_q^{"} = X_q^{"} + X_t \tag{A-25}$$

Generator Terminal Voltage Equation

From the phasor representation of synchronous generator, the equation (2-2) can be written as follows:

$$e_t^2 = e_{td}^2 + e_{tq}^2 \tag{A-26}$$

Re-arranging (2-37), by making use of (2-38) & (2-39)

$$\Delta e_t = K_5\Delta\delta + K_6\Delta E_q^{"} + K_{6d}\Delta E_d^{"} \tag{A-27}$$

Where

$$K_5 = \frac{e_{tdo}}{e_{to}}\frac{X_q^{"}V_{\infty qo}}{\Delta_q^{"}} + \frac{e_{tqo}}{e_{to}}\frac{X_d^{"}V_{\infty do}}{\Delta_d^{"}} \tag{A-28}$$

$$K_6 = \frac{e_{tqo}}{e_{to}}\frac{X_t}{\Delta_d^{"}} \tag{A-29}$$

$$K_{6d} = \frac{e_{tdo}}{e_{to}}\frac{X_t}{\Delta_q^{"}} \tag{A-30}$$

Electrical power equation

The synchronous generator active power in equation (2-14) can be expressed as,

$$P_e = V_{\infty d} i_{td} + V_{\infty q} i_{tq} \tag{A-31}$$

For small perturbations, the electrical power in

$$\Delta P_e = V_{\infty do} \Delta i_{td} + \Delta V_{\infty d} i_{tdo} + V_{\infty qo} \Delta i_{tq} + \Delta V_{\infty q} i_{tqo} \tag{A-32}$$

Re-arranging (2-43) by making use of (2-44) and (2-45) gives,

$$\Delta P_e = K_1 \Delta\delta + K_2 \Delta E_q^{"} - K_{2d} \Delta E_d^{"} \tag{A-33}$$

Where,

$$K_1 = \frac{V_{\infty do}^2}{\Delta_d^{"}} + \frac{V_{\infty qo}^2}{\Delta_q^{"}} + V_{\infty qo} i_{tdo} - V_{\infty do} i_{tqo} \tag{A-34}$$

$$K_2 = \frac{V_{\infty do}}{\Delta_d^{"}} \tag{A-35}$$

$$K_3 = \frac{V_{\infty qo}}{\Delta_q^{"}} \tag{A-36}$$

Model 2

Substituting (2-6) into (2-27) gives,

$$E_q^{'} - X_d^{'} i_{gd} = i_{gd} X_t + V_{\infty q}$$

$$i_{gd} = \frac{E_q^{'} - V_{\infty q}}{X_d^{'} + X_t} \tag{A-37}$$

Re-arranging (A-37) by making use of (2-19) gives,

$$\Delta i_{gd} = \frac{1}{\Delta_d^{'}} \Delta E_q^{'} + \frac{V_{\infty do}}{\Delta_d^{'}} \Delta\delta \tag{A-38}$$

D-axis Flux Linkage Voltage Equation

Re-arranging (2-31) by making use of (A-38) yields,

$$\Delta E_q^{'} = g_3(s)\Delta E_{fd} - g_4(s)\Delta\delta \tag{A-39}$$

or,

$$\Delta E_q^{'} = \frac{K_3}{\left(1+K_3\tau_{do}^{'}s\right)}(\Delta E_{fd} - K_{4d}\,\Delta\delta\,) \tag{A-40}$$

Where,

$$g_3(s) = \frac{K_3}{\left(1+K_3\tau_{do}^{'}s\right)} \tag{A-41}$$

$$g_4(s) = \frac{K_3 K_4}{\left(1+K_3\tau_{do}^{'}s\right)} \tag{A-42}$$

Generator Terminal Voltage Equation:

Substituting (A-38) into (2-6) yields,

$$\Delta e_{tq} = \frac{X_t}{\Delta_d^{'}}\Delta E_q^{'} - \frac{X_d^{'} V_{\infty do}}{\Delta_d^{'}}\Delta\delta \tag{A-43}$$

Re-arranging (2-37) by making use of (2-39) and (A-40) gives,

$$\Delta e_t = K_5\Delta\delta + K_6\Delta E_q^{'} - K_{6d}\Delta E_d^{"} \tag{A-44}$$

Where, $K_5 = \frac{e_{tdo}}{e_{to}}\frac{X_q^{"} V_{\infty qo}}{\Delta_q^{"}} - \frac{e_{tqo}}{e_{to}}\frac{X_d^{'} V_{\infty do}}{\Delta_d^{'}}$ (A-45)

$$K_6 = \frac{e_{tqo}}{e_{to}}\frac{X_t}{\Delta_d^{'}} \tag{A-46}$$

$$K_{6d} = \frac{e_{tdo}}{e_{to}}\frac{X_t}{\Delta_q^{"}} \tag{A-47}$$

Electrical Power Equation:

Re-arranging (2-24) by making use of (A-38) gives,

$$\Delta i_{td} = \frac{1}{\Delta_d^{'}} \Delta E_q^{'} + \frac{V_{\infty do}}{\Delta_d^{'}} \Delta\delta \tag{A-48}$$

Re-arranging (A-50) by making use of (2-43) and (A-48) gives,

$$\Delta P_e = K_1 \Delta\delta + K_2 \Delta E_q^{'} - K_{2d} \Delta E_d^{''} \tag{A-49}$$

$$\text{Where, } K_1 = \left[\frac{V_{\infty do}^2}{\Delta_d^{'}} + \frac{V_{\infty qo}^2}{\Delta_q^{''}} + V_{\infty qo} i_{tdo} - V_{\infty do} i_{tqo} \right] \tag{A-50}$$

$$K_2 = \left[\frac{V_{\infty do}}{\Delta_d^{'}} \right] \tag{A-51}$$

$$K_3 = \left[\frac{V_{\infty qo}}{\Delta_q^{''}} \right] \tag{A-52}$$

Model-3

Substituting (2-28) by (2-3) gives,

$$X_q i_{gq} = V_{\infty d} - i_{gq} X_t$$

$$i_{gq} = \frac{V_{\infty d}}{(X_q + X_t)} \tag{A-53}$$

Re-arranging (A-53) by making use of (2-20) gives,

$$\Delta i_{gq} = \frac{V_{\infty qo}}{(X_q + X_t)} \Delta\delta \tag{A-54}$$

Substituting (A-54) into (2-3) gives,

$$\Delta e_{td} = \frac{X_q V_{\infty qo}}{(X_q + X_t)} \Delta\delta \tag{A-55}$$

Re-arranging (2-37) by making use of (A-43) and (A-55)

$$\Delta e_t = K_5 \Delta\delta + K_6 \Delta E_q^{'} \tag{A-56}$$

Where, $K_5 = \frac{e_{tdo}}{e_{to}} \frac{X_q V_{\infty qo}}{\Delta_q} - \frac{e_{tqo}}{e_{to}} \frac{X_d^{'} V_{\infty do}}{\Delta_d^{'}}$ (A-57)

$$K_6 = \frac{e_{tqo}}{e_{to}} \frac{X_t}{\Delta_d^{'}} \tag{A-58}$$

Electrical Power Equation

Re-arranging (2-23) by making use of (A-54)

$$\Delta i_{tq} = \frac{V_{\infty qo}}{(X_q + X_t)} \Delta\delta \tag{A-59}$$

Re-arranging (2-43) by making use of (A-48) and (A-59) gives,

$$\Delta P_e = K_1 \Delta\delta + K_2 \Delta E_q^{'} \tag{A-60}$$

Where, $K_1 = \left[\frac{V_{\infty do}^2}{\Delta_d^{'}} + \frac{V_{\infty qo}^2}{\Delta_q} + V_{\infty qo} i_{tdo} - V_{\infty do} i_{tqo} \right]$ (A-61)

$$K_2 = \left[\frac{V_{\infty do}}{\Delta_d^{'}} \right] \tag{A-62}$$

Appendix B.

B.1 The parameters of generators

No of gen.	Generator rating (MVA)	X_d (p.u)	$X_d^{'}$ (p.u)	$X_d^{''}$ (p.u)	X_q (p.u)	$X_q^{'}$ (p.u)	$X_q^{''}$ (p.u)	Xl (p.u)	$T_{do}^{'}$ (p.u)	$T_{do}^{''}$ (p.u)	$T_{qo}^{'}$ (p.u)	$T_{qo}^{''}$ (p.u)	H(s)	F (p.u)
G1	3700	1.79	0.355	0.275	1.66	0.57	0.275	0.215	7.9	0.032	0.41	0.055	8	0.001
G2	1450	2.183	0.413	0.339	2.157	1.285	0.332	0.246	5.69	0.041	1.5	0.144	4	0.001
G3	1220	1.798	0.324	0.26	1.778	1.051	0.255	0.193	5.21	0.042	1.5	0.042	4	0.001
G4	2000	1.782	0.444	0.283	1.739	1.201	0.277	0.275	6.07	0.055	1.5	0.152	5.5	0.001
G5	1220	1.798	0.324	0.26	1.778	1.051	0.255	0.193	5.21	0.042	1.5	0.042	4	0.001
G6	1220	1.798	0.324	0.26	1.778	1.051	0.255	0.193	5.21	0.042	1.5	0.042	4	0.001
G7	1220	1.798	0.324	0.26	1.778	1.051	0.255	0.14	5.21	0.042	1.5	0.042	4	0.001
G8	970	0.93	0.302	0.245	0.69	-	0.27	0.244	8	0.03	-	0.06	4	0.001
G9	710	0.92	0.3	0.22	0.51	-	0.29	0.13	5.2	0.029	-	0.034	6	0.001
G10	710	0.92	0.3	0.22	0.51	-	0.29	0.13	5.2	0.029	-	0.034	6	0.001
G11	710	0.92	0.3	0.22	0.51	-	0.29	0.13	5.2	0.029	-	0.034	6	0.001
G12	5910	0.92	0.3	0.22	0.51	-	0.29	0.13	5.2	0.029	-	0.034	6	0.001
G13	5910	0.92	0.3	0.22	0.51	-	0.29	0.13	5.2	0.029	-	0.034	6	0.001
G14	5000	2.183	0.413	0.339	2.157	1.258	0.332	0.246	5.69	0.041	1.285	0.332	4	0.001
G15	5000	2.183	0.413	0.339	2.157	1.258	0.332	0.246	5.69	0.042	1.285	0.332	4	0.001

B.2 Step down transformer parameters (at load terminal)

Step- down Transformer	Nominal Power (MVA)	Winding-1 voltage (kV)	Winding-2 voltage (kV)	Winding-3 voltage (kV)	Shunt Reactor (H) at 20kV	Winding-1 Resistance (pu)	Winding-1 Leakage inductance (pu)	Winding -2 Resistance (pu)	Winding-2 Leakage inductance (pu)	Winding-3 Resistance (pu)	Winding-3 Leakage inductance (pu)	Winding connections
TL1	3000	400	110	20	100	1.047e-3	3.3327e-4	2.095e-4	6.6686e-4	6.35e-4	2.0213e-4	Yg-Yg-D1
TL2	3000	400	110	20	0.01	1.047e-3	3.3327e-4	2.095e-4	6.6686e-4	6.35e-4	2.0213e-4	Yg-Yg-D1
TL3	1850	400	110	20	100	1.047e-3	3.3327e-4	2.095e-4	6.6686e-4	6.35e-4	2.0213e-4	Yg-Yg-D1
TL4	1500	400	110	20	100	1.047e-3	3.3327e-4	2.095e-4	6.6686e-4	6.35e-4	2.0213e-4	Yg-Yg-D1
TL5	2500	400	110	20	0.006	1.047e-3	3.3327e-4	2.095e-4	6.6686e-4	6.35e-4	2.0213e-4	Yg-Yg-D1
TL6	2500	400	110	20	0.008	1.047e-3	3.3327e-4	2.095e-4	6.6686e-4	6.35e-4	2.0213e-4	Yg-Yg-D1
TL7	1500	400	110	20	0.0035	1.047e-3	3.3327e-4	2.095e-4	6.6686e-4	6.35e-4	2.0213e-4	Yg-Yg-D1
TL8	3000	400	110	20	0.03	1.047e-3	3.3327e-4	2.095e-4	6.6686e-4	6.35e-4	2.0213e-4	Yg-Yg-D1
TL9	1500	400	110	20	0.03	1.047e-3	3.3327e-4	2.095e-4	6.6686e-4	6.35e-4	2.0213e-4	Yg-Yg-D1
TL10	1000	400	110	20	0.03	1.047e-3	3.3327e-4	2.095e-4	6.6686e-4	6.35e-4	2.0213e-4	Yg-Yg-D1
TL11	1000	400	110	20	0.03	1.047e-3	3.3327e-4	2.095e-4	6.6686e-4	6.35e-4	2.0213e-4	Yg-Yg-D1

B.3 Step up transformer parameters (at generator terminal)

Gen. Step-up Transformer	Nominal Power (MVA)	Winding-1 voltage (kV)	Winding-2 voltage (kV)	Winding Resistance (pu)	Leakage inductance (pu)	Winding connections
T1	5550	26	400	0.003	9.5493e-4	Yg-Yg
T2	1500	26	400	0.003	9.5493e-4	Yg-Yg
T3	1850	26	400	0.003	9.5493e-4	Yg-Yg
T4	3000	26	400	0.003	9.5493e-4	Yg-Yg
T5	1850	26	400	0.003	9.5493e-4	Yg-Yg
T6	1850	26	400	0.003	9.5493e-4	Yg-Yg
T7	1850	26	400	0.003	9.5493e-4	Yg-Yg
T8	1500	26	400	0.003	9.5493e-4	Yg-Yg
T9	1100	26	400	0.003	9.5493e-4	Yg-Yg
T10	1100	26	400	0.003	9.5493e-4	Yg-Yg
T11	1100	26	400	0.003	9.5493e-4	Yg-Yg
T12	8800	26	400	0.002	6.3662e-4	Yg-Yg
T13	8800	26	400	0.002	6.3662e-4	Yg-Yg
T14	7500	26	400	0.002	6.3662e-4	Yg-Yg
T15	7500	26	400	0.002	6.3662e-4	Yg-Yg

B.4 Load parameters

Load Bus name	Load voltage (kV)	Load Active power (MW)	Load Reactive power (MVar)
SW	110	570	0
S	110	570	0
SE	110	570	0
CS	110	285	0
C	110	428	0
CE	110	285	0
CW	110	428	0
CN	110	570.858	0
NW	110	285.4296	0
N	110	85.713	0
NE	110	85.713	0

B.5 Capacitance parameters

Capacitor no.	C1	C2	C3	C4	C5	C6	C7	C8	C9
Capacitance (µF)	44.45	62.63	62.63	40.53	78.74	81.06	106	106	106

B.6 Transmission line parameters

Node From-To	Length of lines	Number of lines	Positive sequence resistance (Ω/km)	Positive sequence inductance (H/km)	Positive sequence Capacitance (F/km)	Zero sequence resistance (Ω/km)	Zero sequence inductance (H/km)	Zero sequence Capacitance (F/km)
SW-S	180	2	2.282e-2	1.1e-3	1.2775e-8	0.0684	3.3e-3	3.83e-8
SW-CW	220	2	2.282e-2	1.1e-3	1.2775e-8	0.0684	3.3e-3	3.83e-8
SW-CS	180	2	2.282e-2	1.1e-3	1.2775e-8	0.0684	3.3e-3	3.83e-8
S-SE	180	2	2.282e-2	1.1e-3	1.2775e-8	0.0684	3.3e-3	3.83e-8
S-CS	180	2	2.282e-2	1.1e-3	1.2775e-8	0.0684	3.3e-3	3.83e-8
CW-C	140	1	2.282e-2	1.1e-3	1.2775e-8	0.0684	3.3e-3	3.83e-8
C-CE	220	1	2.282e-2	1.1e-3	1.2775e-8	0.0684	3.3e-3	3.83e-8
C-CS	180	2	2.282e-2	1.1e-3	1.2775e-8	0.0684	3.3e-3	3.83e-8
SE-CE	110	2	2.282e-2	1.1e-3	1.2775e-8	0.0684	3.3e-3	3.83e-8
CS-CE	300	1	2.282e-2	1.1e-3	1.2775e-8	0.0684	3.3e-3	3.83e-8
CW-CN	330	1	2.282e-2	1.1e-3	1.2775e-8	0.0684	3.3e-3	3.83e-8
C-CN	220	1	2.282e-2	1.1e-3	1.2775e-8	0.0684	3.3e-3	3.83e-8
CE-CN	340	1	2.282e-2	1.1e-3	1.2775e-8	0.0684	3.3e-3	3.83e-8
CN-NW	130	1	2.282e-2	1.1e-3	1.2775e-8	0.0684	3.3e-3	3.83e-8
CN-N	170	1	2.282e-2	1.1e-3	1.2775e-8	0.0684	3.3e-3	3.83e-8
CN-NE	175	1	2.282e-2	1.1e-3	1.2775e-8	0.0684	3.3e-3	3.83e-8
NE-N	85	1	2.282e-2	1.1e-3	1.2775e-8	0.0684	3.3e-3	3.83e-8
N-NW	65	1	2.282e-2	1.1e-3	1.2775e-8	0.0684	3.3e-3	3.83e-8
N-Nordic_N	170	1	2.282e-2	1.1e-3	1.2775e-8	0.0684	3.3e-3	3.83e-8
NW-Nordic_N	120	1	2.282e-2	1.1e-3	1.2775e-8	0.0684	3.3e-3	3.83e-8
Nordic_N-Nordic	100	1	2.282e-2	6.6362e-4	1.2775e-8	0.0684	3.3e-3	1.991e-3
Nordic-Nordic-N1	200	2	2.282e-2	1.1e-3	1.2775e-8	0.0684	3.3e-3	3.83e-8
Nordic-Nordic-S	200	2	2.282e-2	6.6362e-4	1.2775e-8	0.0684	3.3e-3	1.991e-3
Nordic-S- Nordic-N1	200	2	2.282e-2	6.6362e-4	1.2775e-8	0.0684	3.3e-3	1.991e-3

B.7 Other parameters-

Droop Setting

Nordic_N1_droop=1e-5; Nordic_N2_droop=1e-5; N_droop=1e-5; NE_droop=1e-5;

NW_droop=1e-5;

Generator reference voltages

SW_ref=1.012; S_ref=1.005; SE_ref=1.015; C_ref=1.005; NW_ref=1.015; N_ref=1.005;

NE_ref=1.005; Nordic_C_ref=1.015; Nordic_N1_ref=1.015;

Nordic_N2_ref=1.015; Nordic_S_ref=1.015;

Series inductances

SW_inductance=0.063375; C_inductance=0.2704; N_inductance=0.4056; Nordic_S_inductance=0.6;

Nordic_N_inductance=0.4056;

Reactance calculation

SW_L=SW_inductance/(2*pi*50); C_L=C_inductance/(2*pi*50); N_L=N_inductance/(2*pi*50);

Nordic_S_L=Nordic_S_inductance/(2*pi*50); Nordic_C_L=Nordic_N_inductance/(2*pi*50);

Limit Control of Governor areas

NE_valve_up_limit=1-NE_Pmec; NE_valve_low_limit=NE_Pmec*(-1);

CN_integrator_up_limit=1-CN_Pmec; CN_integrator_low_limit=CN_Pmec*(-1);

CN_limiter_up_limit=3-CN_integrator_up_limit; CN_limiter_low_limit=-3+CN_integrator_low_limit;

N_valve_up_limit=1-N_Pmec; N_valve_low_limit=N_Pmec*(-1);

NW_valve_up_limit=1-NW_Pmec; NW_valve_low_limit=N_Pmec*(-1);

Nordic_N2_valve_up_limit=0.212-N2_Pmec; Nordic_N2_valve_low_limit=N2_Pmec*(-1);

Nordic_N1_valve_up_limit=0.212-N1_Pmec; Nordic_N1_valve_low_limit=N1_Pmec*(-1);